End-to-End Delay Analysis for Routing Protocols in VANETs

by

© Hafez Seliem

A dissertation submitted to the School of Graduate Studies
in partial fulfilment of the requirements for the degree of

Doctor of Philosophy

Faculty of Engineering and Applied Science
Memorial University of Newfoundland

May 2019

St. John's, Newfoundland

Abstract

Vehicular ad-hoc network (VANET) technology enables communication between vehicles, or vehicles and road-side units (RSUs) through wireless communication devices installed on the vehicles. One of the most important goals of VANETs is providing safety applications for passengers. In addition, VANETs provide comfort applications to users. Guaranteeing a reliable and stable routing protocol over VANETs is a very important step. The proposed research attempts to improve routing protocols that decrease the end-to-end delay to suit VANET communication characteristics. In addition, it proposes analysis of the end-to-end delay probability distribution.

More specifically, we derive a closed-form expression for the probability distribution of the re-healing delay in a VANET conditioned on the distance between two VANET clusters. Furthermore, we propose a closed-form expression for the probability distribution of the unconditional re-healing delay. Moreover, we develop a mathematical model to calculate the probability distribution of the end-to-end delay.

On the other hand, using Unmanned Aerial Vehicles (UAVs) or drones in wireless communications and Vehicular Ad-hoc Networks (VANETs) has started to attract attention. We propose a routing protocol that uses infrastructure drones for boosting VANET communications to achieve a minimum vehicle-to-drone packet delivery delay. In addition, we propose a closed-form expression for the probability distribution of the vehicle-to-drone packet delivery delay on a two-way highway. Moreover, based on that closed-form expression, we can calculate

the minimum drone density (maximum separation distance between two adjacent drones) that stochastically limits the worst case of the vehicle-to-drone packet delivery delay.

Furthermore, we propose a drones-active service (DAS) that is added to the location service in a VANET. This service dynamically and periodically obtains the required number of active drones based on the current highway connectivity state by obtaining the maximum distance between each two adjacent drones while satisfying a probabilistic constraint for vehicle-to-drone packet delivery delay. Our analysis focuses on two-way highway VANET networks with low vehicular density. The simulation results show the accuracy of our analysis and reflect the relation between the drone density, vehicular density and speed, other VANET parameters, and the vehicle-to-drone packet delivery delay.

In addition, we propose a new routing protocol called multi-copy intersection-based routing (MCIR) for vehicular ad-hoc networks (VANETs) in urban areas. MCIR is an intersection-based routing protocol that forwards multiple copies of the packets in different road segments. Moreover, it is a beacon-less routing protocol with a carry-and-forward strategy. We show via simulation that the MCIR protocol is superior to other existing routing protocols, especially in low vehicular density scenarios. The results show that MCIR achieves a shorter end-to-end delay and a higher packet delivery ratio in urban VANET communications.

Acknowledgements

As the formal part of my education comes to an end, it is a great pleasure to acknowledge several individuals who have had contributed to who I am today.

After thanking Almighty "ALLAH" for his blessing and guidance to complete this work, I would like to offer my sincere thanks to my supervisor Prof. Mohamed H. Ahmed, and co-supervisors Dr. Mohamed Shehata and Dr. Reza Shahidi for their continues and valuable guidance. I greatly appreciate the time they have spent contributing to this research and to my professional development. Without their guidance and persistent help this dissertation would not have been possible. I would like to acknowledge the financial support provided by my supervisor, the Faculty of Engineering and Applied Science, the School of Graduate Studies, and the Natural Sciences and Engineering Research Council of Canada (NSERC).

A significant part of my education was in Egypt. I would like to thank my elementary, secondary and high schools teachers, my B.Sc. professors and instructors, and my M.Sc. thesis supervisor.

The final word of acknowledgement is reserved for my parents, brothers, and sisters for their unconditional support, and to my lovely wife for her love and patience, without your continuous support and encouragement, nothing is complete. For my daughter Menna, you add a great value to everything.

Co-Authorship Statements

I, Hafez Seliem, hold a principal author status for all the manuscript chapters (Chapter 2 - 6) in this dissertation. However, each manuscript is co-authored by my supervisor and co-researchers, whose contributions have facilitated the development of this work as described below.

- Paper 1 in Chapter 2: H. Seliem, Mohamed H. Ahmed, Mohamed Shehata, "Multi-Copy Intersection-Based Routing Protocol for VANET in Urban Areas," International Journal of Technology and Engineering Studies, vol. 3, no. 4, pp. 159-168, 2017.

  I was the primary author, with authors 2 and 3 contributing to the idea, its formulation and development, and refinement of the presentation.

- Paper 2 in Chapter 3: H. Seliem, Reza Shahidi, Mohamed H. Ahmed, Mohamed S. Shehata, "Probability Distribution of the Re-Healing Delay in a One-Way Highway VANET," IEEE Communications Letters, 22(10), 2056-2059. 2018.

  I was the primary author, with authors 2 - 4 contributing to the idea, its formulation and development, and refinement of the presentation.

- Paper 3 in Chapter 4: H. Seliem, Reza Shahidi, Mohamed H. Ahmed, Mohamed S. Shehata, "On the End-to-End Delay in a One-Way VANET," submitted to IEEE Transactions

on Vehicular Technology, January 2019.

I was the primary author, with authors 2 - 4 contributing to the idea, its formulation and development, and refinement of the presentation.

- Paper 4 in Chapter 5: H. Seliem, Reza Shahidi, Mohamed H. Ahmed, Mohamed S. Shehata, "Delay analysis for Drone-based VANET," IEEE Access, 6, 20125-20137, 2018.

  I was the primary author, with authors 2 - 4 contributing to the idea, its formulation and development, and refinement of the presentation.

- Paper 5 in Chapter 6: H. Seliem, Reza Shahidi, Mohamed H. Ahmed, Mohamed S. Shehata, "Accurate probability distribution for delay in drone-based VANET," to be submitted at IEEE wireless communication letters.

  I was the primary author, with authors 2 - 4 contributing to the idea, its formulation and development, and refinement of the presentation.

Hafez Seliem	Date

Contents

List of Figures

List of Tables

List of Abbreviations

AMR ..... Adaptive Multi-copy Routing

BAHG ..... Backbone Assisted Hop Greedy Routing

CDF ..... Cumulative Distribution Function

DAS ..... Drones-Active Service

DCF ..... Distributed Coordination Function

Drone-BS ..... DroneBase-station

DSRC ..... Dedicated Short Range Communications

EM ..... Emergency Message

FCC ..... Federal Communications Commission

GLS ..... Grid Location Service

GPS ..... Global Positioning Systems

GPSR ..... Greedy Perimeter Stateless Routing Protocol

GyTAR ..... Greedy Traffic-aware Routing Protocol

HLS ..... Hierarchical Location Service

IEEE ..... Institute of Electrical and Electronics Engineers

ITS ..... Intelligent Transport System

LAP ..... Low Altitude Platform

LOS ..... Line of Sight

MAC ..... Medium Access Control

MCIR ..... Multi-copy Intersection-based Routing

NLoS ..... Non-line of Sight

PDF ..... Probability Density Function

PDR ..... Packet Delivery Ratio

RSU ..... Road-side Unit

SRPMT ..... Street-centric Routing Protocol-based on Micro Topology

UAV ..... Unmanned Aerial Vehicle

UVAR ..... UAV-assisted VANET Routing Protocol

V2V ..... Vehicle to Vehicle

VANET ..... Vehicular Ad-hoc Network

WAVE ..... Wireless Access in Vehicular Environments

Chapter 1

Introduction

1.1 Background

Vehicular ad-hoc network (VANET) technology enables communication between vehicles, or vehicles and road-side units (RSUs) through wireless communication devices installed on the vehicles. Many vehicle manufacturers have equipped their new vehicles with global positioning systems (GPSs) and wireless interfaces. In addition, in 1999, the United States Federal Communications Commission (FCC) allocated 75 MHz of spectrum at 5.9 MHz to be used by Dedicated Short Range Communications (DSRC) [1]. DSRC is a short to medium range communications service that was developed to provide vehicle-to-vehicle (V2V) and vehicle-to-roadside communications. DSRC is aimed to provide a high data rate for transmission and a low communication end-to-end delay. The Institute of Electrical and Electronics Engineers (IEEE) has also provided the IEEE 1609 family of standards for wireless access in vehicular environments (WAVE) [2], which defines architecture, and a set of services and interfaces that can provide a secure V2V and vehicle-to-roadside wireless communication.

1.2 Research Motivation

One of the most important goals of VANETs is providing safety applications for passengers. In addition, VANETs provide comfort applications to users (e.g., mobile e-commerce, weather information, and many other multimedia applications).

Routing is a fundamental operation for vehicle communications to select a source-to-destination path in a VANET. The important goal of uni-cast routing protocols in VANET communications is to transmit data from a source to a destination via multi-hop path or greedy forward techniques. The design of effective routing protocols in VANETs has a series of technical challenges. Guaranteeing a reliable and stable routing protocol over a VANET is a very important step. One of the critical issues in VANETs is designing a routing algorithm that is robust to frequent path disruptions caused by vehicles' high mobility.

Scenarios with low vehicular densities have a higher probability of network disconnection. As a result, the packet loss probability increases [3]. To overcome this problem, vehicles can be used as carriers to deliver messages via a carry-and-forward strategy whenever the option of forwarding via wireless transmission is not available. Therefore, most of the existing routing protocols for VANETs use the carry-and-forward strategy as one of their routing strategies to face network disconnection. However, the packets suffer from long end-to-end delay in carry-and-forward strategy, especially in low vehicular densities. Some VANET applications have an end-to-end delay constraint. Consequently, end-to-end delay is a very important issue in VANET routing design. Our research focuses on developing VANET routing protocols for VANET communications that decrease the end-to-end delay. In addition, we propose a mathematical framework to calculate the the end-to-end delay probability distribution.

The proposed research attempts to improve routing protocol that decrease the end-to-end

delay to suit VANET communication characteristics. Our objective is minimize the end-end delay. Eventually, the proposed solution is implemented and evaluated to show its effectiveness through extensive simulation studies.

1.3 Thesis Contribution

This dissertation presents the following novel contributions to end-to-end packet delivery delay in VANETs.

- We propose a new routing protocol called multi-copy intersection-based routing (MCIR) for vehicular ad-hoc networks (VANETs) in urban areas. MCIR is an intersection-based routing protocol that forwards multiple copies of the packets in different road segments.
- We propose a closed-form expression for the probability distribution of the re-healing delay (time taken in the store-and-forward strategy to send a packet from a cluster head to the tail of the next cluster) conditioned on the gap distance between those two clusters on a one-way highway.
- We propose a closed-form expression for the unconditional probability distribution of the re-healing delay.
- We propose an analytical model to study the end-to-end delay in a one-way VANET and derive an analytical formula for the probability distribution of the end-to-end delay.
- We propose a closed form expression for the lower bound on the end-to-end delay probability distribution.

- We propose a closed form expression for the upper bound on the end-to-end delay probability distribution.

- We present a routing protocol that uses infrastructure drones for boosting VANET communications to achieve a minimum vehicle-to-drone packet delivery delay.

- We propose a closed-form expression for the probability distribution of the vehicle-to-drone packet delivery delay on a two-way highway. Based on that closed-form expression, we can calculate the minimum drone density (maximum separation distance between two adjacent drones) that stochastically limits the worst case of the vehicle-to-drone packet delivery delay.

- We propose a drones-active service (DAS) that is added to the location service in a VANET. This service dynamically and periodically obtains the required number of active drones based on the current highway connectivity state by obtaining the maximum distance between each pair of adjacent drones while satisfying a probabilistic constraint for vehicle-to-drone packet delivery delay.

- We propose an analytical expression for the probability distribution of the vehicle-to-drone packet delivery delay on a two-way highway where we consider the vehicle wireless communication range and the cluster length in the analysis.

1.4 Thesis Outline

In this section, we outline the organization of this thesis and give a brief overview of each chapter.

In Chapter 2, we present a new routing protocol called multi-copy intersection-based routing (MCIR) for vehicular ad-hoc networks (VANETs) in urban areas. MCIR is an intersection-based routing protocol that forwards multiple copies of the packets in different road segments. Moreover, it is a beacon-less routing protocol with a carry-and-forward strategy. We show via simulation that the MCIR protocol is superior to other existing routing protocols, especially in low vehicular density scenarios. The results show that MCIR achieves a shorter end-to-end delay and a higher packet delivery ratio in urban VANET communications. In Chapter 3, we presents a closed-form expression for the probability distribution of the re-healing delay (time taken in the store-and-forward strategy to send a packet from a cluster head to the tail of the next cluster) conditioned on the gap distance between those two clusters on a one-way highway. Moreover, a closed-form expression is derived for the unconditional probability distribution of the re-healing delay. Using the derived probability distribution, one can straightforwardly study the impact of VANET parameters on the re-healing delay. Next, based on Chapter 3, in Chapter 4, we present an analytical model to study the end-to-end delay in a one-way VANET. It proposes an analytical formula for the probability distribution of the end-to-end delay. Using the derived probability distribution, the probability that the end-to-end delay is less than a given threshold may be calculated. In addition, one can straightforwardly study the impact of parameters such as wireless communication range, vehicular density, the distance between the source and the destination, and the minimum and maximum vehicles speeds on the end-to-end delay. This can help to better understand data dissemination in VANETs. Moreover, the closed form for the lower bound on the end-to-end delay probability distribution is obtained. In addition, the closed form for a upper bound on the end-to-end delay probability distribution is derived. The accuracy of the analytical results is validated using simulations. Extensive simulation results demonstrate the accuracy of our analysis.

In Chapter 5, we present a routing protocol that uses infrastructure drones for boosting VANET communications to achieve a minimum vehicle-to-drone packet delivery delay. It proposes a closed-form expression for the probability distribution of the vehicle-to-drone packet delivery delay on a two-way highway. In addition, based on that closed-form expression, we can calculate the minimum drone density (maximum separation distance between two adjacent drones) that stochastically limits the worst case of the vehicle-to-drone packet delivery delay. Moreover, it proposes a drones-active service (DAS) that is added to the location service in a VANET. This service dynamically and periodically obtains the required number of active drones based on the current highway connectivity state by obtaining the maximum distance between each two adjacent drones while satisfying a probabilistic constraint for vehicle-to-drone packet delivery delay. Our analysis focuses on two-way highway VANET networks with low vehicular density. The simulation results show the accuracy of our analysis and reflect the relation between the drone density, vehicular density and speed, other VANET parameters, and the vehicle-to-drone packet delivery delay. Next, in Chapter 6, based on Chapter 5, we analytically derive the probability distribution of the vehicle-to-drone packet delivery delay on a bi-directional highway . The model on which the analysis is based considers the vehicle wireless communication range and the cluster length. Finally, in Chapter 7, we summarize the contributions presented in this dissertation and discuss several potential extensions to our work.

REFERENCES

[1] R. Yuan, "North american dedicated short range communications (dsrc) standards," in *Proceedings of Conference on Intelligent Transportation Systems*, Nov 1997, pp. 537–542.

[2] D. Jiang and L. Delgrossi, "Ieee 802.11 p: Towards an international standard for wireless access in vehicular environments," in *Vehicular Technology Conference, 2008. VTC Spring 2008. IEEE*. IEEE, 2008, pp. 2036–2040.

[3] L. Yao, J. Wang, X. Wang, A. Chen, and Y. Wang, "V2x routing in a vanet based on the hidden markov model," *IEEE Transactions on Intelligent Transportation Systems*, vol. 19, no. 3, pp. 889–899, 2018.

Chapter 2

Multi-Copy Intersection-Based Routing Protocol for VANETs in Urban Areas

2.1 Abstract

In this paper, we propose a new routing protocol called multi-copy intersection-based routing (MCIR) for vehicular ad-hoc networks (VANETs) in urban areas. MCIR is an intersection-based routing protocol that forwards multiple copies of the packets on different road segments. Moreover, it is a beacon-less routing protocol with a carry-and-forward strategy. We show via simulation that the MCIR protocol is superior to other existing routing protocols, especially in low vehicular density scenarios. The results show that MCIR achieves a shorter end-to-end delay and a higher packet delivery ratio in urban VANET communications.

2.2 Introduction

Vehicular ad-hoc network (VANET) technology enables communication between vehicles, or vehicles and road-side units (RSU) through wireless communication devices installed on the vehicles. One of the most important goals of VANETs is providing safety applications for passengers. In addition, VANETs provide comfort applications to the users (e.g., mobile e-commerce, weather information, and other many multimedia applications). Routing is a fundamental process for VANET to select a source-to-destination path.

VANET connectivity often changes, especially when the vehicular density is low. Therefore, regular ad-hoc routing protocols with complete path discovery mechanisms are not feasible since the routing path is usually disconnected due to the intermittent nature of the network links. Scenarios with low vehicular densities have a higher probability of network disconnection. As a result, the packet loss probability increases [1]. To overcome this problem, vehicles can be used as carriers to deliver messages via a carry-and-forward strategy whenever the option of forwarding via wireless transmission is not available. Therefore, most of the existing routing protocols for VANETs use the carry-and-forward strategy as one of their routing strategies to counter network disconnection. However, the packets suffer from long end-to-end delays in the carry-and-forward strategy.

Many papers have proposed routing protocols for VANET routing in urban areas. Most routing protocols in urban areas are position-based protocols that depend on the greedy perimeter stateless routing protocol (GPSR) [2]. GPSR protocol uses greedy forwarding to forward packets from a source to a destination. In greedy forwarding, GPSR tries to bring packets closer to the destination in each hop using geographic information. However, in many cases, greedy forwarding can lead to areas where there is no neighbor closer to the destination vehicle except

for the current forwarding vehicle.

Greedy traffic-aware routing (GyTAR) protocol [3] uses digital maps to identify the position of intersections and location service to get the destination location. It selects a forwarding path with the highest vehicular density and the shortest distance. For each intersection, the protocol calculates a score for each road segment candidate that depends on the vehicular density and the Euclidean distance to the destination. A road segment is an area between two adjacent intersections such as the region that is between the intersections I_1 and I_2 in Fig. 2.1. The candidate road segment with the highest score is selected.

On the other hand, backbone assisted hop greedy routing (BAHG) [4] selects the forwarding path with the minimum number of intersections. This is because the shortest path, or the path with the highest connectivity, may include numerous intermediate intersections. As a result, this yields a routing path with a higher hop count. Moreover, it ranks the connectivity of the streets based on the number of lanes.

Street-centric routing protocol based on micro topology (SRPMT) [5] represents the city on a transfer graph, where each edge represents micro topology, while the vertex represents an intersection. Micro topology consists of vehicles and wireless links among vehicles along a street. The edge weights depend on the vehicles mobility, signal fading, wireless channel contention, and existing data traffic. Multi-path for video streaming proposed in [6], distributes the traffic into a set of two or three paths for load balancing.

Adaptive Multi-copy Routing (AMR) [7] adaptively selects between single-copy and multi-copy routing at the intersections depending on the difference between estimated end-to-end delay for the single-copy and the multi-copy. If the difference is greater than a certain threshold, AMR selects multi-copy routing. However, AMR assumes that the average vehicle density and the real-time delay cost of every road segment in the network are available for each vehicle. In

addition, AMR does not eliminate the unneeded copies of the packets.

Most of the above mentioned routing protocols use a single-copy of the generated packets. Moreover, they select the route with the highest vehicular density to avoid network disconnection. However, this single-copy may face disconnected road segments due to low vehicular density. Therefore, most of the previous protocols focus on VANET with high vehicular density. For example, BAHG protocol obtains its results with 600 vehicles in an area of 3 km x 3 km. On the other hand, the authors of SRPMT perform the simulation with 100 to 300 vehicles in an area of 2 km x 1.5 km. Moreover, the authors of GyTAR conduct their simulations with 100 to 350 vehicles in an area of 2.5 km x 2 km. Nevertheless, one of VANET characteristics is that vehicular densities may fluctuate between low and high. Therefore, we need to consider low vehicular density scenarios in the simulation. In addition, it is challenging to estimate the vehicular density and make this information available accurately to all vehicles in the network as in AMR. Moreover, the beacon packets add much overhead to a VANET.

This paper focuses on developing multi-copy intersection-based routing (MCIR) protocol for urban VANET communications. MCIR is a beacon-less routing protocol with a carry-and-forward strategy. In addition, MCIR does not need vehicular density estimation. The proposed protocol deals with low vehicular density by forwarding either one or two copies of each packet at the intersections towards the destination depending on the forwarding vehicle position with respect to the destination position. At each intersection, MCIR finds out which one or two of the four main directions will bring the packets closer to the destination. Next, MCIR forwards the packet in these selected directions. For instance, as shown in Fig. 2.1, at intersection I_1, MCIR forwards the packet up and right, while at intersection I_4, MCIR forwards the packet right only. Meanwhile, the proposed protocol eliminates the unneeded copies of the packets at the intersections to minimize the routing overhead. The proposed protocol improves the

packet delivery ratio and reduces the end-to-end delay. Moreover, on straight road segments, the protocol greedily forwards packets to the next intersection.

The main contributions of this paper are as follows: 1) It proposes a new routing protocol for VANET in urban areas. 2) It analyzes the proposed protocol at low vehicular density and its impact on the routing performance. 3) It compares the proposed protocol with two of the most commonly-used protocols in the literature. The rest of this paper is organized as follows. Section II introduces the system model. Section III provides MCIR protocol design with a detailed example. Section IV presents the performance evaluation for MCIR in terms of packet delivery rate, average end-to-end delay, and routing overhead. Finally, the conclusions and future work are presented in Section V.

2.3 System Model

We assume that each vehicle has the capability to obtain digital maps and its position information, which we consider as a valid assumption since nowadays most of the vehicles have a GPS device [8]. In addition, it is assumed that the source vehicle acquires the destination's location via a location service such as hierarchical location service (HLS) [9] or grid location service (GLS) [10].

Once the destination vehicle's location is obtained, it is included in the packet header. Therefore, the intermediate vehicles do not have to use the location service. However, due to the dynamic nature of the VANET, the destination vehicle may change its location by the time packets arrive at the initial location. In this case, the packet carrier obtains the new location of the destination vehicle via location service and forwards the packet towards the new location [11]. Further, we presume the use of location service is limited only to acquiring the destination

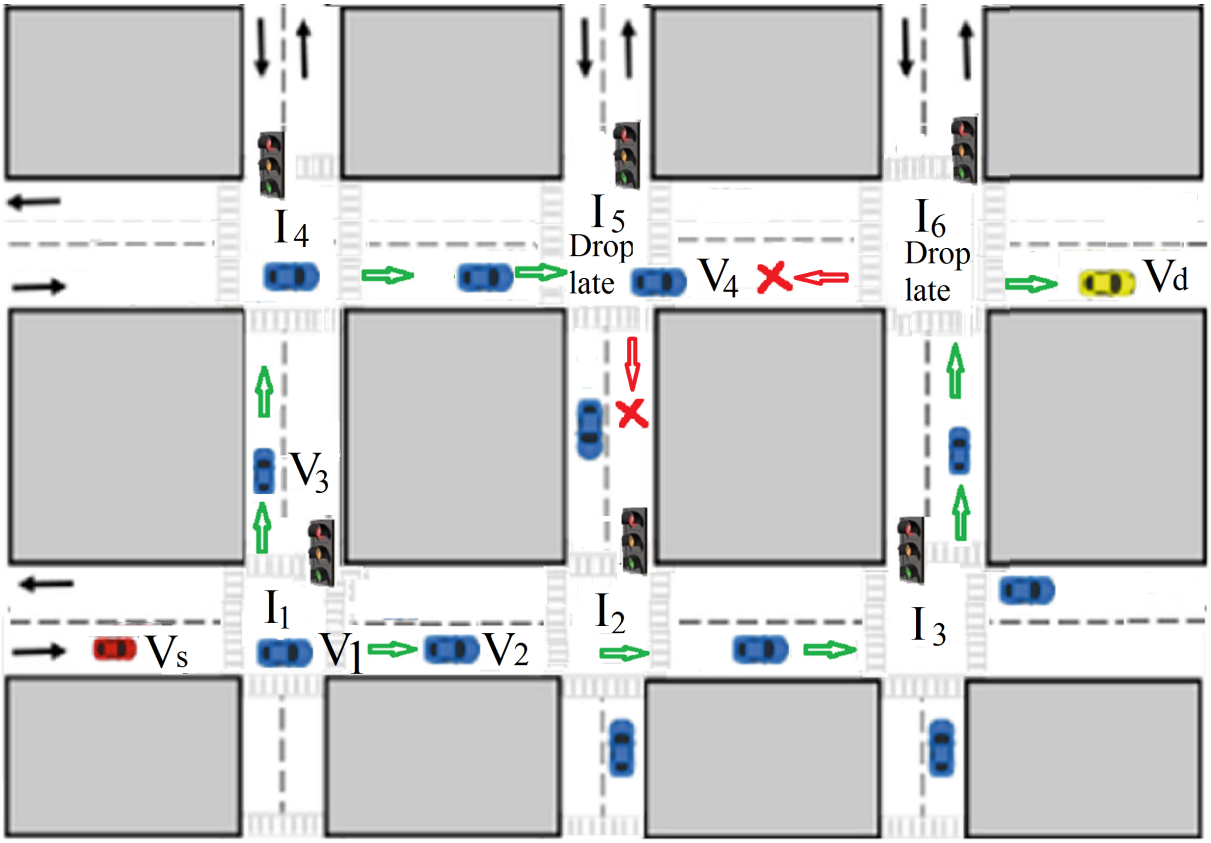

Figure 2.1: Urban grid model

vehicle location.

In addition, we use a grid model for the city environment as shown in Fig. 2.1. This model is based on the Manhattan grid mobility model [12]. In this model, each vehicle is able to adjust its speed based on the movement of the neighboring vehicles and change the lane to overtake other vehicles in multi-lane roads. This model also supports smart intersection management, where vehicles slow down and stop at intersections, or they act accordingly at traffic lights. Moreover, a wrap-around pattern is used such that when a vehicle reaches the border or its destination position, it starts moving towards a new destination position. For instance, as shown in Fig. 2.1, when a vehicle V_1 reaches its destination location at I_3, it starts moving towards a new destination location.

Moreover, we assume that the speeds of the vehicles are uniformly distributed within the interval [V_{min} , V_{max}] [13], while the inter-vehicle distance is exponentially distributed [14]. The medium access control (MAC) layer protocol is the distributed coordination function (DCF) of the IEEE 802.11. In addition, the radio channel propagation model is assumed to follow Nakagami-m distrbution [15]. Packet traffic model follows the constant bit rate (CBR) pattern between a source and a destination that are randomly selected.

2.4 Proposed routing protocol

MCIR protocol has three modes that depend on the location of the forwarding vehicle (the vehicle that has a packet or a flow of packets and wants to forward it towards the destination) and the vehicular density as shown in Fig. 2.2. The three modes are defined as follows.

Greedy Forwarding Mode: In this mode, the current location of the forwarding vehicle and the destination location are stored in the packet header to enable the neighbors to calculate

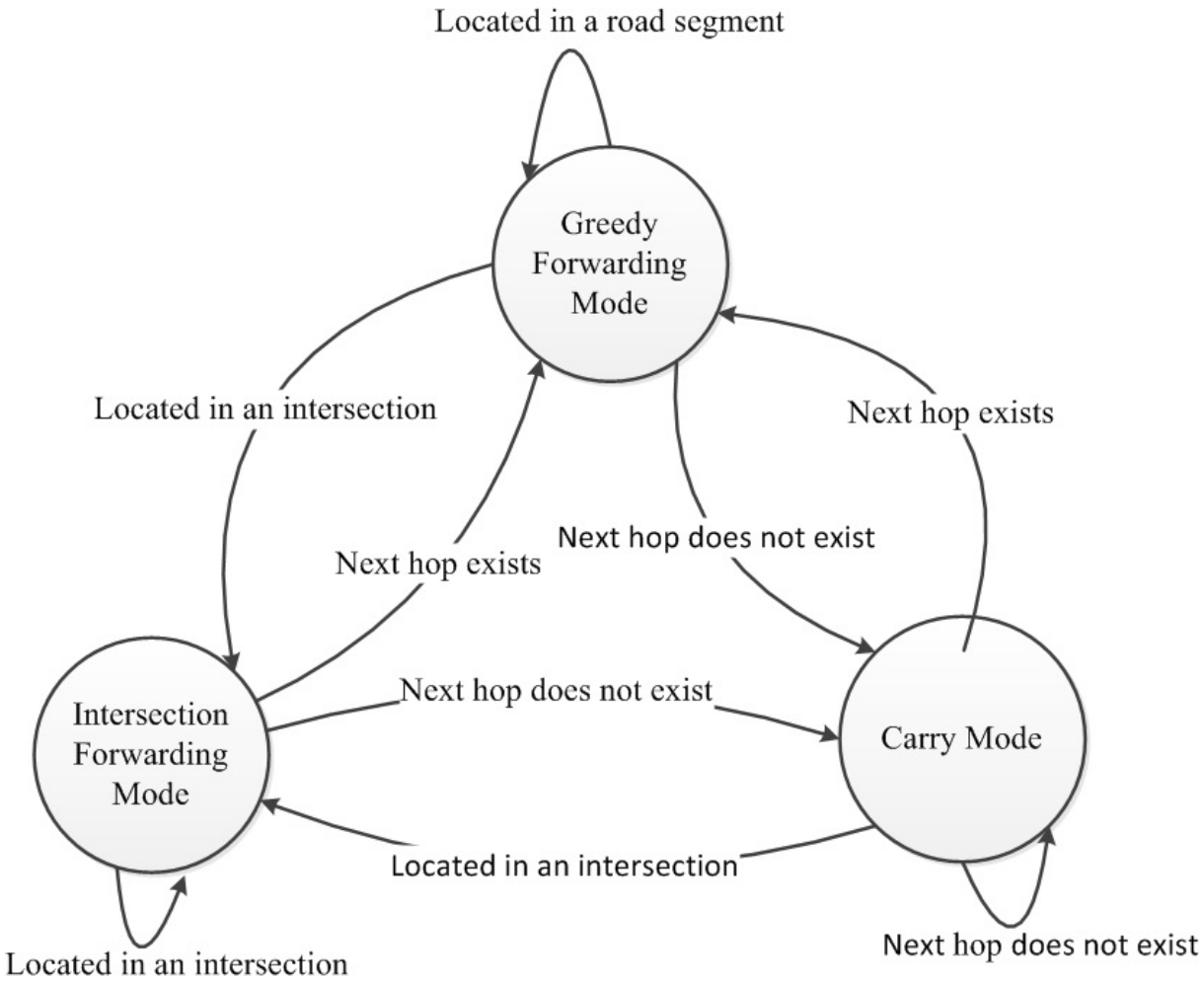

Figure 2.2: MICR Modes.

their progress towards the destination. All neighbors check if they are closer to the destination than the forwarding vehicle. If this condition is true, each neighbor vehicle starts a timer with an interval as follows

$$Timer\ Interval = \frac{R-D}{R}, \tag{2.1}$$

where R is the communication range and D is the Euclidean distance from the neighbor vehicle to the forwarding vehicle. Therefore, the closest neighbor vehicle to the destination vehicle starts the forwarding first. Consequently, it achieves more progress towards the destination, decreases the hop count, and reduces the end-to-end delay. When one neighbor vehicle forwards the packet, all other neighbor vehicles which overhear the packet transmission will drop the packet. On the other hand, the forwarding vehicle must overhear one neighbor forwarding the packet. Otherwise, the forwarding vehicle switches to Carry Mode.

Carry Mode: MCIR switches to Carry Mode when a forwarding vehicle is located at a forwarding area with no neighbors. In this mode, the vehicle carries the packets and keeps in the buffer. When a carry timer (a timer during its period the forwarding vehicle must overhear one neighbor forwards the packet) expires, the forwarding vehicle rebroadcasts the packets and starts the overhearing. Consequently, if one neighbor exists in the forwarding area and is closer to the destination than the forwarding vehicle, this neighbor will be the next hop for the packet. As a result, the forwarding vehicle switches to the Greedy Forwarding Mode and drops the packet after overhearing the neighbor forwarding the packet.

Intersection Forwarding Mode: At the intersection points that are defined by the digital map, MCIR operates in Intersection Forwarding Mode. MCIR forwards multiple copies of the packets in the candidate road segments towards the destination vehicle and eliminates unneeded copies at the next intersections to reduce the overhead. All the vehicles in the candidate road

segments must be closer to the destination than the forwarding node. At the intersections, MCIR forwards the packet if it is the first time the packet reaches this intersection. Otherwise, the packet is dropped. Next, each neighbor vehicle in this intersection checks if it is located in one of the four main directions bringing the packet closer to the destination. This can be achieved by using the digital map and the destination location from the packet header. If this condition is true, the neighbor starts the Greedy Forwarding Mode as mentioned before. In addition, the neighbor vehicle drops the packet and stops the forwarding if one neighbor in the same road segment forwarded the same packet. Before dropping the packet, the neighbor vehicle ensures that it is located in the same road segment of the forwarding neighbor vehicle. For instance, as shown in Fig. 2.1, if V_2 overhears V_3 forwarding the same packet, V_2 does not stop forwarding because V_3 is in a different road segments and MCIR forwards the packets in both road segments. This condition is added because the neighbor vehicle may overhear one vehicle forwarding the packet but in another road segment and MCIR forwards the same packet in one or two road segments. Finally, the forwarding vehicle drops the packet after it ensures that there is one neighbor forwarding the packet. Otherwise, the forwarding vehicle switches to the Carry Mode.

As illustrated in Fig. 2.2, MCIR switches from the Greedy Forwarding Mode or the Intersection Mode to the Carry Mode if the forwarding vehicle does not find a next hop for the packet. In addition, MCIR switches from the Greedy Forwarding Mode or the Carry Mode to the Intersection Mode when the vehicle moves from a road segment to an intersection. The Carry Mode and the Greedy Forwarding Mode are timer-based as MCIR is a beacon-less routing protocol. MCIR has two timers; one operates on the neighbor vehicles to forward the packet in the Greedy Forwarding Mode. The second timer operates on the forwarding vehicle to carry the packet in the Carry Mode until one neighbor exists.

2.4.1 Detailed Example for MCIR

In this sub-section, we present an example to explain the multi-copy forwarding algorithm, which is the main component of the MCIR protocol. In Fig. 2.1, we assume that a source vehicle V_s wants to send a flow of packets to a destination vehicle V_d. Therefore, V_s broadcasts the packet and the intermediate vehicle V_1 will receive it. After V_1 receives the packet from V_s at the intersection I_1 and ensures that this packet has never been replicated and forwarded at I_1, V_1 switches to the Greedy Forwarding Mode.

Since MCIR does not know the vehicular density of the road segments towards the destination, MCIR sends the packet in both directions of the road segments I_1-I_4 and I_1-I_2. Therefore, V_1 switches to the Intersection Forwarding Mode. V_1 broadcasts the packet and starts the overhearing. Each neighbor vehicle ensures that it is located at a candidate road segment. This condition is added to reduce the overhead by forwarding the packet towards the destination only. In this example, I_1-I_4 and I_1-I_2 are candidate road segments for the packet forwarding.

Next, V_2 and V_3 ensure that their distances to the destination V_d is less than the distance between V_1 and V_d. Therefore, V_2 and V_3 start their forwarding timer to forward this packet. After the timer expires, V_2 and V_3 forward the packet in the road segments I_1-I_4 and I_1-I_2, respectively. If V_2 overhears V_3 forwarding the packet, V_2 does not stop forwarding because V_3 and V_2 are not in the same road segment. Simultaneously, V_1 drops the packet after overhearing the packet. Otherwise, V_1 switches to the Carry Mode. This process is then repeated once the packet reaches intersections I_2 and I_4. At intersection I_4, there is only one candidate road segment for the packet which is I_4-I_5. On the other hand, at intersection I_2, there are two candidate road segments which are I_2-I_5 and I_2-I_3. In this example, we assume the packet arrives first at intersection I_5 via I_2; and the current forwarding vehicle V_4 switches to the Intersection

Forwarding Mode at I_5.

Therefore, V_4 starts forwarding the data packet on the road segment I_5-I_6. At the same time, V_4 forwards alarm packet (packet includes only the data packet id, the source id, and the destination id) in the road segment I_5-I_2 to inform all the vehicles in this road segment to drop any received data packet with the same information (id, source id, destination id). This process is added to prevent forwarding the same packet from the intersection I_2 to the intersection I_5. Finally, the same process will be repeated at I_6. In this example, we assume the packet arrives first at intersection I_6 via I_3; and the alarm packet is forwarded in the road segment I_6-I_5. As a result, the destination gets the packet that arrives first.

2.5 Simulation Results

This section presents the performance evaluation of MCIR to investigate the performance impact of multi-copy on routing protocols. We implement our proposed MCIR protocol in NS-2 (V-2.34). For comparison, we implement GPSR, AMR, and SRPMT explained in the Introduction Section. We make two modifications on GPSR to be more suited for VANET and for fair comparison with MCIR. The first modification is the addition of the location service on GPSR to get the location of the destination vehicle, while the second modification is the addition of the carry-and-forward strategy.

The simulation scenarios are configured in a 3 km x 3 km urban grid model with different vehicular densities (defined as the average number of vehicles per unit road length) ranging from 5 vehicles/km to 30 vehicles/km. We use VanetMobiSim [16] to generate realistic vehicle mobility. Results are averaged for 20 simulation runs.Table 1 summarizes the configuration parameters used in the simulation.

Table 2.1: Simulation parameters

Simulation Parameter	Value
Vehicular density (vehicles/km)	5,10, 15, 20, 25, 30
Speed (m/sec)	5 to 15
Simulation time (seconds)	600
Traffic model	CBR Traffic
CBR rate (packets/second)	8
Transmission range (m)	250
Channel date rate (Mbps)	2
Packet size (bytes)	256
Number of sessions	1
Number of intersections	16

Four main important performance metrics are considered. The first metric is the end-to-end delay defined as the difference between the time a data packet arrives at its destination and the time the same packet is originated by the source. This time includes all possible delays as follows

$$Delay = Queue_{\text{delay}} + Carry_{\text{delay}} + Prop_{\text{delay}} + Tr_{\text{delay}}, \tag{2.2}$$

where $Queue_{delay}$ is the queuing delay, $Carry_{delay}$ is the Carry Mode delay, $Prop_{delay}$ is the propagation delay over the wireless channel, and Tr_{delay} is transmission delay. The second metric is the packet delivery ratio (PDR) defined as the ratio of the total number of the data packets received by the destination to the the total number of the data packets sent by the traffic

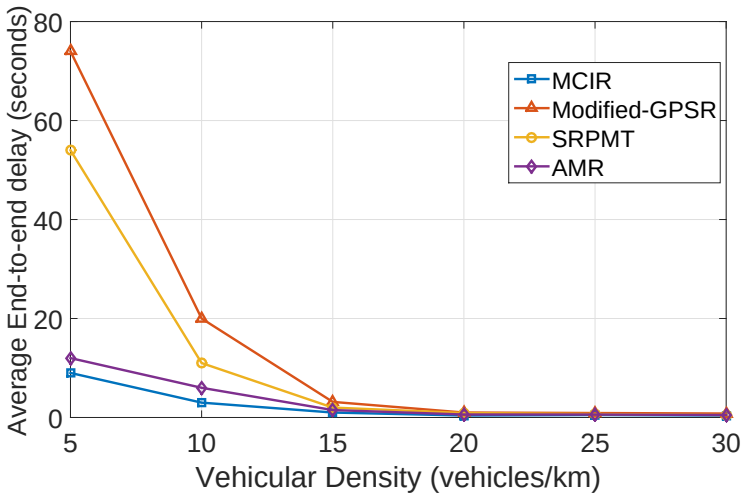

Figure 2.3: Average End-to-end Delay.

sources. Finally, the third metric is the routing overhead defined as follows

$$(Overhead)_{\text{packets}} = \frac{Number\ of\ transmitted\ packets}{Number\ of\ received\ data\ packets}. \tag{2.3}$$

However, the routing overhead in MCIR represents data and the alarm packets, while the overhead in modified-GPSR, AMR, and SRPMT represents beacon and data packets. In addition, the beacon and alarm packets are much smaller than the data packets. Therefore, for fair comparison with MCIR, we consider the fourth metric that represents the routing overhead in the number of transmitted bits as in [5] . It is defined as follows

$$(Overhead)_{\text{bits}} = \frac{Number\ of\ transmitted\ bits}{Number\ of\ received\ data\ bits}. \tag{2.4}$$

Fig. 2.3 shows the average end-to-end delay against the vehicular density for MCIR, SRPMT, AMR, and modified-GPSR protocols. Results show that there is a significant decrease in the average end-to-end delay of MCIR compared with modified-GPSR, SRPMT, and AMR especially at low vehicular density. For instance, at vehicular density of 5 vehicles/km, the average end-to-end delay of MCIR is reduced by 87%, 83%, and 18% compared with modified-GPSR,

SRPMT, and AMR, respectively. However, this improvement decreases to 50%, 3%, and 1% at a vehicular density of 30 vehicles/km due to the increase of the vehicular density that increases the connectivity of the network. In addition, at a vehicular density of 15 vehicles/km, the average end-to-end delay of MCIR is reduced by 66%, 50%, and 25% compared with modified-GPSR, SRPMT, and AMR, respectively. The reason behind this behavior is that a low vehicular density leads to disconnected road segments. As a result, the three routing protocols switch to Carry Mode. Consequently, the packets suffer from a higher end-to-end delay. However, the probability that all copies of the packets in MCIR are in the Carry Mode at the same time is lower than that the single copy in case of modified-GPSR, SRPMT. In addition, it is noticed that MCIR has a slightly shorter end-to-end delay than AMR. This is because AMR switches between single-copy and multi-copy based on estimated vehicular density and end-to-end delay for each road segment. However, it is challenging to estimate those two parameters (vehicular density and end-to-end delay) and make their information available accurately to all vehicles in the network. On the contrary, MCIR does not need those two parameters. Also, the results show that the vehicular density highly impacts the end-to-end delay. With decreasing vehicular density, the average end-to-end delay increases for all values of the vehicular density for the four routing protocols. On the other hand, SRPMT has a slightly shorter end-to-end delay than modified-GPSR due to micro topology considerations in the routing metric, especially at low vehicular density.

Fig. 2.4 shows the PDR against the vehicular density for MCIR, AMR, SRPMT, and modified-GPSR protocols. It is noticed that there is a significant increase in the PDR of MCIR compared with modified-GPSR, AMR, and SRPMT for all values of the vehicular density. For instance, at vehicular density of 5 vehicles/km, the PDR of MCIR is increased by 63% , 45%, and 6% compared with modified-GPSR, SRPMT, and AMR, respectively. However, this im-

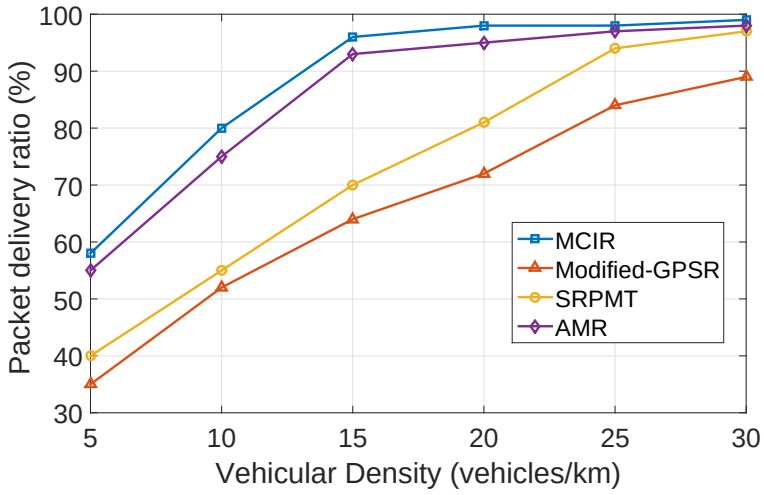

Figure 2.4: Packet delivery Ratio.

provement decreases to 11%, 3%, and 2% at vehicular density of 30 vehicles/km due to the increase of the vehicular density that enhances the connectivity of the network. Three reasons are behind this behavior. Firstly, in SRPMT, AMR, and modified-GPSR, packets are more likely to collide with the beacon packets. On the contrary, MCIR is a beacon-less protocol. Secondly, in the case of SRPMT and modified-GPSR, the single-copy of the packet may be dropped after time out in the queue due to switching to carry-and-forward strategy in the disconnected road segments. Thirdly, modified-GPSR depends on the neighbor table to select the next hop. However, the neighbor table may contain outdated information. Consequently, the packet is dropped after forwarding to a non-existing neighbor. On the other hand, MCIR does not suffer from the three previous problems as it sends multiple copies from the same packet. Therefore, if one copy of the packet is dropped, another copy arrives at the destination. As a result, the PDR of MCIR remains the highest of all of them for all values of the vehicular density. SRPMT appears to have a slightly higher PDR than modified-GPSR due to micro topology consideration in the routing metric, especially at low vehicular densities.

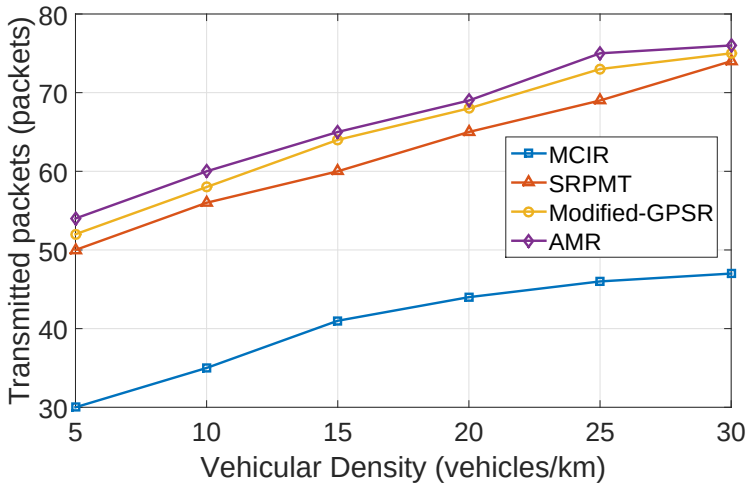

Figure 2.5: Routing overhead represented in transmitted packets.

Fig. 2.5 shows the routing overhead represented in the number of transmitted packets against the vehicular density for MCIR, AMR, SRPMT, and modified-GPSR protocols. It is noticed that MCIR has less routing overhead than SRPMT, modified-GPSR, and AMR for all values of the vehicular density. For instance, at a vehicular density of 5 vehicles/km, the routing overhead of MCIR is decreased by 40%, 42%, and 44% compared with modified-GPSR, SRPMT, and AMR, respectively. There are two reasons for this behavior. Firstly, MCIR is a beacon-less routing protocol. Secondly, MCIR has the highest number of successfully received data packets compared with SRPMT and modified-GPSR. The results confirm that the increase of the vehicular density causes an increase in the routing overhead for all three routing protocols. This is expected because increasing vehicular density leads to an increase in the hop count for the packets. Moreover, the number of transmitted beacon packets increase in the case of SRPMT, AMR, and modified-GPSR with the increase of the vehicular density. SRPMT appears to have a marginally higher routing overhead than modified-GPSR due to the beacon packets to collect vehicle information in local micro topology. In addition, AMR has the highest routing overhead

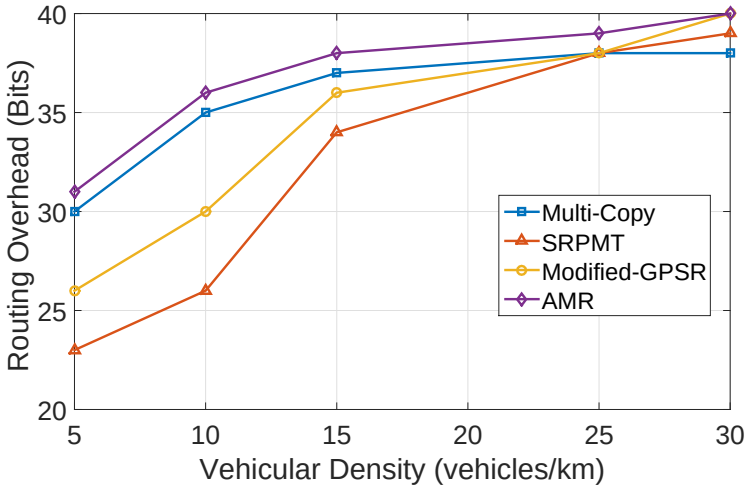

Figure 2.6: Routing overhead represented in transmitted bits.

due to the beacon packets and multi-copy consideration. On the contrary, MCIR is beacon-less and eliminates the unneeded copies.

Fig. 2.6 shows the routing overhead represented in the number of transmitted bits against the vehicular density for MCIR, AMR, SRPMT, and modified-GPSR protocols. It is noticed that MCIR has a higher routing overhead than SRPMT and modified-GPSR at low vehicular density. For instance, at vehicular density of 5 vehicles/km, the routing overhead of MCIR is increased by 11% and 30% compared with modified-GPSR and SRPMT, respectively. This is because MCIR is multi-copy routing protocol, while SRPMT and modified-GPSR are single-copy protocols. In addition, the data packets are larger in size than the beacon packets. On the other hand, the results confirm that MCIR overhead remains constant after reaching its peak. However, Modified-GPSR, AMR, and SRPMT overhead increases with the increasing of the vehicular density. For instance, at vehicular density of 30 vehicles/km, the routing overhead of MCIR is decreased by 12%, 8%, and 112% compared with modified-GPSR, SRPMT, and AMR, respectively. This is expected because increasing vehicular density leads to an increase in the

number of beacon packets in the case of SRPMT, AMR, and modified-GPSR. On the contrary, MCIR is a beacon-less routing protocol. Finally, AMR has the highest routing overhead due to the beacon packets and multi-copy consideration without elimination of the unneeded copies. On the contrary, MCIR is a beacon-less and eliminates the unneeded copies.

2.6 Conclusions

In this paper, we proposed a multi-copy routing protocol that aims to reduce the end-to-end delay and increase the packet delivery ratio. MCIR is a beacon-less routing protocol that forwards multiple copies of the packets and eliminates unneeded copies at the intersections. We have investigated the vehicular density impact on the VANET routing protocols performance. Simulation results confirm that the vehicular density highly impacts the routing performance in urban VANET communications. In addition, results show that MCIR outperforms SRPMT, AMR, and modified-GPSR in terms of the end-to-end delay and packet delivery ratio. In our future work, we will consider an adaptive beacon-less routing protocol that switches between mutli-copy and single-copy based on the vehicular density.

REFERENCES

[1] N. Wisitpongphan, F. Bai, P. Mudalige, V. Sadekar, and O. Tonguz, "Routing in sparse vehicular ad hoc wireless networks," *IEEE J. Sel. Areas Commun*, vol. 25, no. 8, pp.

1538–1556, 2007.

[2] B. Karp and H.-T. Kung, “Gpsr: Greedy perimeter stateless routing for wireless networks,” in *Proc. ACM MobiCom*, 2000, pp. 243–254.

[3] M. Jerbi, S.-M. Senouci, T. Rasheed, and Y. Ghamri-Doudane, “Towards efficient geographic routing in urban vehicular networks,” *IEEE Trans. Veh. Technol*, vol. 58, no. 9, pp. 5048–5059, 2009.

[4] P. K. Sahu, E. H.-K. Wu, J. Sahoo, and M. Gerla, “Bahg: back-bone-assisted hop greedy routing for vanet’s city environments,” *IEEE Trans. Intell. Transp. Syst*, vol. 14, no. 1, pp. 199–213, 2013.

[5] K. Chen, X. Cao, D. Sung *et al.*, “A street-centric routing protocol based on micro topology in vehicular ad hoc networks,” *IEEE Trans. Veh. Technol*, vol. PP, no. 99, pp. 1–1, 2015.

[6] R. Wang, M. Almulla, C. Rezende, and A. Boukerche, “Video streaming over vehicular networks by a multiple path solution with error correction,” in *Proc. IEEE ICC*, 2014, pp. 580–585.

[7] C. K. Joon Yoo, Sunwoong Choi, “The multi-copy diversity for routing in sparse vehicular ad hoc networks,” *Telecommunication Systems*, vol. 50, no. 4, pp. 297–309, 2012.

[8] C. Kaplan, “Gps, cellular, fm speed and safety control devise,” Dec. 26 2006, uS Patent App. 11/645,551.

[9] W. Kieß, H. Füßler, J. Widmer, and M. Mauve, “Hierarchical location service for mobile ad-hoc networks,” *ACM J. SIGMOBILE*, vol. 8, no. 4, pp. 47–58, 2004.

[10] J. Li, J. Jannotti, D. S. De Couto, D. R. Karger, and R. Morris, "A scalable location service for geographic ad hoc routing," in *Proc. ACM MobiCom*, 2000, pp. 120–130.

[11] M. Ayaida, M. Barhoumi, H. Fouchal, Y. Ghamri-Doudane, and L. Afilal, "Phrhls: A movement-prediction-based joint routing and hierarchical location service for vanets," in *Proc. IEEE ICC*, June 2013, pp. 1424–1428.

[12] F. J. Martinez, J.-C. Cano, C. T. Calafate, and P. Manzoni, "Citymob: a mobility model pattern generator for vanets," in *Proc. IEEE ICC*, 2008, pp. 370–374.

[13] H. Wu, R. M. Fujimoto, G. F. Riley, and M. Hunter, "Spatial propagation of information in vehicular networks," *IEEE Trans. Veh. Technol*, vol. 58, no. 1, pp. 420–431, 2009.

[14] N. Wisitpongphan, F. Bai, P. Mudalige, V. Sadekar, and O. Tonguz, "Routing in sparse vehicular ad hoc wireless networks," *IEEE J. Sel. Areas Commun*, vol. 25, no. 8, pp. 1538–1556, 2007.

[15] M. Killat and H. Hartenstein, "An empirical model for probability of packet reception in vehicular ad hoc networks," *EURASIP J. Wirel. Commun. Netw.*, vol. 2009, pp. 4:1–4:12, 2009.

[16] J. Härri, F. Filali, C. Bonnet, and M. Fiore, "Vanetmobisim: generating realistic mobility patterns for vanets," in *Proc. ACM VANET 06*, 2006, pp. 96–97.

Chapter 3

Probability Distribution of the Re-healing Delay in a One-Way Highway VANET

3.1 Abstract

This letter proposes a closed-form expression for the probability distribution of the re-healing delay (time taken in the store-and-forward strategy to send a packet from a cluster head to the tail of the next cluster) conditioned on the gap distance between those two clusters on a one-way highway. Moreover, a closed-form expression is derived for the unconditional probability distribution of the re-healing delay. Using the derived probability distribution, one can straightforwardly study the impact of VANET parameters on the re-healing delay. Also, the probability distribution of the end-to-end delay in VANETs can be derived from the results in this letter. The accuracy of the proposed analysis is validated using simulations.

3.2 Introduction

Vehicular ad-hoc networks (VANETs) enable ad-hoc communication between vehicles, or between vehicles and road-side units (RSUs) or drones [1]. VANET applications usually have time constraints on information dissemination. One example is emergency message (EM) dissemination (when an accident happens or a certain road condition is observed, an update should be broadcast as soon as possible).

VANETs can either be fully-connected, or sparsely-connected [2]. It is a crucial challenge to forward EM packets in sparsely-connected VANETs while satisfying the time constraints. A VANET is usually partitioned into a number of clusters (a cluster of vehicles is fully-connected and the distance between any two clusters is greater than the vehicle communication range). Fig. 3.1 shows an example of two clusters, where the head vehicle of the first cluster and the tail vehicle of the second cluster are labeled. Many proposed VANET routing protocols in the sparsely-connected case use a store-and-forward strategy (when the network is disconnected, packets can be stored and carried by a vehicle until reaching the next cluster). The re-healing delay is the time taken in the store-and-forward strategy to send a packet from a cluster head to the tail of the next cluster. This delay is the main focus of many vehicular active safety applications. Therefore, it is desirable to characterize the re-healing delay in VANETs. Moreover, the probability distribution of the re-healing delay can be used to derive the probability distribution of the end-to-end delay.

Several papers, such as [2]-[8], have analyzed the re-healing delay performance for safety message dissemination in VANETs. An expression for the mean of the re-healing delay was found in [2]. In addition, Ref. [3] derived the probability distribution of the re-healing delay based on an approximate probability distribution of cluster lengths. Morover, Ref. [4] proposed

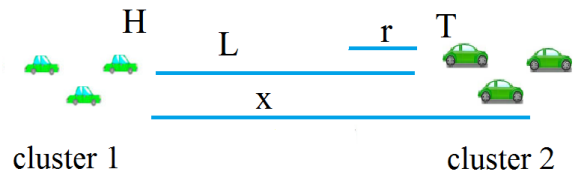

Figure 3.1: Two clusters in a VANET.

an accurate probability distribution of the cluster length, and from this derived the probability distribution of the re-healing delay. The authors in [2]-[4] assumed the same system model (infrastructure-less bi-directional highway with a constant speed model for the vehicles).

Moreover, Refs. [5] and [6] calculated the mean of the re-healing delay to RSUs over a bi-directional highway. While, Ref. [5] considered a constant speed model, Ref. [6] considered a truncated normal distribution for vehicle speed.

On the other hand, Ref. [7] proposed an analytical model for the distribution of the re-healing delay. In addition, Ref. [8] derived closed-form expressions for the CDFs of the distances travelled by the cluster head and tail over time t, and these closed-form expressions were used to derive the probability distribution of the re-healing delay. Both Refs. [7] and [8] assumed the same system model (one-way highway with uniformly-distributed vehicle speeds).

One key difference between the system model in this work and that in many previous papers (e.g., [2] - [5]) is that we assume the speeds of the vehicles are uniformly distributed. Therefore, a vehicle can overtake another one travelling in the same direction. On the contrary, previous papers assumed a constant speed model for each direction, or the same speed for both directions. Therefore, clusters in the same direction could not re-heal except by using RSUs or by using vehicles moving in the opposite direction.

On the other hand, the key differences between this work, and [8] are as follows: 1) while

this letter derives a closed-form expression for the CDF of the conditional re-healing delay, Ref. [8] does not provide a closed-form expression and its analytical method requires numerical integration, 2) in this letter we propose a correction for the derived expression proposed in [7] and [8] for the probability distribution of the conditional re-healing delay, and 3) in this letter we calculate closed-form expressions for the conditional and unconditional probability distributions of the re-healing delay.

The main contributions of this letter are as follows:

- It proposes a closed-form expression for the CDF of the re-healing delay conditioned on the given distance between two clusters in a VANET.
- It proposes a closed-form expression for the CDF of the unconditional re-healing delay in a VANET.
- It compares results from the proposed analysis with simulation results to show the accuracy of our analysis.

The rest of this letter is organized as follows. Section II introduces the system model. Section III gives a closed-form expression for the CDF of the re-healing delay conditioned on the given distance between two consecutive VANET clusters. Then, it proposes a closed-form expression for the unconditional probability distribution of the re-healing delay. Next, Section IV compares the simulation results against analytical results. Finally, the conclusions are presented in Section V.

Table 3.1: List of Notation

L	Gap between two consecutive clusters
r	Vehicle wireless communication range
x	R.V. for re-healing distance
$X(t)$	R.V. for distance cluster head moved in [0,t]
$X'(t)$	R.V. for distance cluster tail moved in [0,t]
T_c	R.V. for duration of re-healing phase
$F_{X(t)}(x)$	CDF of $X(t)$
$F_{X'(t)}(x)$	CDF of $X'(t)$
$f_{X(t)}(x)$	PDF of $X(t)$
$f_{X'(t)}(x)$	PDF of $X'(t)$
λ	Traffic flow rate (vehicles/unit time)
λ_s	Reciprocal of mean distance between vehicles
$v_{\min}$	Minimum allowed speed of vehicle
$v_{\max}$	Maximum allowed speed of vehicle
Δv	$v_{\max}$- $v_{\min}$
$u(\cdot)$	Heaviside unit step function
$\star$	Cross-correlation
s^*	Complex conjugate of s
$\mathscr{L}_x[\cdot]$	Laplace transform with respect to x
$\mathscr{L}_s^{-1}[\cdot]$	Inverse Laplace transform with respect to s

3.3 System model

We consider a highway with vehicles moving in one direction. We assume that the speeds of the vehicles are uniformly distributed within the interval [$v_{\min}$, $v_{\max}$] [7], [8]. We also assume the inter-vehicular distances are exponentially-distributed, and that the inter-vehicular arrival rate is Poisson-distributed with a mean equal to the traffic flow rate λ (vehicles/sec) [7],[8].

In addition, the time required for a vehicle to receive and process a message before it is available for further relaying is negligible as in [4]-[8]. Also, Table 3.1 shows the list of notations used in our analysis. The medium access control (MAC) layer protocol is the distributed coordination function (DCF) of the IEEE 802.11. In addition, the radio channel propagation model is assumed to follow the Nakagami-m distribution [1]. Finally, the packet traffic model follows the constant bit rate (CBR) pattern between a source and a destination that are randomly selected.

3.4 Proposed model

In this section, we find a closed-form expression for the CDF of the re-healing delay conditioned on the distance between two clusters in one-way highway. Then, we derive a closed-form expression for the unconditional re-healing delay distribution.

Firstly, from [8], the closed forms for $F_{X(t)}(x)$ and $F_{X'(t)}(x)$ are equal to 0 for $x < v_{\min}t$ and 1 for $x > v_{\max}t$ and for x between $v_{\min}t$ and $v_{\max}t$, given by the following expressions

$$F_{X(t)}(x) = \frac{\frac{x}{t} - v_{\min}}{\Delta v} e^{\lambda\left(\frac{\frac{xv_{\min}}{v_{\max}} - v_{\min}t}{\Delta v} - t + \frac{x}{v_{\max}}\right)} \left(\frac{v_{\max}t}{x}\right) \frac{\lambda x}{\Delta v},$$

and

$$F_{X'(t)}(x) = 1 - \frac{(v_{\max} - \frac{x}{t})\, e^{-\lambda\left(\frac{v_{\min}t - x}{v_{\max}}\right)} (\frac{x}{v_{\min}t})^{-\lambda x / v_{\max}}}{\Delta v}.$$

Furthermore, from [7], the distribution of the re-healing delay T_c, conditioned on l, the distance between the cluster tail and the next cluster head, was derived. They obtained the following expression

$$P(T_c < t | L = l) = \int_0^{\infty} f_{X(t)}(x) \int_0^{x+r-l} f_{X'(t)}(x')\, dx'\, dx, \tag{3.1}$$

where $l > r$. However, both clusters are moving simultaneously. Therefore, the minimum period of time required for re-healing is $(\frac{l-r}{\Delta v})$ seconds (when the cluster head moves with speed $v_{\max}$ and the next cluster tail with speed $v_{\min}$). Consequently, the distance the head must travel before re-healing is at least $(l-r)v_{\max}/\Delta v$. Hence, x in the previous expression should be corrected to start from $(l-r)v_{\max}/\Delta v$ not 0. Moreover, after considering this correction, the above equation can instead be expressed as

$$P(T_c < t | L = l) = \int_{(l-r)v_{\max}/\Delta v}^{\infty} f_{X(t)}(x)\, F_{X'(t)}(x + r - l)\, dx. \tag{3.2}$$

This can be identified as a windowed cross-correlation between $f_{X(t)}(x)$ and $F_{X'(t)}(x)$. From the theory of the Laplace transform, we know that the Laplace transform of the cross-correlation of two signals g and h is given by the expression $G^*(-s^*) \cdot H(s)$, where G and H are the Laplace transforms of g and h, respectively. Therefore, it is desirable to find the Laplace transforms of $f_{X(t)}(x)$ and $F_{X'(t)}(x)$.

The Laplace transform of $f_{X(t)}(x)$ is equal to

$s \cdot \mathscr{L}_x[F_{X(t)}(x)](s) - F_{X(t)}(0)$. In addition, $F_{X(t)}(0) = 0$ because $F_{X(t)}(x)$ is zero when x less than $v_{\min}t$. Therefore, $\mathscr{L}_x[f_{X(t)}(x)](s)$ is equal to $s \cdot \mathscr{L}_x[F_{X(t)}(x)](s)$.

On the other hand, one can define the random variable X_1' such that $F_{X_1'(t)}(x) = 1 - F_{X'(t)}(x)$.

Therefore,

$$P(T_c < t|L = l) = \int_{\frac{(l-r)v_{\max}}{\Delta v}}^{\infty} f_{X(t)}(x)[1 - F_{X_1'(t)}(x+r-l)]\ dx$$
$$= 1 - F_{X(t)}(\tfrac{(l-r)v_{\max}}{\Delta v}) - \int_{(l-r)v_{\max}/\Delta v}^{\infty} f_{X(t)}(x) F_{X_1'(t)}(x+r-l)\ dx$$
$$= 1 - F_{X(t)}(\tfrac{(l-r)v_{\max}}{\Delta v}) - f_{X(t)} \star F_{X_1'(t)}(r-l),$$
$$= 1 - F_{X(t)}(\tfrac{(l-r)v_{\max}}{\Delta v}) - \mathscr{L}_s^{-1}[s \cdot \mathscr{L}_x[F_{X(t)}(x)](s)\mathscr{L}_x[F_{X_1'(t)}(x)](s)](x),$$

where

$$F_{X_1'(t)}(x) = \frac{(v_{\max} - \frac{x}{t})\ e^{-\lambda\left(\frac{v_{\min}t - x}{v_{\max}}\right)}(\frac{x}{v_{\min}t})^{-\lambda x/v_{\max}}}{\Delta v}. \tag{3.3}$$

It can be found that

$$\mathscr{L}_x[F_{X(t)}(x)](s) = \frac{\frac{v_{\min}e^{-\left(\lambda t + \frac{\lambda v_{\min}t}{\Delta v}\right)}}{s - \frac{\lambda}{v_{\max}} + \frac{\lambda v_{\min}}{-v_{\max}^2 + v_{\min}v_{\max}}} - \frac{e^{-\left(\frac{\lambda v_{\max}t}{\Delta v}\right)}}{t\left(s - \frac{\lambda}{\Delta v}\right)^2}}{\Delta v}, \tag{3.4}$$

and

$$\mathscr{L}_x[F_{X_1'(t)}(x)](s) = \frac{\frac{e^{-\left(\frac{\lambda v_{\min}t}{v_{\max}}\right)}}{t\left(s - \frac{\lambda}{v_{\max}}\right)^2} + \frac{v_{\max}e^{-\left(\frac{\lambda v_{\min}t}{v_{\max}}\right)}}{s - \frac{\lambda}{v_{\max}}} -}{\Delta v}. \tag{3.6}$$

Finally, the closed form for $P(T_c < t|L = l)$ is shown in Eq. (3.5).

3.4.1 CDF of the unconditional re-healing delay

From [7], the probability distribution of the unconditional re-healing delay was derived as follows

$$F_{T_c}(t) = P(T_c < t) = \int_0^{\infty} P(T_c < t|L = l) f_L(l)\ dl, \tag{3.7}$$

$$
\begin{aligned}
&P(T_c < t|L = l) = \frac{v_{\min} - k_3/t}{\Delta v} e^{-\lambda\left(t + \frac{t v_{\min} v_{\max} - v_{\min} k_3}{v_{\max}\Delta v} - \frac{k_3}{v_{\max}}\right)} \left(t v_{\max}/k_3\right)^{\lambda k_3/\Delta v} \left(u(l-r) - u(k_{12})\right) \\
&+ k_1 k_4 k_6 \Big(\frac{k_9(v_{\max}^5 v_{\min} - 3v_{\max}^4 v_{\min}^2 + 3v_{\max}^3 v_{\min}^3 - v_{\max}^2 v_{\min}^4)}{\lambda^2 k_8 \Delta v} \\
&- \frac{k_{10}(v_{\max}^5 v_{\min} - 2v_{\max}^4 v_{\min}^2 + v_{\max}^3 v_{\min}^3)}{\lambda^2 k_8 v_{\max}} + \frac{k_{10}k_{11}(v_{\max}^5 - 2v_{\max}^4 v_{\min} + v_{\max}^3 v_{\min}^2)}{\lambda k_2 v_{\max}^2} \\
&+ \frac{k_9 k_{11}(-v_{\max}^5 + 3v_{\max}^4 v_{\min} - 3v_{\max}^3 v_{\min}^2 - v_{\max}^2 v_{\min}^3)}{\lambda k_2 (\Delta v)^2} \Big) / \left(t^2 (\Delta v)^2\right) \\
&+ v_{\min} k_1 k_4 k_5 \Big(\frac{v_{\max}^2 k_9 \Delta v}{\lambda k_2} + \frac{k_{10}(-v_{\max}^4 + v_{\max}^3 v_{\min})}{v_{\max} k_2 \lambda} - \frac{k_{10}k_{11}(-v_{\max}^3 + v_{\max}^2 v_{\min})}{v_{\max}^2 (2v_{\max} - v_{\min})} \Big) / k_7 \\
&+ v_{\max} k_1 k_4 k_6 \Big(\frac{k_9(-v_{\max}^4 + 3v_{\max}^3 v_{\min} - 3v_{\max}^2 v_{\min}^2 + v_{\max} v_{\min}^3)}{\lambda k_2 \Delta v} + \frac{k_{10} v_{\max} (\Delta v)^2}{\lambda k_2} \\
&- \frac{k_9 k_{11}(v_{\max}^3 - 2v_{\max}^2 v_{\min} + v_{\max} v_{\min}^2)}{(\Delta v)^2 (2v_{\max} - v_{\min})} \Big) / k_7 + \frac{v_{\max} v_{\min} k_1 k_4 k_5 \left(v_{\max} k_9 + k_{10}\Delta v\right)}{(\Delta v)^2 (2v_{\max} - v_{\min})} + k_{13}
\end{aligned}
$$

where

$$
\begin{aligned}
&k_1 = u\left(-\frac{(l-r)(2v_{\max} - v_{\min})}{\Delta v}\right), \quad k_2 = (2v_{\max} - v_{\min})^2, \; k_3 = l - r + v_{\min} t, \; k_4 = e^{-\lambda v_{\min} t / v_{\max}}, \\
&k_5 = e^{(-\lambda t - \lambda v_{\min} t/\Delta v)}, \quad k_6 = e^{(-\lambda t v_{\max}/\Delta v)}, \quad k_7 = t(\Delta v)^2, \quad k_8 = (2v_{\max} - v_{\min})^3, \quad k_9 = e^{k_{11}\lambda/\Delta v}, \\
&k_{10} = e^{-k_{11}\lambda/v_{\max}}, \quad k_{11} = l - r + v_{\max}(l-r)/\Delta v, \quad k_{12} = l - r - t\Delta v, \\
&k_{13} = 0.5 + 0.5\text{piecewise}(v_{\min}\Delta v k_{12} \le 0, \; -sign(k_{12}), \; 0 < v_{\min}\Delta v k_{12}, \; sign(v_{\max} t - \frac{v_{\max}(l-r)}{\Delta v})).
\end{aligned}
\tag{3.5}
$$

---

where $f_L(l)$ is the PDF of the inter-vehicular distances and is equal to $\lambda_s e^{-\lambda_s l}$, where λ_s is the reciprocal of the mean distance between vehicles and is equal to $2\lambda/(v_{\min} + v_{\max})$ as in [7] and [8].

This is of the same form as a Laplace transform if we assume $s = \lambda_s$. Therefore, F_{T_c} is the Laplace transform of $P(T_c < t|L = l)\lambda_s$, where λ_s is now the transform variable. Based on this form as a Laplace transform, the closed form for the CDF of the unconditional re-healing delay

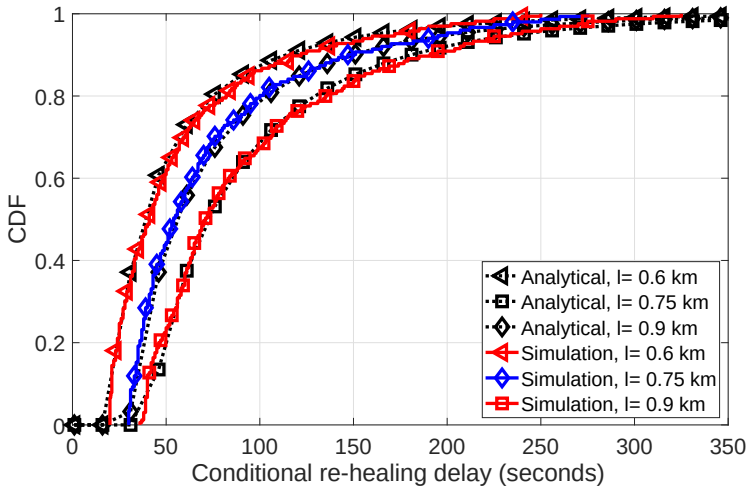

Figure 3.2: Conditional re-healing delay with changing l.

$P(T_c < t)$ can be calculated as shown in Eq. (3.8).

$$P(T_c < t) = 2\lambda e^{-\left(k_2+k_1+\lambda t+\frac{2\lambda(r-v_{\min}t)}{v_{\max}+v_{\min}}\right)}\left(v_{\min}e^{k_2} - v_{\max}e^{k_2} + v_{\max}e^{k_1+\lambda t} - v_{\min}e^{k_1+\lambda t} - \lambda t v_{\max}e^{k_1+\lambda t}\right.$$
$$\left. + \lambda t v_{\min}e^{k_1+\lambda t} + \frac{2\lambda t e^{k_1+\lambda t}(v_{\max}^2 + v_{\min}^2 - 2v_{\max}v_{\min})}{v_{\max}+v_{\min}}\right) / \left(t(v_{\max}+v_{\min})\left(\lambda + \frac{2(\lambda v_{\min} - \lambda v_{\max})}{v_{\max}+v_{\min}}\right)^2\right)$$
$$- e^{-\left(k_2-k_1+\frac{2\lambda r}{v_{\max}+v_{\min}}\right)} + 1$$

where

$$k_1 = 2\lambda v_{\min}t/(v_{\max}+v_{\min}),\ \ k_2 = 2\lambda v_{\max}t/(v_{\max}+v_{\min}) \tag{3.8}$$

Table 3.2: Simulation Parameters

Simulation Parameter	**Values**
λ (veh/s)	0.025, 0.035, 0.045
$v_{\min}$ (m/s)	15
$v_{\max}$ (m/s)	30
Simulation runs	500
Channel date rate (Mbps)	2
Communication range r (m)	300
Packet size (bytes)	512

3.5 Simulation and model validation

This section compares simulation results against analytical results using NS-2 (V-2.34). Also, we used VanetMobiSim [9] to generate realistic vehicle mobilities for a highway segment of length 30 km. We used greedy perimeter stateless routing protocol (GPSR) that greedily forwards the packets and added to it the store-and-forward strategy. In the simulations, one cluster is selected randomly to generate an emergency message, and the head of this cluster carries the message until it is connected to the next cluster. Table 3.2 summarizes the configuration parameters used in these simulations.

3.5.1 Conditional re-healing delay

Fig. 3.2 shows the analytical and simulation results for the CDF of the conditional re-healing delay with the same simulation parameters as in Table II and vehicular density λ equal to 0.025 veh/s, while changing the gap length l to values of (0.6, 0.75, and 0.9 km). It can be seen that the

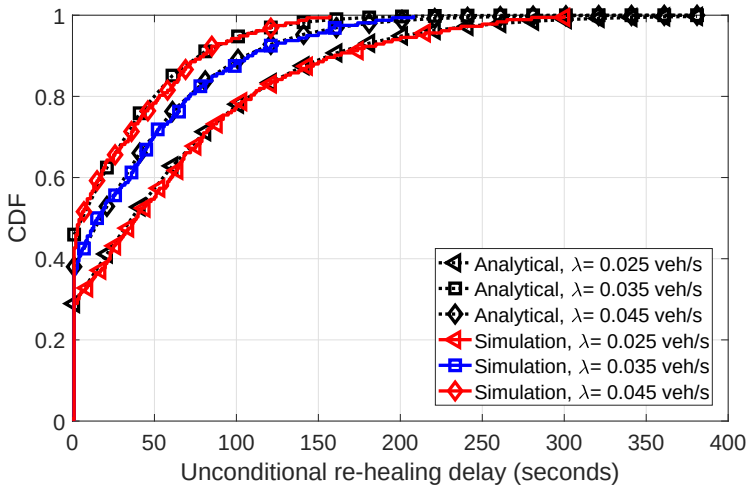

Figure 3.3: Unconditional re-healing delay with changing λ.

two curves (analytical, and simulation) agree closely across all re-healing delay values for the three vehicular densities, confirming the correctness and accuracy of the obtained closed-form expression.

Results show that the gap length highly impacts the CDF of the conditional re-healing delay. With increasing gap length, the CDF of the conditional re-healing delay decreases. This is because increasing the gap length causes an increase in the re-healing delay as we have the same speed in the three cases. Furthermore, it can be noted that the CDF of the conditional re-healing delay is equal to 0 for any values of t that are less than $(l-r)/\Delta v$ seconds. For instance, for a gap length equal to 0.6 km, the CDF of the conditional re-healing delay is equal to 0 for t less than 20 ((600-300)/15) seconds.

3.5.2 Unconditional re-healing delay

Fig. 3.3 shows the analytical and simulation results for the CDF of an unconditional re-healing delay with the same simulation parameters as in Table II, while changing the vehicular density

λ to values of (0.025, 0.035, and 0.045) veh/s. Once again, the two curves (analytical, and simulation) agree closely across all re-healing delay values for the three vehicular densities.

Results show that the vehicular density significantly impacts the CDF of the unconditional single catch-up time. With increasing vehicular density, the CDF of the unconditional re-healing delay increases for all values of the vehicular density. This is because increasing the vehicular density causes an increase in the number of vehicles in each cluster. Consequently, there is a higher probability of a shorter overall re-healing delay. Moreover, increasing the vehicular density causes a decrease in the distance l between VANET clusters.

3.6 Conclusions

In this letter, we found a closed-form expression for the probability distribution of the re-healing delay conditioned on the gap distance between the clusters in a VANET. In addition, a closed-form expression for the unconditional probability distribution of the re-healing delay was derived. Extensive computer simulation results demonstrated the accuracy of the proposed analysis. The closed form for the unconditional re-healing delay characterizes the delay for broadcasting a safety message in a highway VANET. Also, it can be used to derive the end-to-end delay. From the closed form, we found out that the difference between $v_{\max}$ and $v_{\min}$ has a high impact on the re-healing delay. With increasing the speed difference Δv, the CDF of the conditional re-healing delay increases. This is because increasing Δv causes an increase in the relative speed between vehicles. Consequently, the re-healing delay for the same gap distance will be decreased. Due to space limitations, we did not include this plot in the letter. In addition, when the distance a from the current message head to a fixed RSU is less than twice the communication range r, i.e., $a < 2r$, and there is no direct communication path to the RSU

at the initial time, then the conditional re-healing time to the next cluster can be used to find the CDF of the total end-to-end delay in this special case. Due to space limitations, we leave this to future work, although this provides additional evidence of the applicability of the current work to practical scenarios. In our future work, we will consider calculation of the probability distribution of the re-healing delay for a two-way highway.

REFERENCES

[1] H. Seliem, R. Shahidi, M. H. Ahmed, and M. S. Shehata, "Drone-based highway-vanet and das service," *IEEE Access*, vol. 6, pp. 20 125–20 137, 2018.

[2] N. Wisitpongphan, F. Bai, P. Mudalige, V. Sadekar, and O. Tonguz, "Routing in sparse vehicular ad hoc wireless networks," *IEEE J. Sel. Areas Commun*, vol. 25, no. 8, 2007.

[3] Y. Zhuang, J. Pan, Y. Luo, and L. Cai, "Time and location-critical emergency message dissemination for vehicular ad-hoc networks," *IEEE J. Sel. Areas Commun*, vol. 29, no. 1, pp. 187–196, 2011.

[4] J.-J. Huang, "Accurate probability distribution of rehealing delay in sparse vanets," *IEEE Commun. Lett*, vol. 19, no. 7, pp. 1193–1196, 2015.

[5] A. B. Reis, S. Sargento, F. Neves, and O. K. Tonguz, "Deploying roadside units in sparse vehicular networks: What really works and what does not," *IEEE Trans. Veh. Technol*, vol. 63, no. 6, pp. 2794–2806, 2014.

[6] Y. Wang, J. Zheng, and N. Mitton, "Delivery delay analysis for roadside unit deployment in vehicular ad hoc networks with intermittent connectivity," *IEEE Trans. Veh. Technol*, vol. 65, no. 10, pp. 8591–8602, 2016.

[7] H. Wu, R. M. Fujimoto, G. F. Riley, and M. Hunter, "Spatial propagation of information in vehicular networks," *IEEE Trans. Veh. Technol*, vol. 58, no. 1, pp. 420–431, 2009.

[8] R. Shahidi and M. H. Ahmed, "Probability distribution of end-to-end delay in a highway vanet," *IEEE Commun. Lett*, vol. 18, no. 3, pp. 443–446, 2014.

[9] J. Härri, F. Filali, C. Bonnet, and M. Fiore, "Vanetmobisim: generating realistic mobility patterns for vanets," in *Proc. ACM VANET 06*, 2006, pp. 96–97.

Chapter 4

On the End-to-End Delay in a One-Way VANET

4.1 Abstract

Vehicular ad-hoc networks (VANETs) are a focus of much research. In this paper, we present an analytical model to study the end-to-end delay in a one-way VANET. This paper proposes an analytical formula for the probability distribution of the end-to-end delay. Using the derived probability distribution, the probability that the end-to-end delay is less than a given threshold may be calculated. In addition, one can straightforwardly study the impact of parameters such as wireless communication range, vehicular density, the distance between the source and the destination, and the minimum and maximum vehicles speeds on the end-to-end delay. This can help to better understand data dissemination in VANETs. Moreover, closed forms for lower and upper bounds on the end-to-end delay probability distribution are obtained. The accuracy of the analytical results is validated using simulations. Extensive simulation results demonstrate the

accuracy of our analysis.

4.2 Introduction

Vehicular ad-hoc networks (VANETs) are a focus of current research in both the academic research community and automobile industry. The United States Federal Communications Commission (FCC) has allocated 75 MHz of the radio spectrum at 5.9 GHz to be used for Dedicated Short Range Communications (DSRC) [1]. VANET technology enables ad-hoc communication between vehicles, or vehicles and road-side units (RSUs). Many vehicle manufacturers have equipped their new vehicles with global positioning systems (GPSs) [2] and wireless communication devices. One of the most important applications of VANETs is to provide safety applications for passengers. In addition, VANETs provide comfort and commercial applications (e.g., instant messaging, mobile e-commerce, and weather information) [3].

VANET connectivity often changes, especially when the vehicular density is low. Therefore, regular ad-hoc routing protocols are not feasible since the routing path is often disconnected due to the intermittent nature of the network links. As a result, the packet loss probability increases. To overcome this problem, many proposed VANET routing protocols use a store-and-forward strategy. In such a strategy, when the vehicles are connected as a cluster, packets can be relayed quickly within the cluster using wireless communications; when the network is disconnected, packets can be stored and carried by a vehicle, and then the packets are retransmitted when another vehicle ahead is within communication range.

It is always desirable to characterize the end-to-end packet delay in communication networks, especially in wireless ad-hoc networks such as VANETs, (see [4]-[15]). It is also especially important in the case of VANETs without infrastructure, considered here, since no

guarantees exist on this delay, and all vehicles are moving with random speed, making the analysis more challenging.

Many papers have analyzed the delay performance in VANETs. However, most of the proposed analytical models focus mainly on connectivity analysis (propagation speed and time) and the expected value of the end-to-end delay, not on the end-to-end delay probability distribution (see [4]-[10]).

Ref. [4] derived the mean packet propagation delay based on inter-vehicle spacing and vehicular velocity distributions. Ref. [5] derived the expected value of the packet propagation speed and a closed-form expression for a single re-healing delay using a discrete-time Markov model. Both [4] and [5] used the same system model except that [5] used a Gaussian distribution and [4] used the uniform distribution for each vehicle's speed. An analytical model for multiple traffic streams was proposed in [6]. Moreover, an expression for the mean re-healing delay for packet transmission between two disconnected vehicles on a two-way highway was found in [7]. In addition, the authors in [8] derived the expected end-to-end delivery delay from a vehicle to Internet access points. Additionally, the authors in [9] proposed an analytical framework for the expected path delay in bidirectional vehicle traffic. Furthermore, using queuing theory , an analysis for the total delay from source to destination in bi-directional roadways with traffic lights was proposed in [10].

There are analytical studies on VANETs based on the assumption that the vehicle speed does not change over time, which is referred to as the constant speed model. For instance, a probabilistic vehicle-to-RSU packet delivery delay model was proposed in [11]. The model is based on effective bandwidth theory and the effective capacity concept. In addition, the authors in [12] derived a closed-form expressions for the cumulative distribution function (CDF) of the vehicle-to-RSU packet delivery delay in bidirectional highways based on the distance between

RSUs. Ref. [13] derived upper and lower-bounds on the end-to-end delay in epidemic routing in VANETs. However, the authors in [9]-[11] considered a constant speed for the vehicles and a fixed location for the destination (RSU or intersection).

Moreover, in [14], we proposed a closed-form expression for the unconditional probability distribution of the re-healing delay (time taken in the store-and-forward strategy to send a packet from a cluster head to the tail of the next cluster) in a one-way highway VANET, and this closed-form expression provides a basis for our work. On the other hand, in [15], the closed-form expressions for the CDFs of the distances travelled by the cluster head and tail and analytical expression for the end-to-end delay were derived. In this paper, we propose a more accurate probability distribution than that provided in [15], based on the closed form of the re-healing delay proposed in [14]. On the other hand, Ref. [15] is based on an uncorrected analytical form of the unconditional re-healing delay, the correction for which is proposed in [14]. Moreover, this paper proposes a lower-complexity analytical model for the end-to-end delay probability distribution based on the probability mass function (PMF) of the number of gaps from source to destination, and the closed-form expression for the probability density distribution (PDF) of the re-healing delay (this paper model has one summation over iterated convolutions over the closed-form expression for the PDF of the re-healing delay, while our previous work must perform a summation over repeated convolutions of a numerically-calculated double integral). Furthermore, this paper proposes a closed-form expression for the lower and upper bounds of the end-to-end delay probability density distribution, allowing one to rapidly find bounds on the worst-case and best-case end-to-end delay for a VANET. On the other hand, the work in [15] was extended to two-way multi-lane highways in [16]. An analytical expression for the end-to-end delay probability distribution was proposed considering the same system model as in [15], except taking into consideration vehicles travelling in both directions.

Ref. [17] derived closed-form expressions for the PMF of the number of clusters in a VANET conditioned on distance, and we use this result in our work. In addition, that work calculated the expected delivery delay over this number of gaps.

All this previous work shows that great effort has been exerted towards characterizing the end-to-end delay in VANETs. However, [4]-[11] considered a constant speed model for the vehicles or only calculated the expected value for the end-to-end delay. In this paper, we propose an analytical framework for calculation of the CDF of the end-to-end propagation delay conditioned on the initial distance between a source and a destination, while the source and the destination are moving with a uniformly-random distributed speed. Deriving the CDF of the end-to-end delay allows for the determination of its statistics (e.g., PDF, moments, cumulants, and characteristic function). In addition, derivation of the CDF allows one to obtain the probability that the end-to-end delay is less than a given threshold. This allows a service provider, e.g., an intelligent transportation system (ITS) service provider to characterize the end-to-end propagation delay based on VANET parameters such as vehicular density, minimum and maximum speed, wireless communication range, and initial distance between source and destination. Moreover, closed-form expressions for lower and upper bounds on the end-to-end delay probability density distribution are derived, allowing a service provider to rapidly find a bound on the worst-case end-to-end delay for a VANET. The lower bound is important as it represents the worst case for the actual end-to-end delay time.

The main contributions of this paper are as follows:

1. It proposes an analytical framework for the CDF of the end-to-end delay in a VANET.

2. It proposes a closed-form expression for the lower bound of the end-to-end delay probability density distribution.

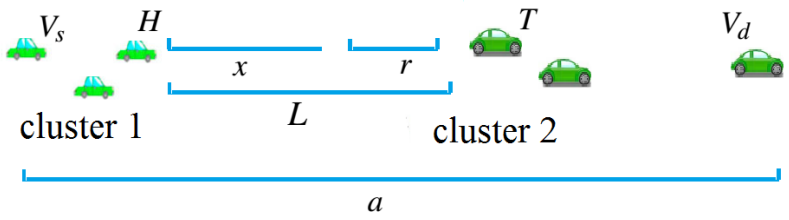

Figure 4.1: Two clusters in a VANET.

3. It proposes a closed-form expression for the upper bound of the end-to-end delay probability density distribution.

4. It compares results from the proposed framework with simulation results to show the accuracy of our analysis.

The rest of this paper is organized as follows. Section II introduces the system model. Section III proposes a formula to determine the CDF of the end-to-end delay in a VANET. Section IV gives a closed-form expression for the lower bound of the end-to-end delay probability density distribution. In addition, Section V proposes a closed-form expression for the lower bound of the end-to-end delay probability density distribution. Next, Section VI compares the simulation results against analytical results. Subsequently, Section VII investigates the VANET parameters (vehicle wireless communication range r, different speed range with the same speed average, different speed average, and distance) and their effect on end-to-end delay. Then, the conclusions and future work are presented in Section VIII, and finally the Appendix presents more detailed derivations of some of the formulae used in Sections V and VI.

Table 4.1: List of notation

L	Gap between two consecutive clusters
a	Distance between (source and destination)
r	Vehicle wireless communication range
T_c	R.V. for duration of the re-healing delay
T_d	End-to-end propagation delay
$F_{T_c}(t)$	CDF of T_c
$f_{T_c}(t)$	PDF of T_c
$F_{X'(t)}(x)$	CDF of R.V. for distance cluster tail moved in [0,t]
$f_{X(t)}(x)$	PDF of R.V. for distance cluster tail moved in [0,t]
T_c	R.V. for duration of re-healing phase
λ	Traffic flow rate (vehicles/unit time)
λ_s	Reciprocal of mean distance between vehicles
$v_{\min}$	Minimum allowed speed of vehicle
$v_{\max}$	Maximum allowed speed of vehicle
Δv	Difference between $v_{\max}$ and $v_{\min}$
$u(\cdot)$	Heaviside unit step function
$\star$	Cross-correlation
$*^i$	Convolution iterated i times
s^*	Conjugate of s
$\mathscr{L}_x[\cdot]$	Laplace transform relative to x
$\mathscr{L}_s^{-1}[\cdot]$	Inverse Laplace transform relative to s
$P_X(x)$	PMF of X
$\mathscr{F}_\omega^{-1}$	Inverse Fourier transform relative to ω

$$F_{T_c}(t) = 2\lambda e^{-\left(k_2+k_1+\lambda t+\frac{2\lambda(r-v_{\min}t)}{v_{\max}+v_{\min}}\right)}\left(v_{\min}e^{k_2} - v_{\max}e^{k_2} + v_{\max}e^{k_1+\lambda t} - v_{\min}e^{k_1+\lambda t} - \lambda t v_{\max}e^{k_1+\lambda t}\right.$$
$$\left. + \lambda t v_{\min}e^{k_1+\lambda t} + \frac{2\lambda t e^{k_1+\lambda t}(v_{\max}^2 + v_{\min}^2 - 2v_{\max}v_{\min})}{v_{\max}+v_{\min}}\right) / \left(t(v_{\max}+v_{\min})\left(\lambda + \frac{2(\lambda v_{\min} - \lambda v_{\max})}{v_{\max}+v_{\min}}\right)^2\right)$$
$$- e^{-\left(k_2-k_1+\frac{2\lambda r}{v_{\max}+v_{\min}}\right)} + 1$$

where

$$k_1 = 2\lambda v_{\min}t/(v_{\max}+v_{\min}),\ \ k_2 = 2\lambda v_{\max}t/(v_{\max}+v_{\min}) \tag{4.1}$$

4.3 System model

A VANET is usually partitioned into a number of clusters [4], [5], where a cluster is a maximal set of vehicles in which every pair of vehicles in the cluster is connected by at least one multihop path. Fig. 1 shows an example of two clusters, where the head vehicle of the first cluster and the tail vehicle of the second cluster are labeled.

We assume that the speeds of the vehicles are uniformly distributed within the interval [$v_{\min}$, $v_{\max}$] [4], [15]. We also assume the inter-vehicle distance is exponentially distributed with parameter λ_s, and that the inter-vehicle arrival is Poisson-distributed with a mean equal to the traffic flow rate λ (vehicles/sec) [3]-[13]. Moreover, vehicle positions and velocities are assumed mutually independent [3]-[8].

In addition, we consider that two vehicles can directly communicate with each other if the Euclidean distance between them is shorter than the radio range r. Moreover, the time required for a vehicle to receive and process a message before it is available for further relaying is neglected as in [3]-[8]. This assumption is reasonable as long as the data rate supported by

IEEE 802.11p is 3 Mbps [18]. Consequently, the transmission delay is on the order of tens of milliseconds [15], [19]. Therefore, it can be neglected compared to the delay time in the store-and-forward strategy. Accordingly, we assume that the end-to-end delay is the sum of the re-healing delays between disconnected vehicles.

Furthermore, as shown in Fig. 1, we consider a highway with vehicles moving in one direction. Also, Table 4.1 shows the list of notations used in our analysis. Moreover, since the vehicle wireless communication range is larger than the highway width, only the 1-D distance along the highway is considered; i.e., the highway width is neglected. The medium access control (MAC) layer protocol is the distributed coordination function (DCF) of the IEEE 802.11. In addition, the radio channel propagation model is assumed to follow the Nakagami-m distrbution [20], [21]. Finally, the packet traffic model follows the constant bit rate (CBR) pattern between a source and a destination that are randomly selected.

4.4 CDF for the end-to-end delay

As mentioned in the system model, we assume that inter-vehicle message transmission within the communication range is instantaneous. Therefore, it is assumed that the only delay in message propagation occurs when the packet is being carried by a vehicle in the carry-forward strategy (a vehicle does not have any vehicles ahead of it within communication range). In addition, a VANET may have many gaps over a stretch of highway. Consequently, the end-to-end delay is equal to the sum of the propagation delays between the source and the destination.

Firstly, from [14], the closed form expression for the unconditional re-healing delay is shown in Eq. (4.1). On the other hand, from [17], the PMF for the number of gaps condi-

tioned on distance is as follows

$$Pr[N_{gaps} = m|D = a] = e^{-\lambda a} \sum_{i=m}^{\lfloor a/r \rfloor} \frac{(-1)^{i-m}}{m!(i-m)!} \left[-\lambda(a-ir)\right]^{i-1} (i + \lambda(a-ir))\, e^{-\lambda(a-ir)}, \tag{4.2}$$

where r is the wireless vehicle communication range, and a is the distance between source and destination. The maximum number of gaps in this distance is $\lfloor a/r \rfloor$.

Therefore, we can obtain the PDF of the end-to-end delay conditioned on the distance between source and destination.

$$Pr[T_d = t|D = a] = \sum_{i=0}^{\lfloor a/r \rfloor} \left[f_{T_c}(t) \; *^i \; f_{T_c}(t)\right] \; Pr[N_{gaps} = i+1|D = a], \tag{4.3}$$

where $*^i$ represents the convolution iterated i times between the unconditional PDF for the re-healing delay and itself. We derived the closed form for the unconditional PDF for the re-healing delay by differentiating $F_{T_c}(t)$. The closed form for $f_{T_c}(t)$ is shown later in Eq. (4.7).

Moreover, the CDF of the end-to-end delay conditioned on the distance

$$Pr[T_d < t|D = a] = \int_0^t \sum_{i=0}^{\lfloor a/r \rfloor} \left[f_{T_c}(t_c) \; *^i \; f_{T_c}(t_c)\right] Pr[N_{gaps} = i+1|D = a]\, dt_c, \tag{4.4}$$

where each term in the summation represents the sum of the delays conditioned on having i gaps in that distance a.

Next, we can switch the order of integration and summation to obtain

$$Pr[T_d < t|D = a] = \sum_{i=0}^{\lfloor a/r \rfloor} \left[F_{T_c}(t) \; *^i \; f_{T_c}(t)\right] Pr[N_{gaps} = i+1|D = a]. \tag{4.5}$$

In addition, we can change the $*^i$ to multiplication by obtaining the Fourier transform for $f_{T_c}(t)$ as shown in Eq. (4.6). One can obtain closed forms of the Fourier transforms of $f_{T_c}(t)$

$$
\begin{aligned}
f_{T_c}(t) &= \frac{2\lambda k_2\,\Delta v e^{k_5-k_6}}{v_{\max}+v_{\min}} + 2k_1\lambda e^{-(k_5+k_6+\lambda t)}\Bigg(\lambda^2 v_{\min} t e^{(k_5+\lambda t)} - \lambda^2 v_{\max} t e^{(k_5+\lambda t)} \\
&- \frac{2\lambda v_{\max}^2 e_6^k - 2\lambda v_{\max}^2 e^{(k_5+\lambda t)} - 2\lambda v_{\max} v_{\min} e^{k_6}}{v_{\max}+v_{\min}} + \frac{2\lambda^2 v_{\max}^2 t e^{(k_5+\lambda t)} + 4\lambda^2 v_{\min}^2 t e^{(k_5+\lambda t)}}{v_{\max}+v_{\min}} \\
&+ \frac{4\lambda^2 v_{\min}^3 t e^{(k_5+\lambda t)}}{(v_{\max}+v_{\min})^2} - \frac{2\lambda v_{\max} v_{\min} t e^{(k_5+\lambda t)} + 6\lambda^2 v_{\max} v_{\min} t e^{(k_5+\lambda t)}}{v_{\max}+v_{\min}} \\
&- \frac{8\lambda^2 v_{\max} v_{\min}^2 t e^{(k_5+\lambda t)} - 4\lambda^2 v_{\max}^2 v_{\min} t e^{(k_5+\lambda t)}}{(v_{\max}+v_{\min})^2}\Bigg)/k_4 - \frac{2k_1 k_3 \lambda e^{-(k_6+k_5+\lambda t)}}{k_7 t^2 (v_{\max}+v_{\min})} - \frac{2k_1 k_3 \lambda^2 e^{-(k_6+k_5+\lambda t)}}{k_4} \\
&- \frac{4k_1 k_3 v_{\max}\lambda^2 e^{-(k_6+k_5+\lambda t)}}{t k_7 (v_{\max}+v_{\min})^2}
\end{aligned}
$$

where

$$
\begin{aligned}
&k_1 = e^{-\left(\frac{2\lambda(r-v_{\min}t)}{v_{\max}+v_{\min}}\right)},\ k_2 = e^{-\left(\frac{2\lambda r}{v_{\max}+v_{\min}}\right)}, \\
&k_3 = v_{\min}e^{k_6} - v_{\max}e^{k_6} + v_{\max}e^{k_5+\lambda t} - v_{\min}e^{k_5+\lambda t} + \frac{2\lambda t v_{\max}^2 e^{k_5+\lambda t} + 2\lambda t v_{\min}^2 e^{k_5+\lambda t} - 4\lambda t v_{\min} v_{\max} e^{k_5+\lambda t}}{v_{\max}+v_{\min}}, \\
&k_4 = e^{k_7} t (v_{\max}+v_{\min}),\ k_5 = \frac{2\lambda v_{\min} t}{v_{\max}+v_{\min}},\ k_6 = \frac{2\lambda v_{\max} t}{v_{\max}+v_{\min}},\ k_7 = \left(\lambda - \frac{2\lambda v_{\max} + 2\lambda v_{\min}}{v_{\max}+v_{\min}}\right)^2
\end{aligned}
\tag{4.7}
$$

---

and $F_{T_c}(t)$. However, it is a challenge to get the inverse Fourier transform of the entire sum as shown in Eq. (4.6).

$$
\begin{aligned}
&Pr[T_d < t | D = a] \\
&= \sum_{i=0}^{\lfloor a/r \rfloor} \mathscr{F}_t^{-1}\left[[f_{T_c}(\omega)]^i\, F_{T_c}(\omega)\right] Pr[N_{gaps} = i+1 | D = a] \\
&= \mathscr{F}_t^{-1}\left[\sum_{i=0}^{\lfloor a/r \rfloor} [f_{T_c}(\omega)]^i\, F_{T_c}(\omega)\right] Pr[N_{gaps} = i+1 | D = a],
\end{aligned}
\tag{4.6}
$$

where, $f_{T_c}(\omega)$ and $F_{T_c}(\omega)$ are the the Fourier transforms of $f_{T_c}(t)$ and $F_{T_c}(t)$, respectively.

4.5 Lower Bound for the End-to-end Delay PDF

The most challenging part of Eqs. (4.3) and (4.5) is the repeated convolution of the unconditional PDF for the re-healing delay. We start by simplifying $F_{T_c}(t)$, the CDF of the unconditional re-healing delay by ignoring some terms. In Eq. (4.1), one can note that $F_{T_c}(t)$ has three main terms (the first term has in the denominator $t(v_{\max}+v_{\min})\left(\lambda+\frac{2(\lambda v_{\min}-\lambda v_{\max})}{v_{\max}+v_{\min}}\right)^2$, the second one is $e^{-\left(k_2-k_1+\frac{2\lambda r}{v_{\max}+v_{\min}}\right)}$, and the third term is equal to 1). In addition, The general form of $F_t(t_c)$ is as follows,

$$\frac{e^{at}(bt+c)}{mt}-e^{kt}+1, \tag{4.8}$$

where a, b, c, m, and k are function of the other parameters (λ, $v_{\max}$, $v_{\min}$, r). It is difficult to obtain the Laplace or Fourier transform of this expression after raising it to the power i. The most challenging problem results from the first term $\frac{e^{at}(bt+c)}{mt}$. Therefore, we can simplify the CDF of the unconditional re-healing delay by replacing the first term with another term that is lower than the first term $\frac{e^{at}(bt+c)}{mt}$ and is a function in the second term e^{kt}. Consequently, we will have a lower bound for the CDF of the unconditional re-healing delay. We replaced it by the following $-\frac{v_{\max}+v_{\min}}{v_{\max}-v_{\min}}e^{-(k_2-k_1)}$, giving a good lower bound. In this case, a lower bound for the unconditional re-healing delay is as follows

$$F_{T_c}(t)=\left(-\frac{v_{\max}+v_{\min}}{\Delta v}e^{\left(\frac{2\lambda r}{v_{\max}+v_{\min}}\right)}-1\right)e^{-\left(k_2-k_1+\frac{2\lambda r}{v_{\max}+v_{\min}}\right)}+1$$

where (4.9)

$$k_1=2\lambda v_{\min}t/(v_{\max}+v_{\min}),\ \ k_2=2\lambda v_{\max}t/(v_{\max}+v_{\min})$$

Therefore, the general form for the lower bound now is as follows

$$F_{T_c}(t) = ae^{bt} + 1$$

$$\textbf{where} \tag{4.10}$$

$$a = -\frac{v_{\max} + v_{\min}}{\Delta v} - e^{\left(\frac{-2\lambda r}{v_{\max}+v_{\min}}\right)}, \;\; b = -k_2 + k_1.$$

In addition, a lower bound on the PDF of the unconditional re-healing delay is as follows

$$f_{T_c}(t) = ce^{bt}, \tag{4.11}$$

where $c = ab$. On the other hand,

$$\mathscr{L}_t[ce^{bt}] = \frac{c}{s-b} \tag{4.12}$$

and

$$\mathscr{L}_s^{-1}\left[\left(\frac{c}{s-b}\right)^i\right] = \frac{t^{i-1}c^i e^{bt}}{(i-1)!}. \tag{4.13}$$

Finally, a lower bound on the PDF of the end-to-end delay conditioned on the distance from source to destination is

$$Pr[T = t|D = a] = \sum_{i=1}^{\lfloor a/r \rfloor} \frac{t^{i-1}c^i e^{bt}}{(i-1)!} e^{-\lambda a} \sum_{k=i+1}^{\lfloor a/r \rfloor} \frac{(-1)^{k-i-1}}{(i+1)!(k-i)!} \left[-\lambda(a-kr)\right]^{k-1} \tag{4.14}$$
$$(i+1+\lambda(a-kr))\, e^{-\lambda(a-kr)},$$

where

$c = \left(\frac{2\lambda t \Delta v}{v_{\max}+v_{\min}}\right)\left(\frac{v_{\max}+v_{\min}}{\Delta v} + e^{\left(\frac{-2\lambda r}{v_{\max}+v_{\min}}\right)}\right)$, and

$b = \frac{-2\lambda t \Delta v}{v_{\max}+v_{\min}}$.

The detailed derivation of the proof for inequalities of this expression is included in the Appendix.

4.6 Upper Bound for the End-to-end Delay

Here, we follow the same methodology for calculating the lower bound of the end-to-end delay. For the upper bound, we replace the first term in the unconditional by the following term

$$\frac{-2\left(-\Delta v+\frac{(2\Delta v)^2}{4v_{\max}+v_{\min}}\right)}{(v_{\max}+v_{\min})\left(1-\frac{2\Delta v}{v_{\max}+v_{\min}}\right)^2}e^{-\left(k_2-k_1+\frac{2\lambda r}{v_{\max}+v_{\min}}\right)} \tag{4.15}$$

In this case, an upper bound for the unconditional re-healing delay is as follows

$$F_{T_c}(t)=\left(\frac{-2\left(-\Delta v+\frac{(2\Delta v)^2}{4v_{\max}+v_{\min}}\right)}{(v_{\max}+v_{\min})\left(1-\frac{2\Delta v}{v_{\max}+v_{\min}}\right)^2}-1\right)e^{-\left(k_2-k_1+\frac{2\lambda r}{v_{\max}+v_{\min}}\right)}+1 \tag{4.16}$$

Therefore, the general form for the lower bound now is as follow

$$F_{T_c}(t)=ae^{bt}+1 \tag{4.17}$$

where

$a=\left(\frac{-2\left(-\Delta v+\frac{(2\Delta v)^2}{4v_{\max}+v_{\min}}\right)}{(v_{\max}+v_{\min})\left(1-\frac{2\Delta v}{v_{\max}+v_{\min}}\right)^2}-1\right)e^{-\left(\frac{2\lambda r}{v_{\max}+v_{\min}}\right)}$,

$b=k_1-k_2$.

In addition, an upper bound on the PDF of the unconditional re-healing delay is as follows

$$f_{T_c}(t)=ce^{bt}, \tag{4.18}$$

where $c=ab$. Then, we follow the same method used before in the lower bound section. Finally, an upper bound on the PDF of the end-to-end delay conditioned on the distance from source to destination is

$$Pr[T=t|D=a] = \sum_{i=1}^{\lfloor a/r \rfloor} \frac{t^{i-1}c^i e^{bt}}{(i-1)!} e^{-\lambda a} \sum_{k=i+1}^{\lfloor a/r \rfloor} \frac{(-1)^{k-i-1}}{(i+1)!(k-i)!} \left[-\lambda(a-kr)\right]^{k-1} \left(i+1+\lambda(a-kr)\right) e^{-\lambda(a-kr)}$$

where

$$c = \left(\frac{-2\lambda t \Delta v}{v_{\max}+v_{\min}}\right)\left(\frac{-2\left(-\Delta v + \frac{(2\Delta v)^2}{4v_{\max}+v_{\min}}\right)}{(v_{\max}+v_{\min})\left(1-\frac{2\Delta v}{v_{\max}+v_{\min}}\right)^2} - 1\right)$$

$$e^{-\left(\frac{2\lambda r}{v_{\max}+v_{\min}}\right)}$$

$$b = \left(\frac{-2\lambda t \Delta v}{v_{\max}+v_{\min}}\right) \tag{4.19}$$

The detailed derivation of the proof for inequalities of this expression is included in the Appendix.

4.7 Simulation and model validation

This section compares simulation results against analytical results. We implemented a routing protocol to for the simulation results in NS- 2 (V-2.34). In addition, we used VanetMobiSim [22] to generate realistic vehicle mobilities. In this mobility model, a one-way highway segment is considered. Table 4.2 summarizes the configuration parameters used in these simulations.

4.7.1 End-to-end Delay

Fig. 4.2 shows the analytical results for the CDF of the end-to-end delay with the same simulation parameters as in Table II and λ=0.08 vehicles/second, while changing the distance between the source and the destination a (4, 5, and 6 km). The analytical results in Fig. 4.2 are plotted using Eq. (4.5). It can be seen that the two curves (analytical, simulation) agree closely across

Table 4.2: Simulation parameters

Simulation Parameter	**Value**
λ (veh/s)	0.07, 0.08, 0.09
Highway length (km)	30
Simulation time (s)	500
$v_{\min}$ (m/s)	15
$v_{\max}$ (m/s)	30
Simulation runs	200
Channel date rate (Mbps)	2
Communication range r (m)	300
a (km)	6

all time values for the three a values, indicating that our analysis is accurate in characterizing the CDF of the end-to-end delay.

However, a small deviation between the analytical and simulations results may be observed. This is because our analysis assumes that the time required for a vehicle to receive and process a message before it is available for further relaying is neglected.

On the other hand, results show that a has a high impact on the CDF of the end-to-end delay. For instance, the CDF of the end-to-end delay at a is equal to 4 km is the highest CDF for all values of T_d. This is because decreasing a causes a decrease in the end-to-end delay.

In addition, decreasing a increases the probability that there are no gaps between the source and the destination based on the PMF of the gaps conditioned on the distance as shown in Eq (4.2).

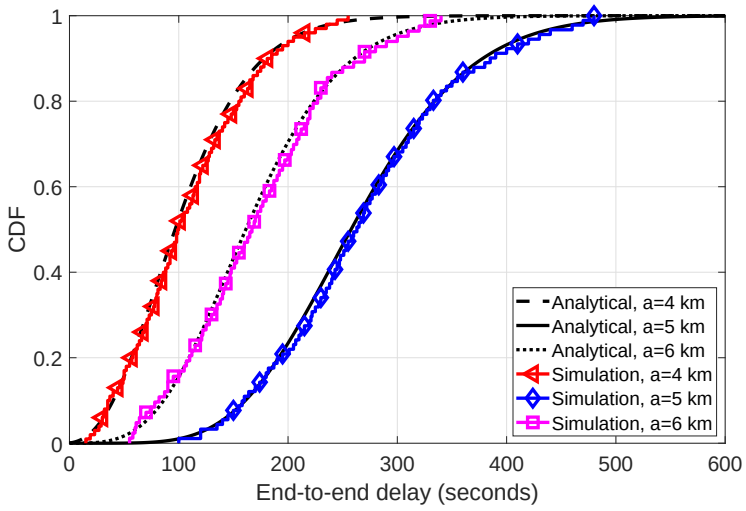

Figure 4.2: End-to-end delay with changing a.

4.7.2 Lower Bound for CDF on the End-to-End Delay

Fig. 4.3 shows the analytical CDF and lower bound results for the CDF of the end-to-end delay with a equal to 6 km and the other parameters as in Table II, while changing the vehicular density λ to values of (0.07, 0.08, and 0.09 vehicles/second). The analytical results in Fig. 4.3 are plotted using Eq. (4.5). In addition, the lower bound results in Fig. 4.3 are plotted using Eq. (4.14).

It can be seen that there is no large difference between the two curves for the three vehicular densities, indicating that our closed form for the lower bound of the end-to-end delay PDF is good in characterizing the end-to-end delay especially at small and large values of t . However, at middle values of t, we can note a slight difference between the lower bound and the analytical results especially at larger values of t.

For instance, at $t = 100$ seconds the values of the analytical CDF for vehicular densities 0.07, 0.08 and 0.09 vehicles/second are 0.09, 0.15, and 0.23, respectively. However, the lower bound

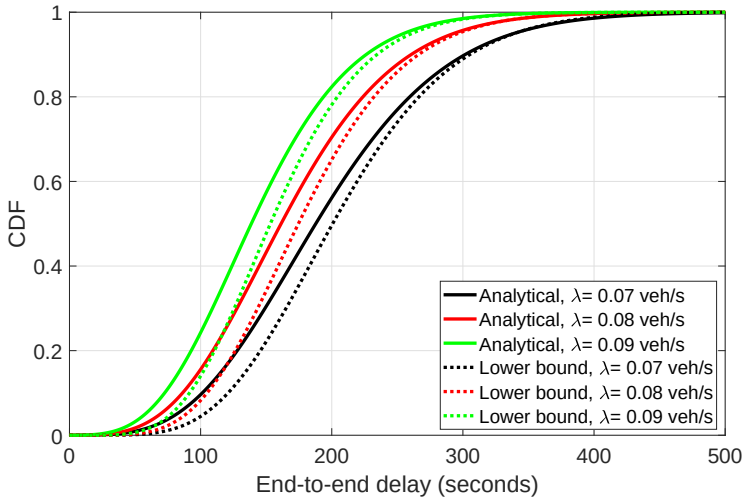

Figure 4.3: Results for lower bound expression with changing λ.

for the CDF for vehicular densities 0.07, 0.08 and 0.09 vehicles/second are 0.04, 0.07, and 0.13, respectively. On the other hand, at $t = 200$ seconds, the values of the analytical CDF for vehicular densities 0.07, 0.08 and 0.09 vehicles/second are 0.55, 0.69, and 0.81, respectively. However, the values of the lower bound of the CDF for vehicular densities 0.025, 0.035 and 0.045 vehicles/second are 0.49, 0.64, and 0.77, respectively.

4.7.3 Upper Bound for CDF on the End-to-End Delay

Fig. 4.4 shows the analytical CDF and lower bound results for the CDF of the end-to-end delay with a equal to 6 km and the other parameters as in Table II, while changing the vehicular density λ to values of (0.07, 0.08, and 0.09 vehicles/second). The analytical results in Fig. 4.4 are plotted using Eq. (4.5). In addition, the upper bound results in Fig. 4.4 are plotted using Eq. (4.19).

It can be seen that there is no large difference between the two curves for the three vehicular densities, confirming that our closed form for the upper bound of the end-to-end delay PDF is

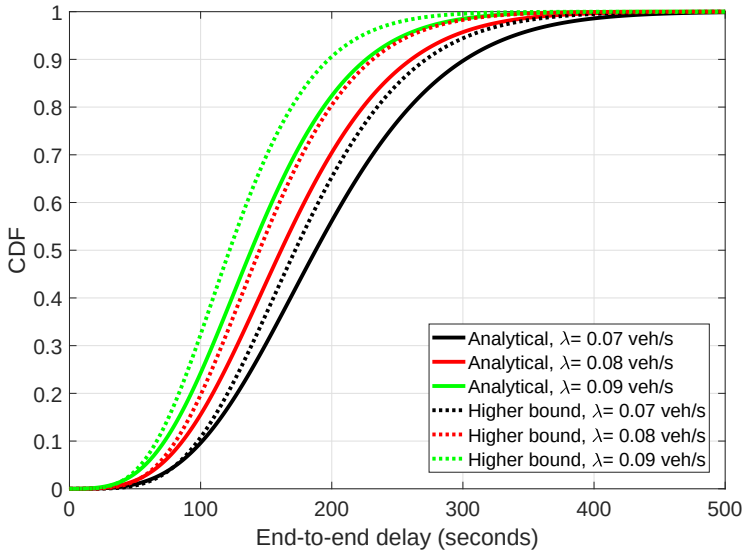

Figure 4.4: Results for upper bound expression with chnaging λ.

good in characterizing the end-to-end delay especially at small values of t . However, at larger values of t, we can note a slight difference between the upper bound and the analytical results.

For instance, at $t = 100$ seconds the values of the analytical CDF for vehicular densities 0.07, 0.08 and 0.09 vehicles/second are 0.09, 0.15, and 0.23, respectively. However, the lower bound for the CDF for vehicular densities 0.025, 0.035 and 0.045 vehicles/second are 0.11, 0.20, and 0.31, respectively. On the other hand, at $t = 200$ seconds, the values of the analytical CDF for vehicular densities 0.07, 0.08 and 0.09 vehicles/second are 0.55, 0.69, and 0.81, respectively. However, the values of the lower bound of the CDF for vehicular densities 0.07, 0.08 and 0.09 vehicles/second are 0.7, 0.81, and 0.9, respectively.

4.7.4 Results compared with related work

Fig. 4.5 shows the analytical results for the proposed model and that proposed on Ref. [15] for the CDF of the end-to-end delay with a equal to 15 km, r equal to 250 m, and (v_{min}, v_{max}) equal

to (15, 25) m/sec, while changing the vehicular density λ to values of (0.07, 0.08, and 0.09 vehicles/second). The analytical results in Fig. 4.5 are plotted using Eq. (4.5).

The results confirm that there a difference between the proposed result and that in Ref. [15] especially for low vehicular densities. This is because the analysis in Ref. [15] is based on the analytical expression of unconditional re-healing delay that proposed in Ref. [4] as follows

$$P(T_c < t|L = l) = \int_0^{\infty} f_{X(t)}(x) \int_0^{x+r-l} f_{X'(t)}(x')\, dx'\, dx, \tag{4.20}$$

where l is the distance between two VANET clusters and $l > r$. However, Ref. [14] proposed a correction for this expression as follows

$$P(T_c < t|L = l) = \int_{(l-r)v_{\max}/\Delta v}^{\infty} f_{X(t)}(x)\, F_{X'(t)}(x+r-l)\, dx. \tag{4.21}$$

This expression is revised because both clusters are moving simultaneously. Therefore, the minimum re-healing delay required is $(\frac{l-r}{\Delta v})$ seconds (when the cluster head moves with speed $v_{\max}$ and the next cluster tail with speed $v_{\min}$). Consequently, the minimum distance the head must travel before re-healing is $(l-r)v_{\max}/\Delta v$. Therefore, x should be corrected to start from $(l-r)v_{\max}/\Delta v$ not 0.

In addition, the difference is decreased at high vehicular densities, as the increase in the vehicular density leads to a decrease in the number of gaps between the source and the destination based on the PMF of the number of gaps as mentioned in Eq. (4.2). Therefore, the difference between the proposed expression for the end-to-end delay and Ref. [15] decreases for high vehicular densities, as the impact of the error in expression for the unconditional re-healing delay does not dominate the CDF of the end-to-end delay values. In the simulation section of Ref. [15], the authors used vehicular density values more than 0.2 vehicles/second. Therefore, the simulations and analytical results were close. On the contrary, for low vehicular densities,

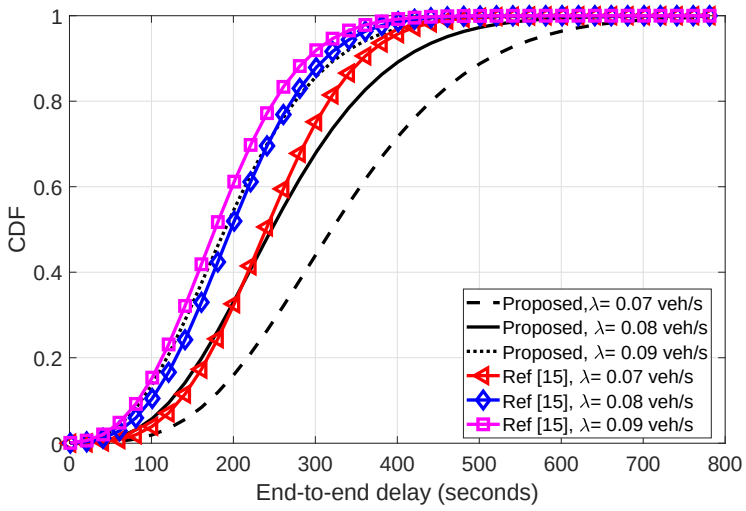

Figure 4.5: Results for the proposed compared with the previous work.

the difference between the proposed expression and that in Ref. [15] is increased. This is because low vehicular density leads to a greater number of gaps. Consequently, the error in Eq. (4.20) has a larger effect on the CDF of the end-to-end delay.

Furthermore, the proposed analytical expression for the end-to-end delay probability distribution has a lower-complexity as it is based on the probability mass function (PMF) of the number of gaps from source to destination, and the closed-form expression for the probability density distribution (PDF) of the re-healing delay (this paper model has one summation over iterated convolutions over the closed-form expression for the PDF of the re-healing delay, while our Ref. [15] is based on a summation over repeated convolutions of a numerically-calculated double integral).

On the other hand, we can note that the vehicular density λ highly impacts the CDF of the end-to-end delay. This is because increasing the vehicular density decreases the catch-up time due to decreased gap length. At the same time, increasing the vehicular density decreases the number of gaps between the source and the destination based on the PMF for the number of

gaps as mentioned in Eq (4.2).

4.8 Impact of other VANET parameters

In this section, we show the impact of VANET parameters (vehicular density λ, vehicle wireless communication range r, varying speed range Δv with the same average speed, and varying average speeds with the same Δv) on the CDF of the end-to-end delay. It was found through simulation that the accuracy was similar to those in the previous section. Therefore, only the analytical plots are shown below for clarity.

4.8.1 Vehicular density

Fig. 4.6 shows the analytical and simulation results for the CDF of the end-to-end propagation delay with a (the distance between the source and the destination) equal to 6 km and the same simulation parameters as in Table II, while changing the vehicular density λ to values of (0.07, 0.08, and 0.09 vehicles/second). The analytical results in Fig. 4.6 are plotted using Eq. (4.5).

One can note that the vehicular density λ highly impacts the CDF of the end-to-end delay. This is because increasing the vehicular density decreases the re-healing delay due to decreased gap length. At the same time, increasing the vehicular density decreases the number of gaps between the source and the destination based on the PMF of the number of gaps as mentioned in Eq. (4.2).

4.8.2 Wireless communication range

Fig. 4.7 shows the analytical results for the CDF of the end-to-end delay with the same simulation parameters as in Table II and λ=0.055 vehicles/second, and the distance between the

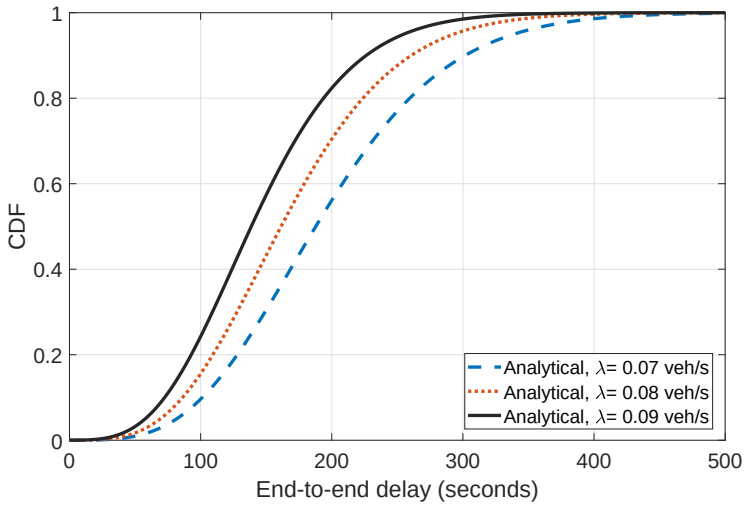

Figure 4.6: End-to-end delay with changing λ.

source and the destination a equal to 6 km, while changing the vehicle wireless communication range r (200, 300, and 400 m). The analytical results in Fig. 4.7 are plotted using Eq. (4.5).

Results show that the value of the radio range r has a high impact on the CDF of the end-to-end delay. For instance, the CDF of the end-to-end delay at r equal to 400 m is the highest CDF for all values of T_d. This is because increasing r causes a decrease in the re-healing delay. In addition, increasing r decreases the re-healing distances between the clusters as well as the number of clusters in the VANET based on the PMF in Eq (4.2).

In addition, especially in high vehicular densities, this difference increases. Therefore, we plot it at a higher vehicular densities (λ=0.8 vehicles/sec). This is because, at low vehicular density, the packet will have excessive store-and-forward stages because the number of gaps (increasing the number of clusters) increases. On the same time, r does not have a large effect much on the re-healing delay in case of the store-and-forward.

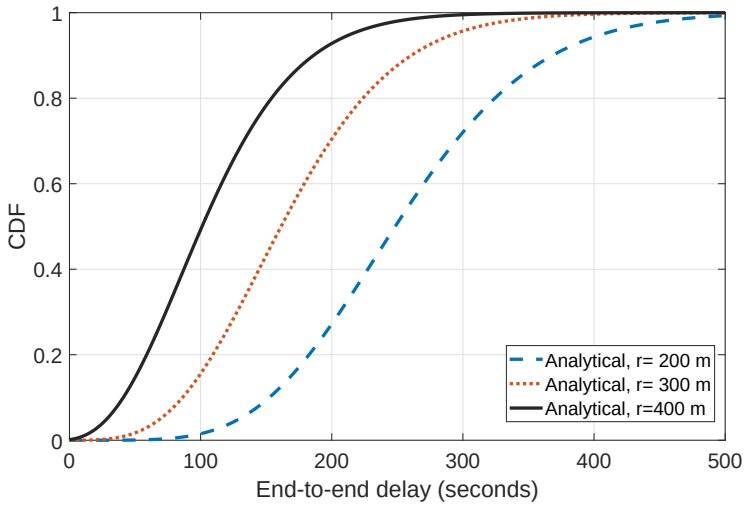

Figure 4.7: End-to-end delay with changing r.

4.8.3 Speed range

Fig. 4.8 shows the analytical results for the CDF of the end-to-end delay with the same simulation parameters as in Table II, λ=0.025 vehicles/second, and the distance between the source and the destination a set to 6 km, while changing the speed range ((15,30), (10,35), (5,40) m/s) and keeping the same value for the average speed 22.5 m/s. The analytical results in Fig. 4.8 are plotted using Eq. (4.5).

Results show that the speed range has an impact on the CDF of the end-to-end delay. For instance, the CDF of the end-to-end delay at Δv equal to 35 m/s is the highest CDF for the all values of t. This is expected because increasing Δv causes an increase in the relative speed between every two successive clusters. As a result, the re-healing delay decreases. Consequently, the CDF of the end-to-end delay increases. This is because the speeds have an impact on the the CDF of the unconditional re-healing delay. Consequently, the end-to-end delay changes.

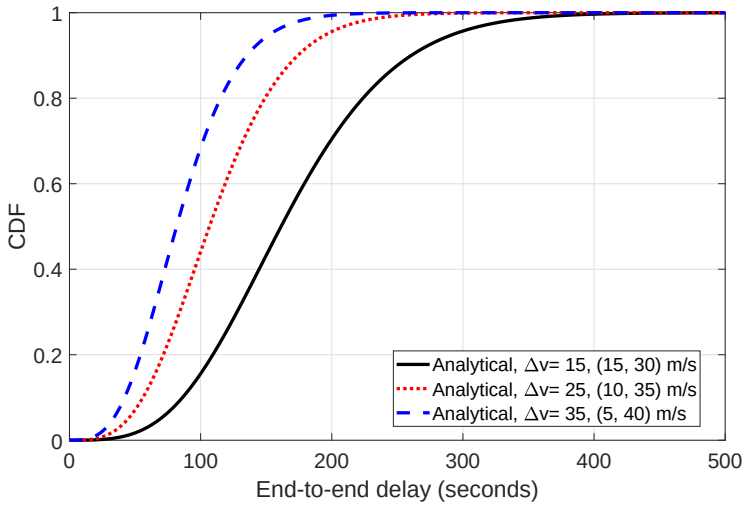

Figure 4.8: End-to-end delay with changing the minimum and maximum speeds.

4.8.4 Average Speed

Fig. 4.9 shows the analytical results for the CDF of the end-to-end delay with the same simulation parameters as in Table II, λ=0.08 vehicles/second, and the distance between the source and the destination a set to 5 km, while changing the average speed (17.5, 22.5, and 27.5 m/s), and keeping the same value for the speed range Δv = 15 m/s. The analytical results in Fig. 4.9 are plotted using Eq. (4.5).

Results show that the average speed has an impact on the CDF of the end-to-end delay. For instance, the CDF of the end-to-end delay for average speed 17.5 m/s is the highest for all values of T_d. This is because in the summation, the values of $v_{\min}$ and $v_{\max}$ have a high impact on the re-healing delay. Based on Eqs. (4.7) and (4.9) for the CDF and PDF the re-healing delay, respectively, there are many terms that have the sum of $v_{\min}$ and $v_{\max}$ in the denominator. Therefore, increasing the sum of $v_{\min}$ and $v_{\max}$, leads to a decrease in the values for PDF and CDF of of the re-healing delay. Consequently, the CDF of the end-to-end delay decreases as it

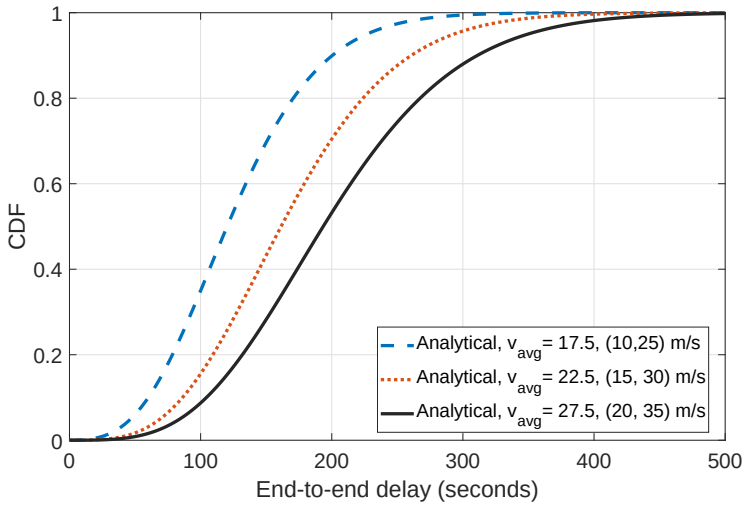

Figure 4.9: End-to-end delay with changing average speed.

depends on the re-healing delay and the number of VANET gaps in between the source and the destination. In our plot, the sum of $v_{\min}$ and $v_{\max}$ in the case of average speed 27.5 m/s is the highest. Therefore, the CDF of the end-to-end delay for average speed 27.5 m/s is the lowest for all values of T_d.

4.9 General Discussion

In this section, we give comments and general discussion related to results from the previous section.

We find that the CDF of the end-to-end propagation delay is based on a convolution between the CDF of the unconditional re-healing delay and the PMF of the number of gaps. Therefore, any parameter that has an impact on both of the CDF of the unconditional re-healing delay and the PMF of the number of gaps, will have the most significant effect on the CDF of the end-to-end delay. Therefore,

1. The vehicular density λ has the most significant impact on the CDF of the unconditional re-healing delay. Increasing λ causes an increase in the CDF of the end-to-end delay. This is because increasing the vehicular density decreases the re-healing delay due to shorter gap lengths. At the same time, increasing the vehicular density decreases the number of gaps between the source and the destination based on the PMF for the number of gaps in Eq. (4.2).

2. The distance between the source and the destination a has the second most significant impact on the CDF of the end-to-end delay. This is because a has an significant impact on the PMF of the number of gaps. With increasing a, the number of gaps between the source and the destination increases. Consequently, it increases in the number of the summation limit on Eq. (4.5).

3. The wireless communication range r has the third most significant impact on the CDF of the end-to-end propagation delay. Increasing r leads to an increase in the CDF of the end-to-end propagation delay. This is because r has an effect on both the CDF of the unconditional re-healing delay and the PMF of the number of gaps.

4. Finally, the speed parameters ($v_{\min}$, $v_{\max}$, Δv) have the fourth most significant impact on the CDF of the end-to-end delay. This is because the speeds have an impact only on the the CDF of the unconditional re-healing delay.

4.10 Conclusions

In this paper, we obtained an analytical formula for the end-to-end delay probability distribution based on the PMF of the number of gaps from source to destination and the closed form

expression of the re-healing delay in one way VANET. In addition, a closed-form expression for the lower bound of the end-to-end delay probability density distribution was derived, allowing a service provider to rapidly find a bound on the worst-case end-to-end delay for a VANET. Furthermore, we found a closed-form expression for the upper bound of the probability distribution of the end-to-end delay conditioned on the gap distance between the clusters in a VANET. Extensive computer simulation results demonstrated the accuracy of our analysis. Simulation results verified the accuracy of our analytical framework and reflected the relation between the end-to-end delay and the VANET parameters such as wireless communication range, vehicular density, the distance between the source and the destination, and minimum and maximum vehicle speed on the end-to-end delay. In our future work, we will consider a two-way highway.

REFERENCES

[1] C. Campolo and A. Molinaro, "Multichannel communications in vehicular ad hoc networks: a survey," *IEEE Communications Magazine*, vol. 51, no. 5, pp. 158–169, 2013.

[2] C. Kaplan, "Gps, cellular, fm speed and safety control devise," Dec. 26 2006, uS Patent App. 11/645,551.

[3] P. K. Sahu, E. H.-K. Wu, J. Sahoo, and M. Gerla, "Bahg: back-bone-assisted hop greedy routing for vanet's city environments," *IEEE Trans. Intell. Transp. Syst*, vol. 14, no. 1, pp. 199–213, 2013.

[4] H. Wu, R. M. Fujimoto, G. F. Riley, and M. Hunter, "Spatial propagation of information in vehicular networks," *IEEE Trans. Veh. Technol*, vol. 58, no. 1, pp. 420–431, 2009.

[5] Z. Zhang, G. Mao, and B. D. Anderson, "On the information propagation process in mobile vehicular ad hoc networks," *IEEE Trans. Veh. Technol*, vol. 60, no. 5, pp. 2314–2325, 2011.

[6] ——, "On the information propagation process in multi-lane vehicular ad-hoc networks," in *Proc. IEEE ICC*, 2012, pp. 708–712.

[7] N. Wisitpongphan, F. Bai, P. Mudalige, V. Sadekar, and O. Tonguz, "Routing in sparse vehicular ad hoc wireless networks," *IEEE J. Sel. Areas Commun*, vol. 25, no. 8, pp. 1538–1556, 2007.

[8] J. Jeong, S. Guo, Y. Gu, T. He, and D. H. Du, "Trajectory-based data forwarding for light-traffic vehicular ad hoc networks," *IEEE Trans. Parallel Distrib*, vol. 22, no. 5, pp. 743–757, 2011.

[9] J. He, L. Cai, J. Pan, and P. Cheng, "Delay analysis and routing for two-dimensional vanets using carry-and-forward mechanism," *IEEE Trans. Mobile Comput*, vol. 16, no. 7, pp. 1830–1841, 2017.

[10] C. Guo, D. Li, G. Zhang, and Z. Cui, "Data delivery delay reduction for vanets on bi-directional roadway," *IEEE Access*, vol. 4, pp. 8514–8524, 2016.

[11] A. Abdrabou and W. Zhuang, "Probabilistic delay control and road side unit placement for vehicular ad hoc networks with disrupted connectivity," *IEEE J. Sel. Areas Commun*, vol. 29, no. 1, pp. 129–139, 2011.

[12] A. Abdrabou, B. Liang, and W. Zhuang, "Delay analysis for sparse vehicular sensor networks with reliability considerations," *IEEE Trans. Wirel. Commun*, vol. 12, no. 9, pp. 4402–4413, 2013.

[13] J. Yoo, S. Choi, and C.-k. Kim, "The capacity of epidemic routing in vehicular networks," *IEEE Commun. Lett*, vol. 13, no. 6, 2009.

[14] H. Seliem, R. Shahidi, M. H. Ahmed, and M. S. Shehata, "Probability distribution of the re-healing delay in a one-way highway vanet," *IEEE Commun. Lett*, vol. 22, no. 10, pp. 2056–2059, Oct 2018.

[15] R. Shahidi and M. H. Ahmed, "Probability distribution of end-to-end delay in a highway vanet," *IEEE Commun. Lett*, vol. 18, no. 3, pp. 443–446, 2014.

[16] ——, "On the analytical calculation of the probability distribution of end-to-end delay in a two-way highway vanet," *IEEE Access*, 2017.

[17] S.-I. Sou and Y. Lee, "End-to-end performance for scf-based vehicular routing over multiple communication gaps," *IEEE Commun. Lett*, vol. 18, no. 6, pp. 1015–1018, 2014.

[18] K. A. Hafeez, L. Zhao, B. Ma, and J. W. Mark, "Performance analysis and enhancement of the dsrc for vanet's safety applications," *IEEE Transactions on Vehicular Technology*, vol. 62, no. 7, pp. 3069–3083, 2013.

[19] C. Campolo, A. Molinaro, A. Vinel, and Y. Zhang, "Modeling prioritized broadcasting in multichannel vehicular networks," *IEEE Trans. Veh. Technol*, vol. 61, no. 2, pp. 687–701, 2012.

[20] M. Killat and H. Hartenstein, "An empirical model for probability of packet reception in vehicular ad hoc networks," *EURASIP J. Wirel. Commun. Netw.*, vol. 2009, pp. 4:1–4:12, 2009.

[21] K. Chen, X. Cao, D. Sung *et al.*, "A street-centric routing protocol based on micro topology in vehicular ad hoc networks," *IEEE Trans. Veh. Technol*, vol. PP, no. 99, pp. 1–1, 2015.

[22] J. Härri, F. Filali, C. Bonnet, and M. Fiore, "Vanetmobisim: generating realistic mobility patterns for vanets," in *Proc. ACM VANET 06*, 2006, pp. 96–97.

Chapter 5

Drone-Based Highway-VANET and DAS Service

5.1 Abstract

Wireless communications between vehicles is a focus of research in both the academic research community and automobile industry. Using Unmanned Aerial Vehicles (UAVs) or drones in wireless communications and Vehicular Ad-hoc Networks (VANETs) has started to attract attention. This paper proposes a routing protocol that uses infrastructure drones for boosting VANET communications to achieve a minimum vehicle-to-drone packet delivery delay. This paper proposes a closed-form expression for the probability distribution of the vehicle-to-drone packet delivery delay on a two-way highway. In addition, based on that closed-form expression, we can calculate the minimum drone density (maximum separation distance between two adjacent drones) that stochastically limits the worst case of the vehicle-to-drone packet delivery delay. Moreover, this paper proposes a drones-active service (DAS) that is added to the

location service in a VANET. This service dynamically and periodically obtains the required number of active drones based on the current highway connectivity state by obtaining the maximum distance between each two adjacent drones while satisfying a probabilistic constraint for vehicle-to-drone packet delivery delay. Our analysis focuses on two-way highway VANET networks with low vehicular density. The simulation results show the accuracy of our analysis and reflect the relation between the drone density, vehicular density and speed, other VANET parameters, and the vehicle-to-drone packet delivery delay.

5.2 Introduction

Wireless communications between vehicles is a focus of research in both the academic research community and automobile industry. Many vehicle manufacturers have equipped their new vehicles with global positioning systems (GPSs) [1] and wireless communication devices. Vehicular ad-hoc network (VANET) technology enables ad-hoc communication between vehicles, or vehicles and fixed infrastructure-road-side units (RSUs) through wireless communication devices installed on the vehicles. VANETs are currently a widely-discussed and researched area in wireless communications. Moreover, the United States Federal Communications Commission (FCC) has allocated 75 MHz of the radio spectrum at 5.9 GHz to be used by Dedicated Short Range Communications (DSRC) [2]. DSRC is a short-to-medium-range communications service that was developed to provide vehicle-to-roadside and vehicle-to-vehicle (V2V) communications. Moreover, DSRC are aimed at providing communications with a high data rate and low end-to-end delay.

VANETs have many applications; the most important of them are active safety applications that can be used to assist drivers to avoid collisions and to coordinate between them at crowded

intersections and highway entries [3]. Moreover, VANETs can intelligently detect and convey road status information, such as real-time traffic congestion, average speed, surface condition, or high-speed tolling, to vehicles in the vicinity of specific sites. Moreover, VANETs also provide comfort applications to users, for example: mobile e-commerce, weather information, Internet access and many other multimedia applications.

Some VANET applications place more emphasis on hard delay constraints than high data rates. For example, for accident avoidance applications where certain events such as air bag ignition or brake events occur, the message must be delivered in a certain amount of time to avoid more accidents. Therefore, it is important to calculate the probability distribution of the VANET delay or determine its statistics (e.g., CDF, moments, and characteristic function).

The high mobility of vehicles is the main and most critical factor in VANET systems. The mobility of vehicles is affected by driver behavior, and constraints on mobility such as roads, road restrictions and junctions, traffic lights and high speeds. We need to consider these characteristics for design decisions in such networks. There are two typical communication scenarios in which VANETs operate. The first scenario is a highway scenario where the environment is straightforward without obstacles. The second scenario is an urban scenario where vehicles are often separated by buildings, trees, and other obstacles.

Many papers have proposed connectivity analysis (propagation speed and time) and delay probability distribution for vehicle-to-infrastructure (V2I) communications in VANETs based on fixed infrastructure-RSUs. For instance, the authors in [4] proposed a probabilistic model for vehicle-to-RSU packet delivery delay. Their model is based on effective bandwidth theory and the effective capacity concept in order to obtain the maximum distance between infrastructure-RSUs that stochastically limits vehicle-to-RSU packet delivery delay to a certain upper bound.

In addition, a mathematical framework for the vehicle-to-RSU packet delivery delay distri-

bution based on the distance between fixed RSUs that is uniformly distributed over the road was proposed in [5]. However, they did not consider the RSU wireless communication coverage in their model.

Moreover, the authors in [6] proposed a trajectory-based data forwarding scheme, tailored for data forwarding for roadside reports in sparse VANETs. They derived the expected end-to-end delivery delay from a vehicle to Internet access points. Additionally, the authors in [7] proposed an analytical framework for the expected path delay in bidirectional vehicular traffic. Using this analytical model, a shortest-path algorithm was applied to select the path with the lowest expected delay.

On the other hand, an optimal infrastructure-RSU-placement model for hybrid VANET sensor networks was proposed in [8]. It applies the center particle swarm optimization approach after it formulates the problem as an integer linear-programming optimization problem. In addition, Ref. [9] presents an analysis for the total delay of broadcasting alert messages in VANETs along a highway such that alert messages can be transmitted to the nearest RSU within a given delay bound. They derived a closed-form expression for the expected value of the total delay of broadcasting alert messages based on the distance between RSUs.

Unmanned aerial vehicles (UAVs) or drones are semi-autonomous or fully-autonomous unmanned aircrafts that have storage space and some on-board intelligence. Therefore, drones can be equipped with communication devices which makes them a possible option to improve connectivity and efficiency for many communication systems. Integration of wireless communication systems and UAVs has started to attract attention. For instance, the authors in [10] proposed drone-base-stations (drone-BSs) that can be used in cellular wireless networks. Consequently, drone-BSs provide a dynamic deployment ability that offers service where the demand exists. In addition, the drone-cell size depends on many parameters (e.g., UAV altitude,

spectrum frequency, environment, and the transmitted power).

Many papers have proposed their solutions for integrating drones in wireless communication systems. On the other hand, only a few papers have proposed using drones in VANETs. For instance, the authors in [11] proposed VDNet as a routing protocol for vehicle-to-vehicle (V2V) communications based on drones to decrease the average end-to-end packet delivery delay. In VDNet, some vehicles are equipped with an on-board drone, which can relay messages in a multi-hop route, deliver data messages directly to the destination, and collect location information while flying above the traffic.

Moreover, Ref. [12] proposed connectivity-based traffic density aware routing using UAVs (CURVE) as a routing protocol for VANETs in urban scenario using drones through cooperative and collaborative communication. The drones exchange information with the vehicles to select the most appropriate next intersection to deliver the data packets successfully to their destinations.

In addition, the authors of [13] proposed an intersection UAV-assisted VANET routing protocol (UVAR) that uses drones. UVAR is based on the drones collecting information about the state of the vehicles' connectivity, and exchanging this information with vehicles through "Hello" messages. Moreover, when a VANET has a gap (connectivity between vehicles on the ground is not possible as the distance between two vehicles is greater than the vehicle wireless communication range), UVAR uses the drones as a relay.

This paper proposes a routing protocol for V2I communications where we replace the infrastructure RSUs with infrastructure drones. While, the vehicles transmit their real-time information and Internet requests to the infrastructure drones, the drones represent gateways to the Internet and the infrastructure of other systems such as the intelligent transport system (ITS). However, it is difficult, in terms of infrastructure cost (number of drones), to get VANETs with

full connectivity by covering all gaps in the highway. On the contrary, using a small number of drones causes long vehicle-to-drone delays due to having to carry packets for a longer distance, especially in VANETs with low vehicular density. This is because the vehicles use the carry-and-forward strategy through these gaps until reaching the next drone. This paper proposes a closed-form expression to characterize the vehicle-to-drone delay probability distribution in bidirectional highway VANETs with low vehicular density where the sensed data packet is destined to the infrastructure drones.

The closed-form expression of vehicle-to-drone packet delivery delay probability distribution offers a design tool that can determine the maximum separation distance between two adjacent drones while satisfying a probabilistic requirement of vehicle-to-drone packet delivery delay. Consequently, we can calculate the minimum number of drones required to cover a two-way highway road. Moreover, it can be used for the optimization of drone placement. In this paper, we use this closed-form expression to change the drones' locations based on the highway connectivity state. The proposed closed-form expression takes into account the likelihood of a carrier vehicle exiting the road at any road junction, the spatial distribution of road junctions, the vehicular density over the highway, and the drone communication range.

The main contributions of this paper are as follows: 1) it analyzes the drone wireless communication coverage in VANETs based on the drone altitude and the other environment communication parameters, 2) it proposes a closed-form expression of the vehicle-to-drone packet delivery delay probability distribution for the proposed protocol and reflects the relation between the vehicle-to-drone packet delivery delay and the drone density, 3) it proposes an algorithm to determine the minimum required number of active drones based on the current state of the vehicles connectivity while satisfying a probabilistic requirement for vehicle-to-drone packet delivery delay, and 4) it compares results from the proposed closed-form with simula-

tion results to show the accuracy of our analysis.

The rest of this paper is organized as follows. Section II introduces the system model. Section III discusses the drone wireless communication coverage in VANETs. Section IV presents the problem formulation and the closed-form expression for characterizing the vehicle-to-drone packet delivery delay probability distribution. In addition, Section V proposes a drones-active service to determine the minimum required number of active drones based on the current highway state. Next, Section VI compares simulation results against analytical results. Finally, the conclusions and future work are presented in Section VII.

5.3 System model

In our analysis, we consider a two-way highway with vehicles moving in one of two opposite directions as shown in Fig. 5.1. In addition, each direction is a straight line with a fixed length of a meters and has two drones, one at each end. Moreover, the vehicles are moving in the forward and opposite directions with a constant speed of v_f and v_b, respectively. The constant speed assumption over the observation period helps to investigate the worst case scenario in V2Is where vehicles moving in one direction have the same speed between two adjacent drones (we do not consider vehicles overtaking other vehicles). In addition, y is the distance that the vehicle travels while carrying the packet before forwarding to the next drone as shown in Fig. 5.1.

Moreover, we assume the road junctions are distributed randomly on the highway as depicted in Fig. 5.1. Some vehicles may join and others may leave at any road junction along the highway. In addition, we assume that the number of road junctions within the highway follows a Poisson distribution with a parameter λ_c and a vehicle can leave the highway at any road

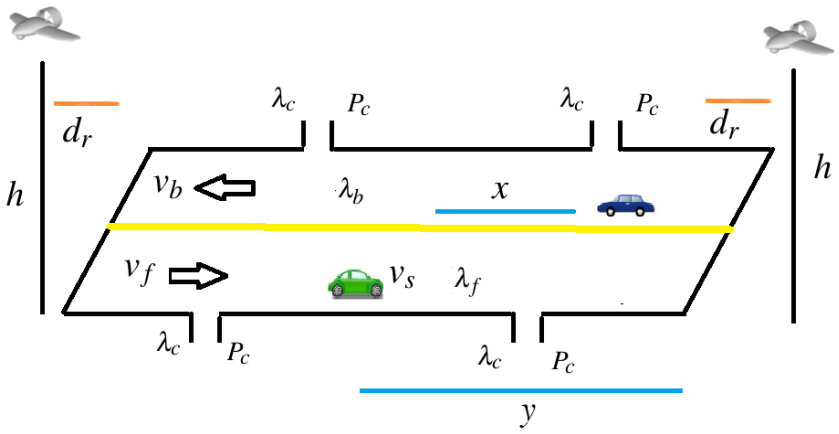

Figure 5.1: System model for bidirectional highway.

junction with a probability P_c as assumed in [5].

Additionally, we assume the inter-vehicular distances between the vehicles are exponentially distributed [4], [14], and the number of vehicles in each direction is Poisson-distributed with vehicular densities λ_f and λ_b for the forward and backward directions, respectively. In a more realistic VANET scenario, the vehicular density and the vehicle exit probability at the road junctions change with time. For instance, at the junction of a big company or a city, the probability of vehicle exit in the morning (people go to their work) or the end of the day (people return back from their work) is higher than other times (at the night period). Therefore, the drones can change their placement and the inter-drone distance while satisfying the probabilistic constraint of the vehicle-to-drone packet delivery delay based on the current highway state.

In addition, we assume that the source of packets is any moving vehicle and the destination is an infrastructure drone which has access to the Internet and other infrastructure systems. In addition, a vehicle acting as the packet source sends one replica of the packets in the opposite direction of the highway. Therefore, packets are carried either by their source vehicles or a

Table 5.1: List of notation

a	Gap between two consecutive drones
d_r	Vehicle wireless communication range
X	R.V. for inter-vehicle distance
Y	R.V. for distance between a vehicle and the drone
T	End-to-end propagation delay
P_{LoS}	The carrier frequency
c	The speed of light
P_{NLoS}	The probability of non-LoS connection
h	The drone's altitude
r	The distance between a vehicle and a drone
$F_{T_c}(t)$	CDF of T_c
$f_{T_c}(t)$	PDF of T_c
λ	Traffic flow rate (vehicles/unit time)
λ_f	Exponential mean distance in the forward direction
λ_b	Exponential mean distance in the backward direction
λ_c	The expected number of junctions
P_c	The probability that vehicle exits at any junction
v_f	Speed for the forward direction
v_b	Speed for the backward direction
$u(\cdot)$	Heaviside unit step function

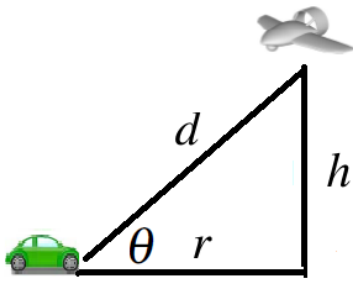

Figure 5.2: Air-to-ground path-loss model.

carrier vehicle moving in the opposite direction of the highway. In the case of high vehicular density, a connected multihop vehicle-to-drone path can be found with a high probability; however, this case is out of the scope of the proposed work. Our analysis focuses on the worst case where the original packet is stored by its source vehicle until it is within the communication range of the next drone.

Moreover, we assume that the VANET includes a location service such as a hierarchical location service (HLS) [15] or grid location service (GLS) [16]. Moreover, the transmission range between vehicles is assumed to be smaller than the distance between two adjacent drones a. In addition, we assume that the medium access control (MAC) layer protocol is the distributed coordination function (DCF) of the IEEE 802.11 standard. Finally, it is assumed that the packet traffic model follows the constant bit rate (CBR) pattern between a source vehicle and an infrastructure drone.

5.4 Drone Wireless Communication Coverage

There is a growing number of papers related to the wireless communication range of drone base-stations (BSs) in cellular networks. For instance, the authors in [17] proposed an air-to-ground path-loss model for low altitude platforms (LAPs), like drone-BSs at heights of less than

3 km. In their model, there are two main propagation categories, corresponding to the receivers with line-of-sight (LoS) connections and the ones without LoS (NLoS) connections which the receivers still receive the signal from LAPs due to strong diffractions and reflections.

Moreover, Ref. [18] proposed a channel path-loss model for drone-BSs in urban areas with respect to intersections and roof-top heights of buildings. It adopts an ITU channel model by optimizing parameters of the selected ITU model such that it can be used for altitudes both strictly lower and higher than building roof-tops.

In addition, the optimal altitude of a single drone-BS to obtain a required wireless communication coverage while minimizing the transmit power is found in [19]. Moreover, a closed-form expression for the probability of LoS connection between a LAP and a receiver is proposed in [20] and formulated as follows

$$P_{LoS} = \frac{1}{1 + e^{-b(\frac{180}{\pi}\theta - a)}}, \tag{5.1}$$

where a and b are constant values depending on the environment (rural, urban, etc), and θ is the elevation angle. This elevation angle is equal to $\arctan\left(\frac{h}{r}\right)$, where h and r are the drone's altitude and its horizontal distance from the vehicle, respectively as shown in Fig. 5.2, Eq. (5.1) shows that the probability of having a LoS connection is increased as the elevation angle increases. Consequently, the probability of LoS will increase, if the drone altitude increases for a fixed r.

On the other hand, based on [20], the mean path-loss channel model for drone-to-vehicle communications will be as follows

$$PL(dB) = 20\log_{10}\left(\frac{4\pi f_c d}{c}\right) + P_{LoS}\,\eta_{LoS} + P_{NLoS}\,\eta_{NLoS}, \tag{5.2}$$

where c is the speed of light, f_c is the carrier frequency, and the probability of non-LoS connection $P_{NLoS} = 1 - P_{LoS}$. Moreover, d is the distance between the drone and the vehicle that

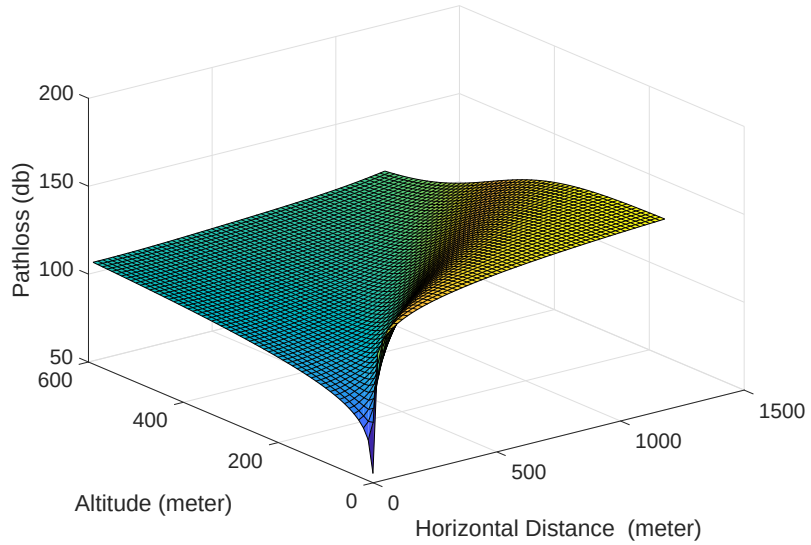

Figure 5.3: 3D plot between the drone's altitude, the drone's horizontal distance, and path-loss.

is equal to $\sqrt{h^2 + r^2}$ as shown in Fig. 5.2. In addition, η_{LoS} and η_{NLoS} depend on the environment and they are the average additional loss to the free space propagation for LoS and NLoS connections, respectively.

Therefore, in a VANET, the wireless communication coverage for the drones depends on the drone altitudes, the path-loss threshold in the VANET, and the carrier frequency f_c.

Based on Eq. (5.1) and Eq. (5.2), Fig. 5.3 shows a 3D plot between the drone's altitude, the drone's horizontal distance from the vehicle, and the mean path-loss propagation channel for drone-to-vehicle communication where a = 9.6, b = 0.28 as in [19], and f_c = 5.9 GHz. It is noticed that an increase in drone altitude does not always lead to an increase in the mean-path loss. There is a decrease in the mean path-loss when the drone altitude is between 200 meters and 400 meters for the same horizontal distance.

On the other hand, based on Eqs. (1) and (2), Fig. 5.4 shows the mean path-loss propagation channel for drone-to-vehicle communication against the horizontal distance between the vehicle

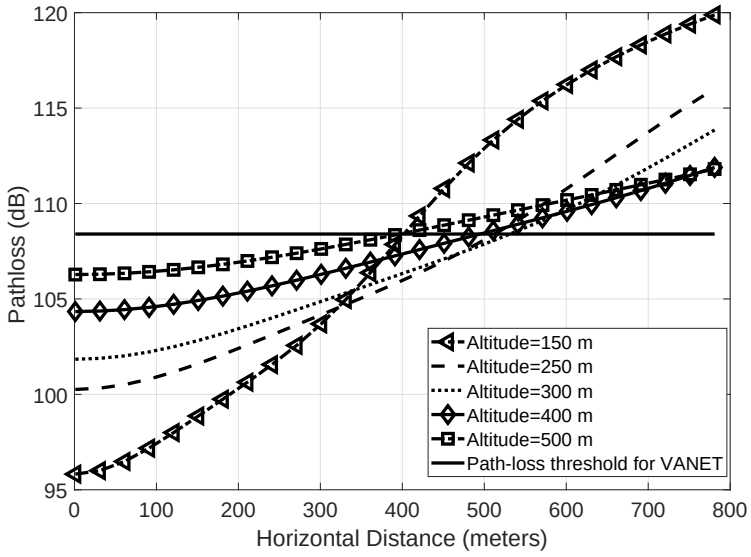

Figure 5.4: Path-loss for different drone altitudes.

and the drone altitudes where $a = 9.6$, $b = 0.28$ as in [19], and $f_c = 5.9$ GHz. Moreover, we use diffrent drone altitudes: 150, 250, 300, 400, and 500 meters. In additon, based on experimental results, the authors in [21] found the mean path-loss threshold for VANETs at $f_c = 5.9$ GHz and 750 MHz. The path-loss threshold for $f_c = 5.9$ GHz in [21] is 108 dB.

Therefore, the drone wireless communication coverage at any altitude in Fig. 5.4 is found by obtaining the intersection point between the mean path-loss threshold line and the drone altitude line. It is noticed that the wireless communication range for a drone altitude of 150 and 500 meters is close to 400 meters. On the other hand, the wireless communication range for a drone altitude of 300 meters is close to 540 meters. In addition, the main factor affecting the optimal altitude is the mean path-loss threshold. For instance, if we were to change the mean path-loss threshold to 110 dB, the optimal altitude would be at 400 meters and the range would be close to 640 meters.

The reason behind this behavior in both figures is that at low drone altitudes the probability

of NLoS becomes greater than that of LoS, due to reflections by buildings and other obstacles, and the additional loss of a NLoS connection is higher than a LoS connection. However, when the drone's altitude increases, the LoS probability increases as well and in turn mean path-loss decreases. On the contrary, the mean path-loss is also dependent on the distance between the vehicle and the drone. Consequently, after a specific height, the distance between the vehicle and the drone factor dominates the mean path-loss. Therefore, after this specific height, when the drone altitude increases, the mean path-loss increases.

5.5 Problem Formulation and the analysis

In this section, we follow the same methodology proposed in [5]. However, in this paper, the drone wireless communication range d_r is considered in the model, while, the authors in [5] did not consider the wireless communication range for the RSU. In this paper, we aim to obtain a closed-form expression for the vehicle-to-drone packet delivery delay cumulative distribution function (CDF) $F_T(t)$ in terms of a (the distance between each pair of adjacent drones), d_r (drone wireless communication range that depends on drone altitude and mean path-loss threshold), road-junction density and probability of vehicles exit at those junctions, and vehicular density on the two-way highway road as shown in Fig. 5.1. Using this closed form, we can obtain the minimum number of drones (maximum a) that satisfies a certain vehicle-to-drone delay constraint $T_{\max}$ with a violation probability of at most ε as follows

$$\begin{aligned} &\text{maximize} \quad a \\ &\text{subject to} \quad 1 - F_T(T_{\max}, a) \leq \varepsilon. \end{aligned} \tag{5.3}$$

As we mentioned in the system model, we consider in the model that the source vehicle sends the packet in the forward and opposite directions (two replicas of the same packet) and

consider the packet that reaches the infrastructure earlier. Consequently, the vehicle-to-drone packet delivery delay will be less than if we were to just transmit the packet in one direction. Therefore, the probability that the vehicle-to-drone packet delivery delay T is less than t can be formulated as follows

$$Pr(T \leq t) = Pr(T \leq t, I = 1) + Pr(T \leq t, I = 0), \tag{5.4}$$

where T is a random variable representing the vehicle-to-drone packet delivery delay and I is a random variable representing the number of extra replicas of the packet. In addition, the first term $Pr(T \leq t, I = 1)$ represents the case when the source vehicle sends the packet in the forward and opposite directions. On the other hand, the second term $Pr(T \leq t, I = 0)$ represents the case when the source carrier vehicle sends the packet only in the forward direction.

First, we need to get a closed-form expression for the term $Pr(T \leq t | I = 1)$ (the conditional CDF of the vehicle-to-drone packet delivery delay given $I = 1$). It can be formulated as follows

$$Pr(T \leq t, I = 1) = Pr(T \leq t | I = 1) Pr(I = 1). \tag{5.5}$$

Moreover, from Fig. 5.1, we can limit Y (the distance between the source vehicle and the drone in the forward direction) to be between 0 and $(a - 2d_r)$. On the other hand, X (the distance between the source vehicle and the first vehicle in the opposite direction) will be between 0 and ∞. Therefore, Eq. (5.5) can be expressed as follows

$$\begin{aligned} Pr(T \leq t, I = 1) = \int_0^{\infty} \int_0^{a-2d_r} & Pr(T \leq t | I = 1, X = x, Y = y) \\ & Pr(I = 1 | X = x, Y = y) f(x, y) \; dy \; dx, \end{aligned} \tag{5.6}$$

where d_r is the drone communication range. Moreover, the first term $Pr(T \leq t | I = 1, X = x, Y = y)$ represents the probability the delay T is less than t conditioned on one replica of the packet

in the opposite direction besides the original copy in the forward direction. This term can be formulated as follows

$$Pr(T \leq t|I=1,Y=y,X=x) = \quad u\left(t - \min\left(\frac{a-\delta-d_r+x}{v_b}, \frac{y-d_r}{v_f}\right)\right), \tag{5.7}$$

where $u(\cdot)$ is the Heaviside unit step function. In addition, we can remove $\min(\cdot)$ in Eq. (5.7) as follows

$$Pr(T \leq t|I=1,Y=y,X=x) = \begin{cases} u\left(t - \dfrac{y-d_r}{v_f}\right), \\ \text{if } \ 0 \leq y \leq \min\left(\dfrac{(a-d_r+x)v_f + d_r v_b}{v_b+v_f}, a-2d_r\right), \\ u\left(t - \dfrac{a-y-d_r+x}{v_b}\right), \\ \text{if } \ \min\left(\dfrac{(a-d_r+x)v_f + d_r v_b}{v_b+v_f}, a-2d_r\right) \leq y \leq a-2d_r. \end{cases} \tag{5.8}$$

On the other hand, the term $f(x,y)$ is the joint probability density function (PDF) of X and Y. In addition, Y is uniformly distributed since the vehicle location is uniformly distributed over the range $[0, a-2d_r]$. On the contrary, as we mentioned in the system model, the inter-vehicle distance, X, is exponentially distributed since the vehicles form a Poisson process. Consequently, we can obtain the expression for $f(x,y)$ as follows

$$f(x,y) = \frac{\lambda_f + \lambda_b}{a-2d_r} e^{-(\lambda_f+\lambda_b)x}, \quad x > 0. \tag{5.9}$$

Moreover, the term $Pr(I=1|X=x,Y=y)$ represents the probability that the packet carrier vehicle will not leave the highway at any road junction. As we mentioned in the system model, we assume that a vehicle can leave the highway at any road junction with a probability P_c and the number of road junctions within the highway follows a Poisson distribution with a parameter λ_c. Therefore, within a distance of y, the vehicle will leave with probability $P_l(y)$,

where $P_l(y) = 1 - e^{-\lambda_c P_c y}$ as proposed in [5]. As a result, the probability that the packet carrier vehicle will not leave the highway at any road junction can be expressed as follows

$$Pr(I = 1 | X = x, Y = y) = e^{-\lambda_c P_c (a - \delta - d_r + x)}. \tag{5.10}$$

Finally, by substituting (Eq. 5.9) and Eq. (5.10) into Eq. (5.6), we can formulate the first term on the right side on Eq. (5.4) as follows

$$\begin{aligned} Pr(T \leq t, I = 1) = & \int_0^{\infty} f(x,y) \int_0^{m} u\left(t - \frac{y - d_r}{v_f}\right) e^{-\lambda_c P_c (a - y - d_r + x)} dy \; dx \\ & + \int_0^{\infty} f(x,y) \int_m^{a - 2d_r} u\left(t - \frac{a - y - d_r + x}{v_b}\right) e^{-\lambda_c P_c (a - y - d_r + x)} dy \; dx, \end{aligned} \tag{5.11}$$

where $m = \min\left(\dfrac{(a - d_r - y + x) v_f + d_r v_b}{v_b + v_f}, \; a - 2d_r\right)$.

Moreover, we can remove the $\min(\cdot)$ term in the integration. In this case, Eq.(5.11) can be formulated as follows

$$\begin{aligned} Pr(T \leq t, I = 1) = & \int_0^{b_1} \int_0^{b_2} k_1 \; dy \, dx + \int_{b1}^{\infty} \int_0^{a - 2d_r} k_1 \; dy \, dx \\ & + \int_0^{b_1} f(x,y) \int_{b_2}^{a - 2d_r} u\left(t - \frac{a - y - d_r + x}{v_b}\right) e^{-\lambda_c P_c (a - y - d_r + x)} dy \; dx, \end{aligned} \tag{5.12}$$

where

$k_1 = f(x,y) u\left(t - \dfrac{y - d_r}{v_f}\right) e^{-\lambda_c P_c (a - y - d_r + x)}$,

and

$b_1 = \dfrac{a v_b - d_r (v_f + 3 v_b)}{v_f}$, $b_2 = \dfrac{(a - d_r - y + x) v_f + d_r v_b}{v_b + v_f}$.

On the contrary, we need to obtain a closed-form expression for the second term on the right side of Eq. (5.4) in the case of $I = 0$, where there is no replica for the packet in the opposite direction. This term can be formulated as follows,

$$Pr(T \leq t, I = 0) = \int_0^{\infty} \int_0^{a-2d_r} Pr(T \leq t | I = 0, X = x, Y = y) \\ Pr(I = 0 | X = x, Y = y) f(x,y) \; dy \; dx, \tag{5.13}$$

where the term $Pr(T \leq t | I = 0, Y = y, X = x)$ will be

$$Pr(T \leq t | I = 0, Y = y, X = x) = u\left(t - \frac{y - d_r}{v_f}\right). \tag{5.14}$$

Moreover, the term $Pr(I = 0 | X = x, Y = y)$, the probability that the carrier vehicle will not leave the highway over the distance $(y - d_r)$ is proposed in [5] as follows

$$Pr(I = 0 | X = x, Y = y) = 1 - e^{-\lambda_c P_c (a - y - d_r + x)}. \tag{5.15}$$

Therefore, the second term on the right side of Eq. (5.4) can be obtained as follows,

$$Pr(T \leq t, I = 0) = \int_0^{\infty} f(x,y) \int_0^{a-2d_r} u\left(t - \frac{y - d_r}{v_f}\right) (1 - e^{-\lambda_c P_c (a - y - d_r + x)}) dy \; dx \tag{5.16}$$

Using Eq. (5.4), Eq. (5.12), and Eq. (5.16), we can obtain an expression for the CDF of the vehicle-to-drone packet delivery delay as given in Eq. (5.17).

Finally, we obtained a closed-form expression for the first three terms in Eq. (5.17) (they include $u(t - \frac{y - d_r}{v_f})$ factors in the integrands) which is shown in Eq. (5.18). Moreover, the closed-form expression for the last term in Eq. (5.17) (which has a $u\left(t - \frac{a - y - d_r + x}{v_b}\right)$ factor) is given in Eq. (5.19).

$$Pr(T \leq t) = \int_0^{b_1} m_1 \int_0^{b_2} u\left(t - \frac{y-d_r}{v_f}\right) m_2 \, dy \, dx + \int_{b_1}^{\infty} m_1 \int_0^{a-2d_r} u\left(t - \frac{y-d_r}{v_f}\right) m_2 \; dy \, dx$$
$$+ \int_0^{\infty} m_1 \int_0^{a-2d_r} u\left(t - \frac{y-d_r}{v_f}\right)(1-m_1) dy \; dx + \int_0^{b_1} m_1 \int_{b_2}^{a-2d_r} u\left(t - \frac{a-y-d_r+x}{v_b}\right) m_2 \, dy \; dx,$$

where

$$m_1 = \frac{\lambda_f + \lambda_b}{a-2d_r} e^{-(\lambda_f+\lambda_b)x}, \; m_2 = e^{-\lambda_c P_c (a-y-d_r+x)}, b_1 = \frac{a v_b - d_r(v_f+3v_b)}{v_f},$$
$$b_2 = \frac{(a-d_r-y+x)v_f + d_r v_b}{v_b + v_f}. \tag{5.17}$$

5.6 Drones-Active Service

There are many papers that have proposed routing protocols for VANET communications based on a location service as in [22–24]. The main role of the location service is to obtain the updated locations of vehicles. Many papers have proposed designs of this location service such as HLS [15], and GLS [16].

In this paper, a drones-active service (DAS) is proposed. The DAS is a computational service that is based on the location service. By using the proposed closed-form expression, the service operator provides the number of drones needed to serve the VANET over the highway in the lowest vehicular density e.g., at the night period. However, DAS switches on some of these drones according to the vehicular density λ_f, λ_b changes and vehicle exit probability at the road junctions P_c.

In a realistic VANET scenario, the vehicular density and the vehicle exit probability at the road junctions change with the time. For instance, at the junction of a big company or a city, the probability of vehicle exit in the morning (people go to their work) or the end of the day

(people return back from their work) is higher than other times (during the night).

$$Term_1 = \begin{cases} k_5 + k_{34}\lambda(k_{10}+k_{13}) & \textbf{if } a \le k_1 \textbf{ and } k_{15} \le k_2 \\ k_6 + k_{34}\lambda(k_9+k_{13}) & \textbf{if } a > k_1 \textbf{ and } k_{15} \le k_2 \\ k_5 + k_{34}\lambda\,(k_{18}+k_{10}+k_8) & \textbf{if } a \le k_1 \textbf{ and } k_{11} \le k_4 \\ k_6 + k_{34}\lambda\,(k_{18}+k_9+k_8) & \textbf{if } a > k_1 \textbf{ and } k_{11} \le k_4 \\ k_5 + k_{34}\lambda\,(k_7+k_{17}+k_{10}+k_{12}-k_{16}) & \textbf{if } a \le k_1 \textbf{ and } k_{11} \ge k_4 \textbf{ and } k_3 < k_{14} \\ k_6 + k_{34}\lambda\,(k_7+k_{17}+k_{12}+k_9-k_{16}) & \textbf{if } a > k_1 \textbf{ and } k_{11} \ge k_4 \textbf{ and } k_3 < k_{14} \end{cases} \tag{5.18}$$

where

$k_1 = 3d_r + v_f t,\ k_2 = \frac{t^2(128d_r - 64a + 64tv_b)^2}{256},\ k_3 = (32768d_r - 1638a + 16384tv_b)^2,$

$k_4 = 4t\left(v_b k_{29} + t(v_b+v_f)\left(v_f + \frac{d_r - a/2 + tv_b/2 + k_{29}/(2v_b+2v_f)}{t}\right)^2\right),$

$k_5 = (\lambda_f+\lambda_b)k_{33}\left(\frac{a-2d_r}{\lambda_f+\lambda_b} + k_{19} - \frac{k_{27}e^{a\lambda_c P_c - 2d_r\lambda_c P_c}}{\lambda_c P_c k_{30}}\right),\ k_6 = \lambda k_{33}\left(k_{19} + \frac{d_r+tv_f}{\lambda} - \frac{k_{22}k_{27}}{\lambda_c P_c k_{30}}\right),$

$k_7 = \frac{k_{20} - k_{20}k_{25}e^{\lambda_c P_c k_{28}}}{k_{21}\lambda_c P_c},\ k_8 = \frac{k_{20}k_{26}\left(k_{23} - e^{-\lambda_c P_c k_{29}/(v_f+v_b)}\right)}{k_{21}\lambda_c P_c},\ k_9 = \frac{k_{26}(k_{22}-1)}{k_{30}\lambda_c P_c}, k_{10} = \frac{k_{26}\left(e^{\lambda_c P_c(a-2d_r)} - 1\right)}{k_{30}\lambda_c P_c}$

$k_{11} = \frac{\left(2d_r(v_f+v_b) - k_{32} - a(v_f+v_b) + v_f(a-d_r) + d_r v_b + tv_b(v_f+v_b)\right)^2}{v_f+v_b},\ k_{12} = \frac{k_{22}(k_{25}-k_{26})}{\lambda_c P_c k_{30}},$

$k_{13} = \frac{k_{26}(k_{22}-1)(k_{23}-1)}{\lambda_c P_c k_{30}},\ k_{14} = 1073741824\,k_{24},\ k_{15} = 64k_{24},\ \ k_{16} = \frac{(k_{25}-k_{26})}{\lambda_c P_c k_{30}},$

$k_{17} = \frac{(k_{25}-1)}{\lambda_c P_c k_{30}},\ k_{18} = \frac{(k_{26}-1)}{\lambda_c P_c k_{30}},\ k_{19} = \frac{k_{27}}{\lambda_c P_c k_{30}},\ k_{20} = e^{\frac{k_{31}\lambda_c P_c}{v_f+v_b}},\ k_{21} = \lambda + \lambda_c p_c - \frac{\lambda p_c v_f}{v_f+v_b},$

$k_{22} = e^{\lambda_c P_c(d_r+v_f t)},\ k_{23} = e^{-\left(\frac{k_{29}k_{30}}{v_f}\right)},\ k_{24} = \left(d_r - a/2 + v_b t/2 + v_f t\right)^2,$

$k_{25} = e^{-k_{28}k_{30}(v_f+v_b)/v_f},\ k_{26} = e^{k_{29}k_{30}/v_f},\ k_{27} = e^{-\lambda_c P_c(a-dr)},\ k_{28} = d_r + v_f t - \frac{k_{31}}{v_f+v_b},$

$k_{29} = v_f(a-d_r) - k_{32} + d_r v_b,\ k_{30} = \lambda + \lambda p_c,\ k_{31} = v_f(a-d_r) + d_r v_b,$

$k_{32} = (v_f+v_b)(a-2d_r),\ k_{33} = \frac{1}{a-2d_r}, k_{34} = k_{33}k_{27},\ \lambda = \lambda_f + \lambda_b.$

$$
Term_2 = \begin{cases}
-k_6 k_{30}\lambda \left(k_{15} + \frac{k_{19}k_{21}(k_{18} - e^{-k_{24}\lambda_c P_c/(v_f+v_b)})}{k_{20}} \right) & \textbf{if } k_{11} \le k_{10} \\
-k_6 k_{30}\lambda u(v_b t - dr) \left(\frac{k_{23}(k_{14}-1)}{\lambda_c P_c k_{26}} + \frac{k_8 k_9 e^{a\lambda_c P_c} - e^{(d_r k_{26} - k_{26} v_b t + a\lambda_c P_c - 2d_r \lambda_c P_c)}}{k_7} \right) & \textbf{if } k_4 \le k_{28} + d_r v_f \\
\textbf{and } k_1 \le k_2 \textbf{ and } k_{10} \le k_{11} & \\
-k_6 k_{30}\lambda \left(k_{15} + \frac{k_8 k_{21} - e^{a\lambda_c P_c}(k_{17} - k_{18})}{k_7} \right) & \textbf{if } k_4 \ge k_{28} + d_r v_f \textbf{ and } k_1 \le k_2 \textbf{ and } k_{10} \le k_{11} \\
-k_6 k_{30}\lambda \left(0.5 sign\left(2d_r - a + \frac{k_{26} + d_r v_f + v_b v_f t}{v_f + v_b} \right) - 0.5 \right) & \\
\left(k_{16} - k_{12} + \frac{k_{19}}{k_{20}} + \left(\frac{k_{23}(k_{22} - k_{14})}{\lambda_c P_c k_{26}} - \frac{k_8 k_9 e^{a\lambda_c P_c}(k_{13} - e^{(-k_{14}\lambda_c P_c (d_r - t v_b))})}{k_7} \right) \right) & \\
\textbf{if } k_3 \le k_5 \textbf{ and } k_4 \le k_{28} + d_r v_f \textbf{ and } k_1 \le k_2 \textbf{ and } k_{10} \le k_{11} & \\
-k_6 k_{30}\lambda \left(k_{16} - k_{12}\frac{k_{23}(k_{21} - k_{12})}{\lambda_c P_c k_{26}} + \frac{k_{19}}{k_{20}} + \frac{k_8 k_9 e^{a\lambda_c P_c}(k_{13} - k_{17} k_{21})}{k_7} \right) & \\
\quad \textbf{if } k_3 \le k_5 \textbf{ and } k_4 \ge k_{28} + d_r v_f \textbf{ and } k_1 \le k_2 \textbf{ and } k_{10} \le k_{11} &
\end{cases} \tag{5.19}
$$

where

$k_1 = 64t^2\left(d_r - 0.5a + v_b t + 0.5 t v_f\right)^2$, $k_2 = \frac{t^2\left(128 d_r - 64a + 64 v_f t\right)^2}{256}$, $\lambda = \lambda_f + \lambda_b$

$k_3 = \frac{v_f\left(d_r(v_f+v_b) - a(v_f+v_b) + v_f(a-d_r) + d_r v_b + t v_b (v_f+v_b)\right)}{(v_f+v_b)}$, $k_4 = v_f(a-d_r) + d_r v_b + t v_f v_b$,

$k_5 = -\frac{v_b\left(2d_r(v_f+v_b) - a(v_f+v_b) + v_f(a-d_r) + d_r v_b\right)}{(v_f+v_b)}$, $k_6 = e^{-\lambda_c P_c (a-dr)}$, $k_7 = \lambda_c \lambda_c P_c$, $k_8 = e^{-\lambda_c P_c v_b t}$,

$k_9 = e^{-d_r \lambda_c P_c}$, $k_{10} = 4t(v_b + v_b)\left(v_f(a-d_r) - k_{28} + d_r v_b + t\left(v_b + \frac{2d_r - a + t v_f + \frac{k_{24}}{v_f} - \frac{k_{24}}{v_f+v_b}}{2t} \right)^2 \right)$,

$k_{11} = (v_f + v_b(2d_r - a + t_v f + \frac{k_{24}}{v_f} + \frac{k_{24}}{v_f+v_b})^2 + 4k_{24} v_f t$, $k_{12} = \frac{k_{22} k_{19} e^{-\left(\frac{k_{25}\lambda_c P_c v_f}{k_{27}(v_f+v_b)}\right)}}{k_{20}}$,

$k_{13} = k_2 e^{-k_{25}\lambda_c P_c / k_{27}}$, $k_{14} = e^{k_{26}(d_r - v_b t)}$, $k_{15} = \frac{k_{23}(k_{21}-1}{\lambda_c P_c k_{26}}$, $k_{16} = \frac{k_{23}(k_{22}-1}{\lambda_c P_c k_{26}}$,

$k_{17} = e^{-k_{24}\lambda_c P_c / v_f}$, $k_{18} = e^{-k_{24} k_{26}/v_f}$, $k_{19} = e^{k_{29}\lambda_c P_c/(v_f+v_b)}$, $k_{20} = \lambda P_c\left(\lambda + \lambda_c P_c - \frac{\lambda P_c v_f}{v_f+v_b}\right)$,

$k_{21} = e^{k_{24} k_{26}/v_f}$, $k_{22} = e^{k_{26} k_{25}/k_{27}}$, $k_{23} = e^{\lambda_c P_c (a-d_r)}$, $k_{24} = v_f(a-d_r) - k_{28} + d_r v_b$,

$k_{25} = d_r - a + t v_b + \frac{k_{29}}{v_f+v_b}$, $k_{27} = \frac{v_f}{v_f+v_b}$, $k_{28} = (a - 2d_r)(v_f + v_b)$, $k_{29} = v_f(a-d_r) + d_r v_b$,

The proposed DAS detects the vehicular density of the highway after every specified time period. In addition, DAS has the values of the probability of vehicle exit at different times. Then, based on the vehicle-to-drone delivery delay constraint, the detected vehicular density, and the the probability of vehicle exit at that time, DAS uses our proposed closed-form expression to obtain the maximum distance between two adjacent drones satisfying the delay constraint.

After that, the DAS finds the required number of drones for the highway at that time based on the calculated maximum distance. Finally, if the maximum distance increases, the DAS switches off some drones e.g., requiring their batteries to be recharged, and the other drones change their location based on the calculated maximum distance between them. On the contrary, if the maximum distance decreases, the DAS switches on some drones again to reach the required number of drones for the highway at that time.

However, in the obtained closed-form expression, the maximum distance is not on the right side. Therefore, after detection of the new value for the vehicular density, DAS can increase/decrease the current distance with d meters, and check the CDF threshold. If the CDF is more than/less than the threshold, DAS can increase/decrease the distance another time by d meters. Then, the algorithm repeats this step until it reaches the CDF delay threshold. The distance in that iteration is the maximum distance between two adjacent drones satisfying the delay constraint. Then, DAS saves this maximum distance and the related parameters (vehicular distance, vehicle exit probability) in a table to use them directly.

Next, DAS decides which drones will be off/on based on this distance. The first priority is for the drone that needs to recharge or closest to consuming its battery. Secondly, if all drones have equal battery charges or they depend on solar energy and do not need to recharge, all drones move the same distance. Then, the drones at the end of the highway will be turned off.

When λ decreases again, each drone returns to the last position and these drones are switched on again.

This method benefits from the mobile nature of the drones and VANET. The DAS approach takes into account the temporal vehicular density variation and the probability of vehicle exit. DAS helps to ensure the minimum number of active drones that can satisfy the required constraint on the vehicle-to-drone packet delivery delay. DAS can switch off some drones that need to recharge their batteries or based on any other configuration. Algorithm 1 explains the DAS in detail.

5.7 Simulation and model validation

This section compares our simulation results against those from our analysis. We implement our proposed protocol in NS-2 (v. 2.34). In addition, we use VanetMobiSim [25] to generate realistic vehicle mobilities with considering the mobility model mentioned in Section III. In this mobility model, a bi-directional highway segment is considered. Table 5.2 summarizes the configuration parameters used in the simulation. The following subsections presents the results for simulations and the analysis with different parameters (the vehicular density, drone density, junctions density, probability of exit at junction, and the forward and backward speeds). However, for clarity of the plots, we include the plots for the simulations in Fig. 5.5 only. It was found through simulation that the accuracy in the others figures were similar to those in Fig. 5.5.

Table 5.2: Simulation parameters

Simulation Parameter	Value
a (km)	6
Exit Probability P_c	0.03
Road junctions density λ_c	0.002
v_f (m/s)	25
v_b (m/s)	30
Simulation runs	500
Simulation time (seconds)	600
Vehicles' communication range (m)	250
Channel date rate (Mbps)	2
Drone altitude (m)	300
Drone communication range (m)	550

5.7.1 Drone density

Fig. 5.5 shows the analytical and simulation results for the CDF of the vehicle-to-drone packet delivery delay with the same simulation parameters as in Table 5.2, while changing the distance between each two drones a to values of (a=3, 4, and 6) km. In Fig. 5.5, the analytical results are plotted using the closed-form in Eq. (5.17).

It can be seen that the two curves (analytical, simulation) agree closely across all time values for all figures, indicating that our analysis is accurate in characterizing the CDF of the the vehicle-to-drone packet delivery delay. However, a small deviation between the analytical and simulations results may be observed. This is because our analysis focuses on the worst case

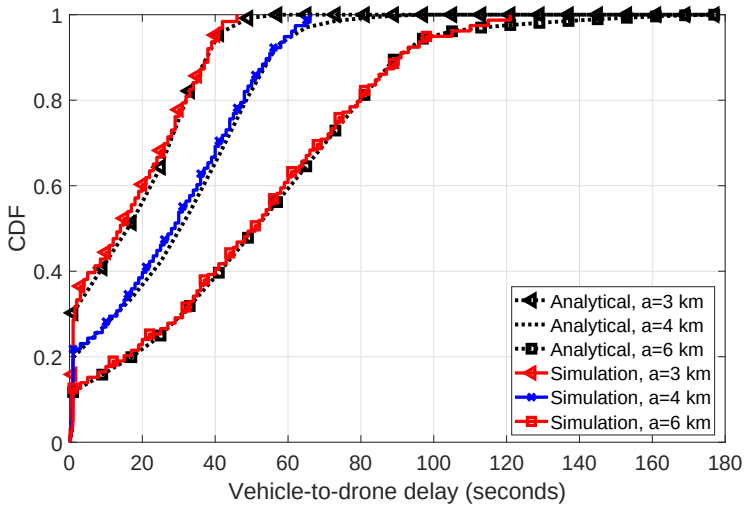

Figure 5.5: Vehicle-to-drone delay with changing a.

where the original packet is stored by its source vehicle, or the next vehicle in the opposite direction, until it is within communication range of a drone. However, the source vehicle may forward the packets to a neighboring vehicle. As a result, the vehicle-to-drone packet delivery delay decreases. In addition, our analysis assumes that the time required for a vehicle to receive and process a message before it is available for further relaying is negligible. The small deviations increase in the case of a high vehicular density because in that case, the probability of forwarding the packet to a neighbor vehicle is increased. However, this case is beyond the scope of this paper.

In addition, one can note that a (drone density) highly impacts the CDF of the vehicle-to-drone packet delivery delay. With increasing the drone density, the CDF of the vehicle-to-drone packet delivery delay increases for all values of the drone density. For instance, the CDF of the vehicle-to-drone packet delivery delay at a equal to 3 km is the highest CDF for the all values of t. This is because increasing the drones density leads to a decrease in a. As a result, the source vehicle carries the packet for a shorter distance. Consequently, the vehicle-to-drone

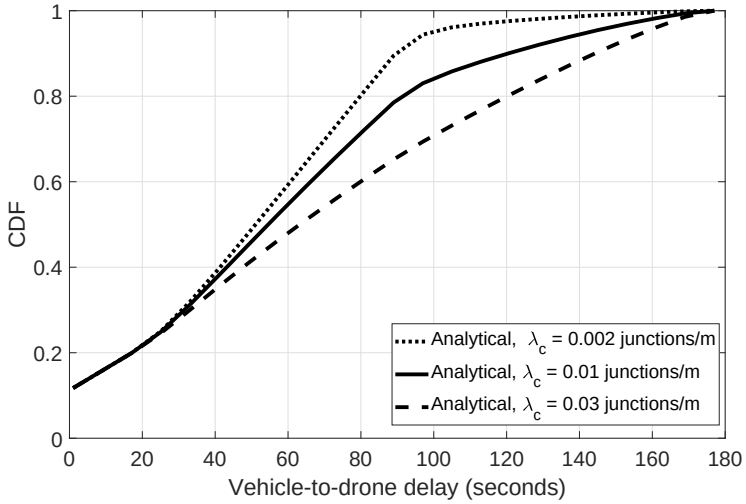

Figure 5.6: Vehicle-to-drone delay with changing junction density λ_c.

packet delivery delay decreases.

5.7.2 Junction density

Fig. 5.6 shows the analytical results for the CDF of the vehicle-to-drone packet delivery delay with the same parameters as in Table 5.2, while changing the junction density λ_c to values of (0.002, 0.01, and 0.03) junctions/m.

The results show that the junction density λ_c impacts the CDF of the vehicle-to-drone packet delivery delay. By increasing the junction density, the CDF of the vehicle-to-drone packet delivery delay decreases for all values of the drone density. For instance, the CDF of the vehicle-to-drone packet delivery delay for λ_c equal to 0.03 junctions/m is the lowest CDF for the all values of t. This is because increasing the junction density leads to an increase in the probability that the vehicle (packet carrier) exits from the highway at any of those junctions. As a result, the drone receives the second replica from the packet that takes a longer time to reach the next drone. Consequently, the vehicle-to-drone packet delivery delay increases.

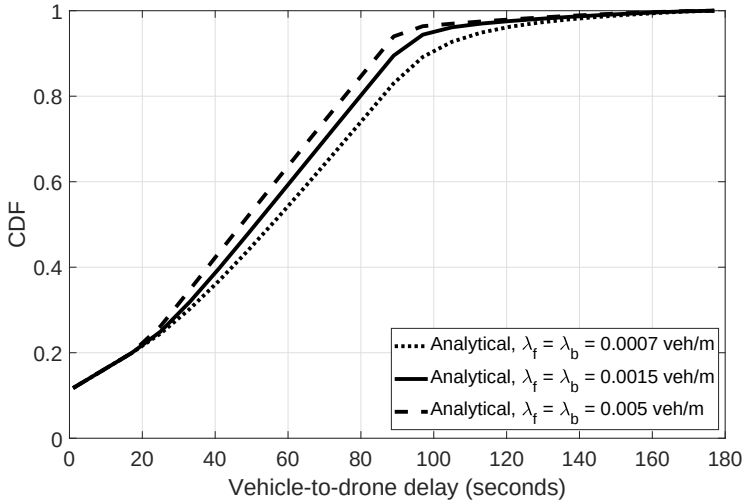

Figure 5.7: Vehicle-to-drone delay with changing vehicular density.

5.7.3 Vehicular density

Fig. 5.7 shows the analytical results for the CDF of the vehicle-to-drone packet delivery delay with the same parameters as in Table 5.2, while changing the vehicular density λ_f and λ_b to values of (0.0007, 0.0015, and 0.005) vehicles/m.

In addition, one can note that the vehicular densities λ_f and λ_b impact the CDF of vehicle-to-drone packet delivery delay. By increasing the vehicular density, the CDF of the vehicle-to-drone packet delivery delay increases for all values of time. For instance, the CDF of the vehicle-to-drone packet delivery delay at 0.005 veh/m is the highest CDF for the all values of t. This is because increasing the vehicular density decreases the vehicle-to-drone distance and the time required to forward the packet to a drone.

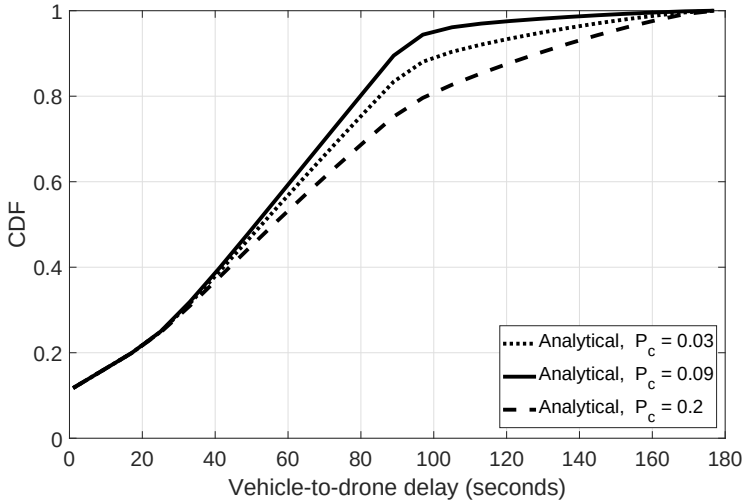

Figure 5.8: Vehicle-to-drone delay with changing P_c.

5.7.4 Exit probability

Fig. 5.8 shows the analytical results for the CDF of the vehicle-to-drone packet delivery delay with the same parameters as in Table 5.2, while changing the probability of exit P_c to values of (0.03, 0.09, and 0.2).

One can note that the probability of exit P_c impacts the CDF of vehicle-to-drone packet delivery delay. By increasing the vehicular density, the CDF of the vehicle-to-drone packet delivery delay decreases for all values of P_c. For instance, the CDF of the vehicle-to-drone packet delivery delay at P_c equal to 0.2 is the lowest CDF for the all values of t. This is because increasing the probability of exit leads to an increase in the probability that the vehicle (packet carrier) exits from the highway at any junctions. As a result, the drone receives the second replica from the packet that takes a longer time to reach the next drone. Consequently, the vehicle-to-drone packet delivery delay increases.

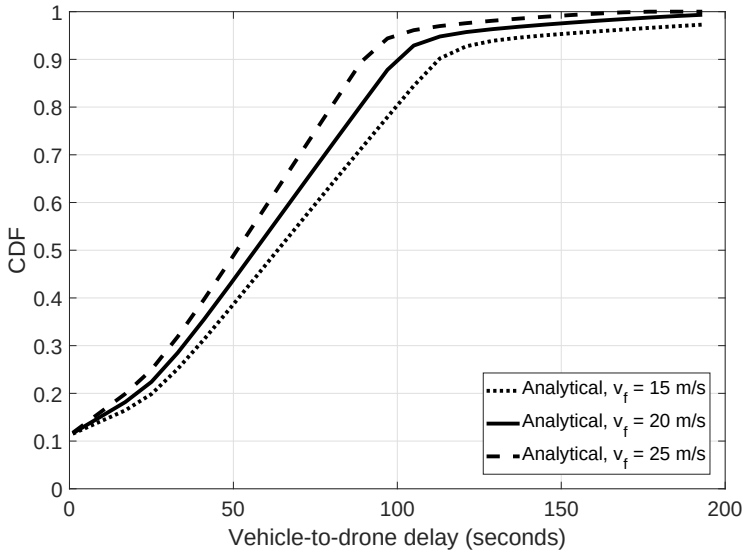

Figure 5.9: Vehicle-to-drone delay with changing v_f.

5.7.5 Forward speed

Fig. 5.9 shows the analytical results for the CDF of the vehicle-to-drone packet delivery delay with the same parameters as in Table 5.2, while changing the forward speed v_f to values of (15, 25, and 35) m/s.

Results show that the forward speed has an impact on the CDF of vehicle-to-drone delivery delay. With increasing v_f, the CDF of the vehicle-to-drone packet delivery delay increases for all values of v_b. For instance, the CDF of the vehicle-to-drone delivery delay at v_f = 35 m/s is the highest CDF for all values of t considered. This is expected because increasing v_f causes an decrease in the time required to reach the drone in the forward direction.

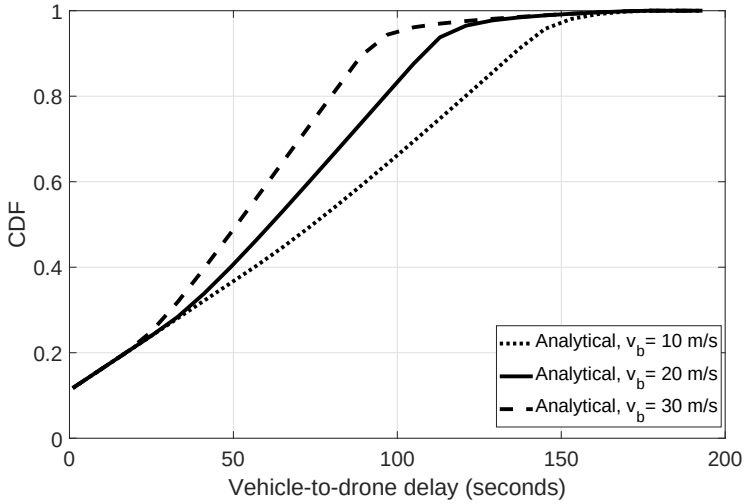

Figure 5.10: Vehicle-to-drone delay with changing v_b.

5.7.6 Backward speed

Fig. 5.10 shows the analytical results for the CDF of the vehicle-to-drone packet delivery delay with the same parameters as in Table 5.2, while changing the backward speed v_b to values of (10, 20, and 30) m/s.

Results show that the backward speed has an impact on the CDF of vehicle-to-drone delivery delay. With increasing v_b, the CDF of the vehicle-to-drone packet delivery delay increases for all values of v_b. For instance, the CDF of the vehicle-to-drone delivery delay at v_b equal to 30 m/s is the highest CDF for all values of t. This is expected because increasing v_b causes an decrease in the time required to reach the drone in the backward direction. As a result, the vehicle-to-drone delivery delay decreases.

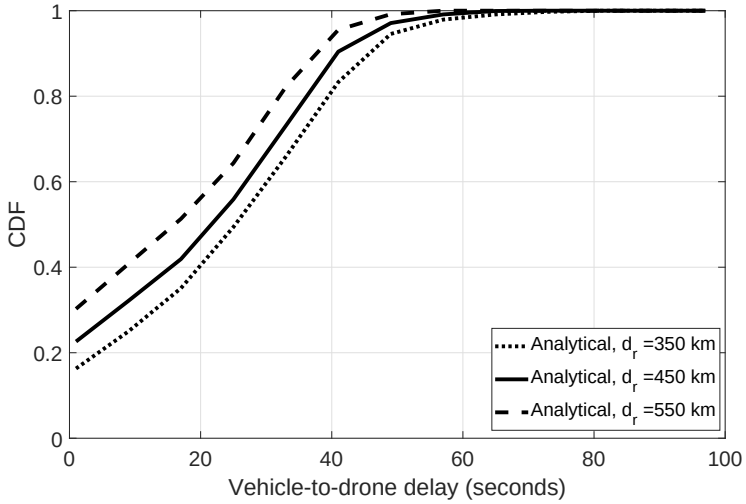

Figure 5.11: Vehicle-to-drone delay with changing d_r.

5.7.7 Drone communication range

Fig. 5.11 shows the analytical results for the CDF of the vehicle-to-drone packet delivery delay with the same parameters as in Table 5.2, and $x = 3$ km,while changing the drone communication range d_r to values of (350, 450, and 550) m.

Results show that the value of the drone communication range d_r has an impact on the CDF of the vehicle-to-drone delivery delay. With increasing the d_r, the CDF of the vehicle-to-drone packet delivery delay increased for all values of d_r. For instance, the CDF of the vehicle-to-drone delivery delay at d_r equal to 550 m is the highest CDF for the all values of t. This is because an increase in d_r while keeping the distance between a vehicle and a drone constant, results in a lower distance necessary for the message to forward the packets to the drone.

5.7.8 Results compared with the previous work

Our model is a generalization of the model in [5]. Our model considers the drone communication range d_r in the model. On the contrary, Ref. [5] considers a zero communication range for the RSUs. Therefore, our model's results are equal to those in [5] in the case that both models use a constant velocity model except when d_r equals zero.

On the other hand, to make sure the expression is not linear, we compare our results to those in [5], but subsitiute the value of a in Ref. [5] by $(a-2d_r)$. Fig. 5.12 compares the results from the proposed analysis and that from Ref. [5] for the CDF of the vehicle-to-drone packet delivery delay with the same parameters as in Table 5.2, while changing the drone range a to values of (4, 5, and 6) km.

The results show there is a big difference at t=0. In our model, we consider the drone range. Therefore, when the source vehicle is located within the drone range, the vehicle-to-drone range is zero as we assume the delay for wireless communication is zero. Therefore, in our model, the CDF of vehicle-to-drone delay at t equal zero is greater than zero for all values of a. However, Ref. [5] considers a zero wireless communication range for the RSUs. Therefore, the CDF of the vehicle-to-drone delay at t=0 is close to zero for all values of a.

5.7.9 DAS simulation results

We implemented the DAS algorithm in NS-2 based on the proposed closed-form expression and the maximum of the objective function mentioned in (Eq. 5.3) ($1-F_T(T_{\max},a) \leq \varepsilon$). Fig. 5.13 shows the simulation results of the DAS algorithm at different vehicular densities and probability of exit with the same parameters as in Table 5.2, and ε equal 0.006 while changing $T_{\max}$ to values of (30, 40, 50, and 60) seconds. Analytical results are not added here, as we use

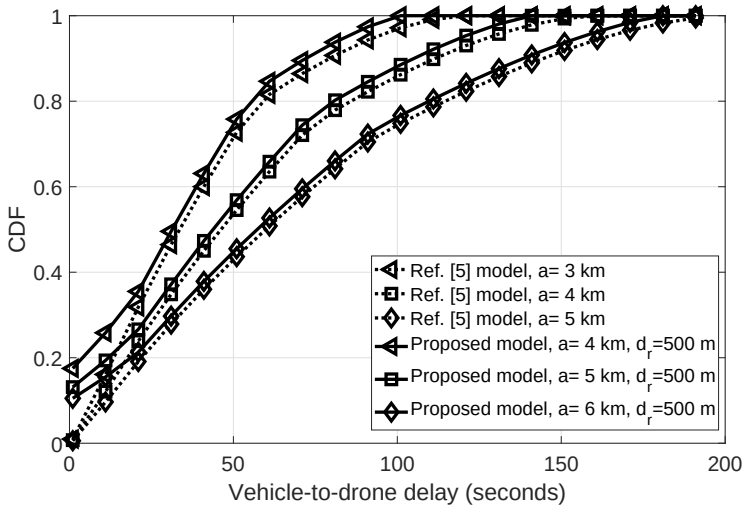

Figure 5.12: Results compared with the previous work.

the analytical closed form inside the simulation, giving the same result.

Results show that the value of $T_{\max}$ has a high impact on a. With increasing $T_{\max}$, the value of a increases for all values of $T_{\max}$. For instance, the highest values of a are at $T_{\max}$ equal to 60 seconds. This is because an increase in $T_{\max}$ leads to a longer a that still satisfies the probability delay constraint. As a result, the number of required drones will be different based on the new values of a, where the drone density equals $1/a$.

5.8 Conclusions

In this paper, we proposed a routing protocol that uses infrastructure drones for boosting VANET communications to achieve a minimum vehicle-to-drone packet delivery delay. This paper proposed a closed-form expression for the probability distribution of the vehicle-to-drone packet delivery delay on a two-way highway. In addition, based on that closed-form expression, we calculated the minimum drone density (maximum separation distance between two adjacent

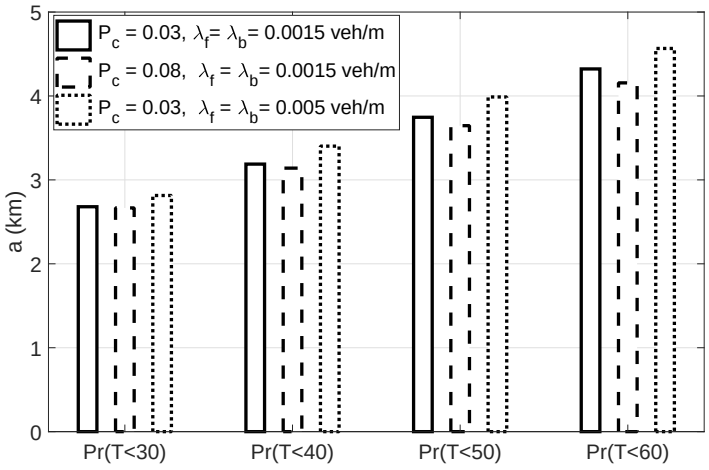

Figure 5.13: DAS simulation results.

drones) that stochastically limits the worst case of the vehicle-to-drone packet delivery delay. Moreover, we proposed a drones-active service (DAS) that is added to the location service in a VANET to dynamically and periodically obtain the required number of active drones based on the current highway connectivity state by obtaining the maximum distance between each two adjacent drones while satisfying a probabilistic constraint for vehicle-to-drone packet delivery delay. The simulation results show the accuracy of our analysis and reflect the relation between the drone density, vehicular density and speed, other VANET parameters, and the vehicle-to-drone packet delivery delay. In our future work, we will consider infrastructure-less drones with V2V communication. In addition, we will formulate the problem as an optimization problem to achieve the minimum end-to-end delay for V2V communication with a minimum number of drones. Moreover, we will formulate an optimization problem to obtain the optimal placement

for the drones in VANETs using DAS.

REFERENCES

[1] C. Kaplan, "Gps, cellular, fm speed and safety control devise," Dec. 26 2006, uS Patent App. 11/645,551.

[2] C. Campolo and A. Molinaro, "Multichannel communications in vehicular ad hoc networks: a survey," *IEEE Commun. Mag*, vol. 51, no. 5, pp. 158–169, 2013.

[3] B. Hassanabadi and S. Valaee, "Reliable periodic safety message broadcasting in vanets using network coding," *IEEE Trans. Wireless Commun*, vol. 13, no. 3, pp. 1284–1297, 2014.

[4] A. Abdrabou and W. Zhuang, "Probabilistic delay control and road side unit placement for vehicular ad hoc networks with disrupted connectivity," *IEEE J. Sel. Areas Commun*, vol. 29, no. 1, pp. 129–139, 2011.

[5] A. Abdrabou, B. Liang, and W. Zhuang, "Delay analysis for sparse vehicular sensor networks with reliability considerations," *IEEE Trans. Wireless Commun*, vol. 12, no. 9, pp. 4402–4413, 2013.

[6] J. Jeong, S. Guo, Y. Gu, T. He, and D. H. Du, "Trajectory-based data forwarding for light-traffic vehicular ad hoc networks," *IEEE Trans. Parallel Distrib*, vol. 22, no. 5, pp. 743–757, 2011.

[7] J. He, L. Cai, J. Pan, and P. Cheng, "Delay analysis and routing for two-dimensional vanets using carry-and-forward mechanism," *IEEE Trans. Mobile Comput*, vol. 16, no. 7, pp. 1830–1841, 2017.

[8] C.-C. Lin and D.-J. Deng, "Optimal two-lane placement for hybrid vanet-sensor networks," *IEEE Trans. Ind. Electron*, vol. 62, no. 12, pp. 7883–7891, 2015.

[9] C. Liu, H. Huang, and H. Du, "Optimal rsus deployment with delay bound along highways in vanet," *Journal of Combinatorial Optimization*, vol. 33, no. 4, pp. 1168–1182, 2017.

[10] I. Bor-Yaliniz and H. Yanikomeroglu, "The new frontier in ran heterogeneity: Multi-tier drone-cells," *IEEE Commun. Mag*, vol. 54, no. 11, pp. 48–55, 2016.

[11] X. Wang, L. Fu, Y. Zhang, X. Gan, and X. Wang, "Vdnet: an infrastructure-less uav-assisted sparse vanet system with vehicle location prediction," *Wireless Communications and Mobile Computing*, vol. 16, no. 17, pp. 2991–3003, 2016.

[12] O. S. Oubbati, A. Lakas, N. Lagraa, and M. B. Yagoubi, "Cruv: connectivity-based traffic density aware routing using uavs for vanets," in *Proc. IEEE ICCVE*, 2015, pp. 68–73.

[13] ——, "Uvar: An intersection uav-assisted vanet routing protocol," in *Proc. IEEE WCNC*, 2016, pp. 1–6.

[14] R. Shahidi and M. H. Ahmed, "Probability distribution of end-to-end delay in a highway vanet," *IEEE Commun. Lett*, vol. 18, no. 3, pp. 443–446, 2014.

[15] W. Kieß, H. Füßler, J. Widmer, and M. Mauve, "Hierarchical location service for mobile ad-hoc networks," *ACM J. SIGMOBILE*, vol. 8, no. 4, pp. 47–58, 2004.

[16] J. Li, J. Jannotti, D. S. De Couto, D. R. Karger, and R. Morris, "A scalable location service for geographic ad hoc routing," in *Proc. ACM MobiCom*, 2000, pp. 120–130.

[17] A. Al-Hourani, S. Kandeepan, and A. Jamalipour, "Modeling air-to-ground path loss for low altitude platforms in urban environments," in *Proc. IEEE GLOBECOM*, 2014, pp. 2898–2904.

[18] I. Bor-Yaliniz, S. S. Szyszkowicz, and H. Yanikomeroglu, "Environment-aware drone-base-station placements in modern metropolitans," *IEEE Wireless Communications Letters*, vol. PP, no. 99, pp. 1–1, 2017.

[19] M. Mozaffari, W. Saad, M. Bennis, and M. Debbah, "Drone small cells in the clouds: Design, deployment and performance analysis," in *Proc. IEEE GLOBECOM*, 2015, pp. 1–6.

[20] A. Al-Hourani, S. Kandeepan, and S. Lardner, "Optimal lap altitude for maximum coverage," *IEEE Commun. Lett*, vol. 3, no. 6, pp. 569–572, 2014.

[21] H. Fernández, L. Rubio, V. M. Rodrigo-Peñarrocha, and J. Reig, "Path loss characterization for vehicular communications at 700 mhz and 5.9 ghz under los and nlos conditions," *IEEE Antennas Wireless Propag. Lett*, vol. 13, pp. 931–934, 2014.

[22] P. Sermpezis, G. Koltsidas, and F.-N. Pavlidou, "Investigating a junction-based multipath source routing algorithm for vanets," *IEEE Commun. Lett*, vol. 17, no. 3, pp. 600–603, 2013.

[23] M. Ayaida, H. Fouchal, L. Afilal, and Y. Ghamri-Doudane, "A comparison of reactive, grid and hierarchical location-based services for vanets," in *Proc. IEEE VTC*, 2012, pp. 1–5.

[24] M. Jerbi, S.-M. Senouci, T. Rasheed, and Y. Ghamri-Doudane, "Towards efficient geographic routing in urban vehicular networks," *IEEE Trans. Veh. Technol*, vol. 58, no. 9, pp. 5048–5059, 2009.

[25] J. Härri, F. Filali, C. Bonnet, and M. Fiore, "Vanetmobisim: generating realistic mobility patterns for vanets," in *Proc. ACM VANET 06*, 2006, pp. 96–97.

Chapter 6

Accurate Probability Distribution Calculation for Drone-Based Highway-VANETs

6.1 Abstract

This letter analytically derives the probability distribution of the vehicle-to-drone packet delivery delay on a bi-directional highway. The model on which the analysis is based considers the vehicle wireless communication range and the cluster length. In addition, the proposed analysis finds that the same calculation in related work underestimates the maximum inter-drone distance, stochastically limiting the vehicle-to-drone packet delay using the drone active service (DAS). The accuracy of the proposed analysis is validated using simulations.

6.2 Introduction

A vehicular ad-hoc network (VANET) is a mobile ad-hoc network between vehicles, or vehicles and infrastructure units (road-side units or drones). VANETs have many applications as safety applications used to avoid collisions. Moreover, VANETs have commercial and comfort applications. While there are constraints on the packet delivery delay for safety applications, comfort applications can tolerate seconds or minutes for the same delay. For this reason, it is important to analyze the statistical characteristics of the packet delivery delay for safety messages in VANETs such as the probability distribution function and moments.

There are many papers that have analyzed the probability characteristics of the vehicle-to-infrastructure (V2I) packet delivery delay in VANETs. For instance, the expectation of the packet delivery delay from a vehicle to Internet access points was derived in [1] . Moreover, the expected value of the vehicle-to-RSU delay was derived analytically in [2]. Furthermore, the authors in [3] proposed a closed-form expression for the expected delay of broadcast alert messages up to reception by the nearest RSU in a highway VANET.

In addition, the authors in [4] presented a probabilistic analysis using effective bandwidth theory for the vehicle-to-RSU packet delay where RSUs were uniformly distributed over the highway. Furthermore, the authors in [5] proposed a mathematical framework for the vehicle-to-RSU packet delay cumulative density function (CDF) in the worst case. Moreover, based on drones that are uniformly distributed over the highway, a closed-form expression for the worst-case vehicle-to-drone packet delay CDF was proposed in [6]. Also, they accounted for the drone wireless communication range and proposed a drone active service (DAS) that updates the inter-drone distance.

The main difference between this proposed analysis and those in the previously-mentioned

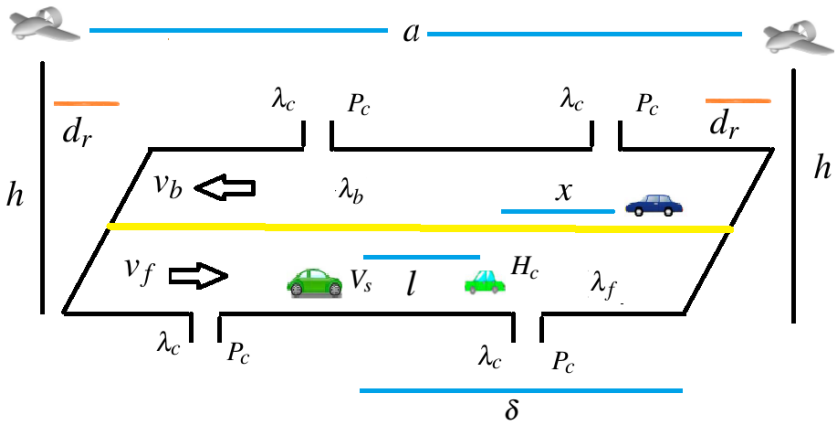

Figure 6.1: System model for the considered highway.

works (e.g., [1] - [5]) is that we focus on the probability distribution of the vehicle-to-drone delay, not just the expected value. Using the proposed analysis, we can calculate the maximum inter-drone distance which stochastically limits the delay to a certain upper bound. Consequently, the minimum number of drones required to be uniformly distributed over a two-way highway to satisfy such probabilistic constraints can be determined.

On the other hand, the main difference between this work and that in [5] and [6] is that our analysis considers the vehicles' wireless communication range and the VANET cluster length. Therefore, our analysis is more accurate, especially for higher values of the vehicular density where the vehicle can forward the packet to the next neighboring vehicle. On the contrary, [5] and [6] focus on the worst case only when the packet is carried by its original source vehicle until arriving within the communication range of the next infrastructure unit (RSUs in [5] or drones in [6]). Therefore, they did not consider the scenario where the packet can be forwarded between vehicles before reaching the next drone/RSU.

The main contributions of this letter are as follows: 1) it proposes an analytical expression for the vehicle-to-drone packet delivery delay probability distribution, and (2) it compares re-

sults from the proposed mathematical framework with simulation results and previous work to validate our analysis.

The rest of this letter is organized as follows. Section II introduces the system model. Section III presents the proposed analysis and the obtained expression. Then, Section IV compares the proposed analysis results against simulation results and previous work. Finally, conclusions and future work are given in Section V.

6.3 System model

We use the same system model proposed in [5] and [6]. However, in this model, we take into consideration the vehicle wireless communication range to derive a more accurate probability distribution of the vehicle-to-drone packet delay. In our model, we consider a bi-directional highway as shown in Fig. 6.1. In addition, we assume the vehicles in each direction are moving with constant speeds of v_f and v_b in the forward and backward directions, respectively (the forward direction is the direction towards the final destination, and the backward direction is the opposite direction). Furthermore, we assume that the number of vehicles in each direction follows a Poisson distribution and the inter-vehicular distances are exponentially-distributed [6]. Moreover, for each segment of length a, we have two drones with a wireless communication d_r, one at each end, as in [6]. In addition, y is the distance from the source vehicle to the next drone in the forward direction. On the other hand, we assume the VANET consists of a group of one or more disconnected VANET clusters. A VANET cluster consists either of a single vehicle not within the communication range of any other vehicle, or a group of fully connected vehicles, each within the wireless communication range of at least one other vehicle in the same cluster [7].

Table 6.1: List of Notation

a	Inter-drone distance
d_r	Drone wireless communication range
h	Altitude for the drone
X	R.V. representing the inter-vehicle distance
v_f	Forward direction speed
v_b	Backward direction speed
Δ	R.V. for distance between the drone and a vehicle
r	Vehicle communication range
P_c	Probability the vehicle leaves the highway at any junction
λ_c	Expected number of junctions
$u(\cdot)$	Heaviside unit step function
λ_f	Forward direction exponential rate parameter
λ_b	Backward direction exponential rate parameter

Moreover, with a probability P_c, we assume a vehicle can exit from the highway at any road junction. In addition, we assume the number of road junctions is Poisson-distributed with parameter λ_c as shown in Fig. 6.1. Furthermore, we assume that any vehicle can be the source of packets and an infrastructure drone is the destination. Moreover, one replica of the packets is sent in the opposite direction of the highway (the direction opposite to that for the source vehicle direction) by the cluster head in the forward direction. Consequently, packets are forwarded to the drone either by the cluster head or a moving vehicle in the opposite direction.

6.4 Proposed analysis

The proposed analysis follows the same methodology proposed in [6]. However, in this letter, the vehicle wireless communication range r is considered, which was not the case in the model and analysis in [6]. In this letter, our goal is to derive an analytical expression for the vehicle-to-drone packet delivery delay cumulative distribution function (CDF) in terms of a (inter-drone distance), d_r (drone wireless communication range), r (vehicle wireless communication range), λ_c (reciprocal of mean distance between those junctions), and λ_f and λ_b (forward and backward directions exponential rate parameters), as depicted in Fig. 6.1. Using the proposed analysis, one can calculate the minimum number of infrastructure drones corresponding to the maximum value of the inter-drone distance (a) that stochastically limits the vehicle-to-drone packet delivery delay to a certain upper bound $T_{\max}$ with a violation probability of at most ε, which can be expressed as follows

$$\begin{aligned} &\text{maximize} \quad a \\ &\text{subject to} \quad 1 - F_T(T_{\max}, a) \leq \varepsilon. \end{aligned} \tag{6.1}$$

In addition, we consider that the cluster head sends the packet in the forward and opposite directions and the analytical calculation considers the packet received earlier by the destination (infrastructure drone). In this case, the vehicle-to-drone packet delivery delay will be less than that if the cluster head just sent the packet in the forward direction. Furthermore, the probability that the vehicle-to-drone packet delay T is less than t can be represented as follows

$$Pr(T \leq t) = Pr(T \leq t, C = 1) + Pr(T \leq t, C = 0), \tag{6.2}$$

where C is a random variable representing the number of replicas forwarded from the packet. Therefore, the term $Pr(T \leq t, C = 1)$ is the joint cumulative probability the cluster head sends

one extra replica of the packet in the opposite direction besides sending the original packet in the forward direction, in a given time interval [0,t]. On the contrary, the term $Pr(T \leq t, C = 0)$ is the joint cumulative probability the cluster head sends the original packet in the forward direction only, in a given time interval [0,t].

We first derive an analytical expression for the first term $Pr(T \leq t, C = 1)$. The joint probability of the vehicle-to-drone packet delivery delay T and the number of replicas C can be represented as follows

$$Pr(T \leq t, C) = Pr(T \leq t|C)Pr(C). \tag{6.3}$$

On the other hand, as shown in Fig. 6.1, δ, the distance in the forward direction between the source vehicle V_s and the next drone, is between 0 and $a - 2d_r$, where d_r is the drone wireless communication range. On the contrary, X (the distance between the cluster head in the forward direction and the first moving vehicle that receives the packet from the cluster head in the opposite direction) lies between 0 and ∞. In addition, l, the cluster length (the distance between the the source vehicle and the cluster's head (H_c) is between 0 and ∞. Consequently, we can represent Eq. (6.3) for the case C=1 as follows

$$\begin{aligned} Pr(T \leq t, C = 1) = \int_0^{\infty} f(l) \int_0^{\infty} \int_0^{a-2d_r} Pr(T \leq t|C = 1, X = x, \Delta = \delta) \\ Pr(C = 1|X = x, \Delta = \delta) f(\delta, x) \; d\delta \; dx \; dl, \end{aligned} \tag{6.4}$$

Furthermore, the term $Pr(T \leq t|C = 1, X = x, \Delta = \delta)$ is the conditional probability of the vehicle-to-drone packet delay in the case when the packet is transmitted in the forward and backward directions. This term can be expressed as follows

$$Pr(T \leq t|C = 1, \Delta = \delta, X = x) = u\left(t - \min\left(\frac{a - \delta - d_r + x}{v_b}, \frac{\delta - d_r - l}{v_f}\right)\right). \tag{6.5}$$

Moreover, $\min(\cdot)$ in Eq. (6.5) can be removed as follows

$$= \begin{cases} u\left(t - \dfrac{\delta - d_r - l}{v_f}\right) & \text{if } 0 \le \delta \le \min(b_1, a-2d_r) \\ u\left(t - \dfrac{a-\delta-d_r+x}{v_b}\right) & \text{if } \min\left(b_1, a-2d_r\right) \le \delta \le a-2d_r, \end{cases}$$

$$\text{where} \qquad b_1 = \frac{(a-d_r+x)v_f + (l+d_r)v_b}{v_b + v_f}. \tag{6.6}$$

Therefore,

$$\begin{aligned} Pr(T \le t | C=1) = & \int_0^\infty f(l) \int_0^\infty \int_0^{min(b_1, a-2d_r)} f(\delta, x) u\left(t - \frac{\delta - d_r - l}{v_f}\right) f(\lambda_c, P_c)\, d\delta\, dx\, dl \\ + & \int_0^\infty f(l) \int_0^\infty \int_{b_1}^{a-2d_r} f(\delta, x) u\left(t - \frac{a-\delta-d_r+x}{v_b}\right) f(\lambda_c, P_c)\, d\delta\, dx\, dl. \end{aligned} \tag{6.7}$$

Moreover, $f(\delta, x)$ represents the joint probability density function (PDF) of Δ and X. In addition, as we mentioned in the system model, the source vehicle location is uniformly-distributed over the distance a, i.e., the random variable Δ is uniformly-distributed. On the other hand, as the vehicles form a Poisson process, X is exponentially-distributed. Consequently, $f(\delta, x)$ can be formulated as follows

$$f(\delta, x) = \frac{\lambda_f + \lambda_b}{a - 2d_r} e^{-(\lambda_f + \lambda_b)x}, \qquad 0 \le \delta \le a - 2d_r, x > 0. \tag{6.8}$$

In addition, $f(\lambda_c, P_c)$ is the probability that the cluster head vehicle does not exit at any road junction over the highway before arriving within the wireless communication range of the next drone. The authors in [6] obtained the expression for this probability as follows

$$f(\lambda_c, P_c) = e^{-\lambda_c P_c (a - \delta - 2d_r + x)}. \tag{6.9}$$

In addition, the PDF of the cluster length is derived in [7] as follows

$$f(l) = \frac{\lambda_f}{e^{-\lambda_f r} - 1} \sum_{i=0}^{\lfloor l/r \rfloor} \frac{\left(-\lambda_f (l - i\, r)\right)^{i-1}}{-m!} \left(\lambda_f (l - i\, r) + m\right) e^{-\lambda_f i\, r}. \tag{6.10}$$

$$Pr(T \leq t) = \sum_{k=0}^{\left\lfloor \frac{b_3}{r} \right\rfloor} \int_0^r f(kr+l) \int_0^{b_2} \int_0^{b_1} f(\delta,x) u\left(t - \frac{\delta - d_r - l}{v_f}\right) f(\lambda_c, P_c)\ d\delta\ dx\ dl$$
$$+ \sum_{k=0}^{\left\lfloor \frac{b3}{r} \right\rfloor} \int_0^r f(kr+l) \int_0^{b_2} \int_{b_1}^{a-2d_r} f(\delta,x) u\left(t - \frac{a - \delta - d_r + x}{v_b}\right) f(\lambda_c, P_c)\ d\delta\ dx\ dl$$
$$+ \sum_{k=0}^{\infty} \int_0^r f(kr+l) \int_0^{\infty} \int_0^{a-2d_r} f(\delta,x) u\left(t - \frac{\delta - d_r - l}{v_f}\right) \left(1 - e^{-\lambda_c P_c (a-\delta-2d_r+x)}\right)\ d\delta\ dx\ dl,$$

where

$$b_1 = \frac{(a - d_r + x)v_f + (kr + l + d_r)v_b}{v_b + v_f},\ b_2 = \frac{(a - 3d_r - kr - l)v_b - v_f d_r}{v_f},\ b_3 = \frac{(a - 3d_r)v_b - v_f d_r}{v_b} \tag{6.12}$$

On the other hand, in the case of $C = 0$, by following the same methodology for the analysis of the $C = 1$ case, the expression for the CDF in that case can be formulated as follows

$$Pr(T \leq t | C = 0) =$$
$$\int_0^{\infty} f(l) \int_0^{\infty} \int_0^{a-2d_r} f(\delta,x) u\left(t - \frac{\delta - d_r - l}{v_f}\right) f(\lambda_c, P_c)\, d\delta\, dx\, dl, \tag{6.11}$$

where $f(\lambda_c, P_c)$ is $1 - e^{-\lambda_c P_c (a-\delta-2d_r+x)}$ as in [5] and [6].

Using Eqs. (6.2), (6.3), (6.7), and (6.11), the CDF of the vehicle-to-drone packet delivery delay can be simplified as represented in Eq. (6.12).

6.5 Simulation and model validation

The proposed system model is implemented in NS-2 (v. 2.34). Moreover, VanetMobiSim [8] is used to generate vehicle mobility scenarios. Table 6.2 summarizes the configuration parameters used in the simulation.

Table 6.2: Simulation parameters

Simulation Parameter	Value
a (km)	5, 6.5, 8
v_b (m/s)	30
P_c	0.02
λ_c	0.002
v_f (m/s)	25
Simulation runs	600
Simulation time (seconds)	600
Vehicles wireless communication range (m)	300
Drone wireless communication range (m)	550

6.5.1 Inter-drone distance

With the parameter values in Table 6.2, the simulation and analytical results for the CDF of the vehicle-to-drone packet delivery delay are shown in Fig. 6.2, while varying the inter-drone distance a to values of (5, 6.5, and 8) km.

It can be noted that the two curves (simulation, and analytical) agree closely for the three inter-drone distances across all delay values, reflecting the correctness and accuracy of the proposed analysis. In addition, the results show the impact of the inter-drone distance parameter a on the CDF of the vehicle-to-drone delay. When the inter-drone distance a decreases, the CDF values increases. This is because increasing a causes the vehicle to carry the packet for a longer distance and we have the same speed in the three cases. Consequently, the vehicle-to-drone delay increases.

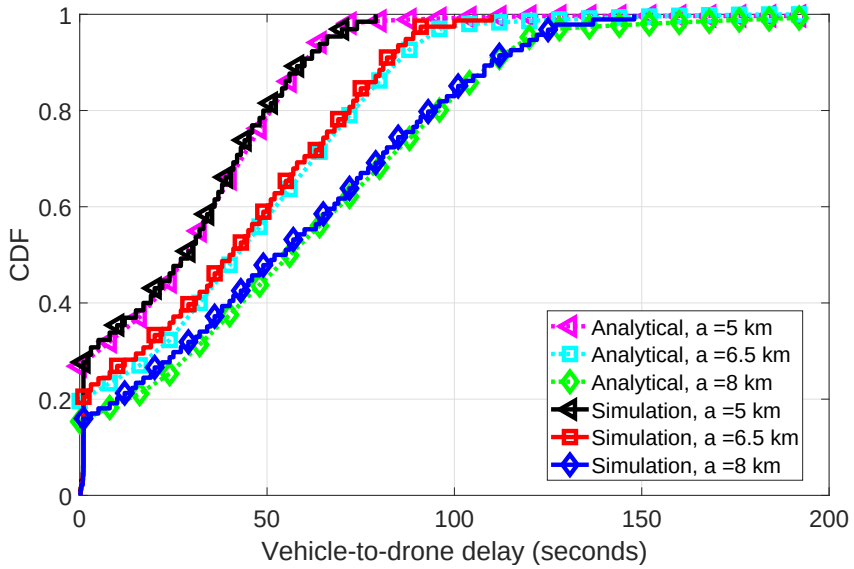

Figure 6.2: Inter-drone distance a and the CDF of the delay.

6.5.2 Proposed analysis results compared with previous work

As mentioned in Section I, a closed-form expression for the vehicle-to-drone packet delay probability distribution in the worst case was proposed in [6]. On the other hand, the analysis here yields a more accurate probability distribution by considering the VANET cluster length and wireless communication range for vehicles. With the parameter values in Table 6.2, the analytical results of the proposed analysis and those from [6] are shown in Fig. 6.3, while changing the vehicular densities λ_f and λ_b to values of (0.002, 0.005, 0.008) vehicle/m.

It can be noted that in the results for the three values of the vehicular densities, the CDF values of our model are higher than those of [6]. This is expected, as [6] took into consideration the worst case only. In addition, the results show that there is a big difference between both analyses especially at higher vehicular density values. At lower vehicular density values (like 0.002 veh/m), the difference between the two curves decreases. This is because at lower

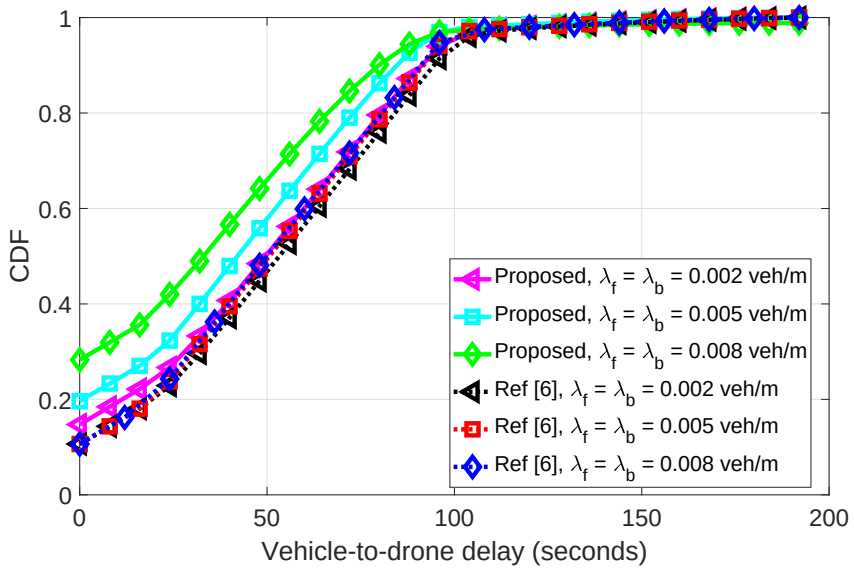

Figure 6.3: Results from proposed analysis vs. those from Ref. [6].

vehicular density values, the cluster length is shorter and the cluster head carries the packets for a longer distance (very close to the worst case where the cluster head is the vehicle source as in [6]). On the other hand, at higher vehicular densities, the differences are very high. This is because the probability of having a longer cluster length increases. Consequently, the cluster head carries the packet for a shorter time. Moreover, the results show that the vehicular densities have a lower impact on the CDF of the delay in [6]. This is because in [6], the vehicular density has an impact only in the opposite direction on the random variable x.

6.5.3 Drone-active service results

Fig. 6.3 shows the DAS simulation results of the proposed analysis and those from [6] with the parameter values in Table 6.2, and based on Eq. 6.1 where ε equal 0.05 and $T_{\max}$= 50 seconds, while changing the vehicular densities λ_f and λ_b to values of (0.001, 0.005, 0.009) veh/m.

Results show that the DAS calculation in our case always yields a higher inter-drone distance

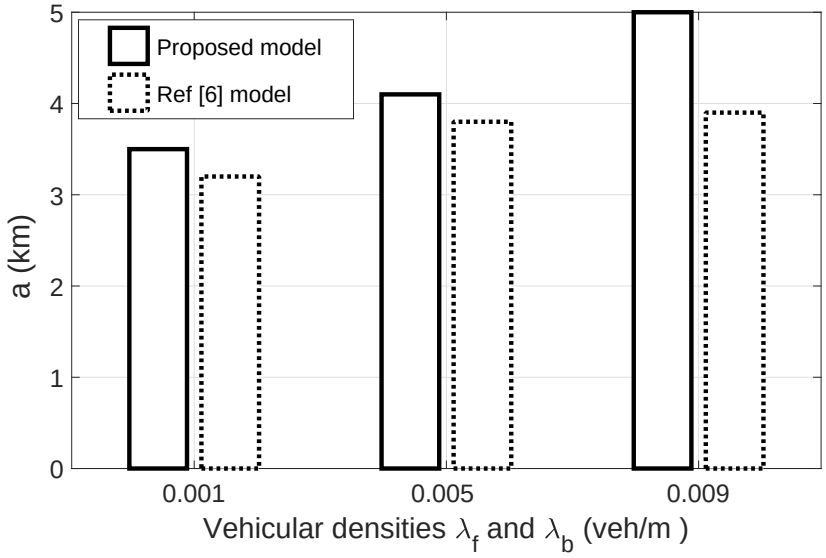

Figure 6.4: DAS Results compared with those from Ref. [6].

a than that from the DAS calculation from [6] for the same parameters. Consequently, our analysis requires a lower number of drones to cover the highway than that required in the case of the analysis from [6]. At lower values of vehicular density, this difference decreases. This is because at lower vehicular density values, the cluster lengths are shorter. On the other hand, at higher vehicular densities, the differences are very high. This is because the probability of having a longer cluster length increases.

6.6 Conclusions

In this letter, we propose an analytical expression for the probability distribution of vehicle-to-drone packet delay on a bi-directional highway. This analysis is more accurate than in previous works that focus on the worst case only. The drone-active service (DAS) can benefit from our analysis. Our analysis is more accurate and the CDF from this analysis is always higher than

that proposed in [6]. Also, the DAS calculation requires a lower number of drones than that required in the case of the analysis from [6]. In future work, infrastructure-less drones can be considered.

REFERENCES

[1] J. Jeong, S. Guo, Y. Gu, T. He, and D. H. Du, "Trajectory-based data forwarding for light-traffic vehicular ad hoc networks," *IEEE Trans. Parallel Distrib*, vol. 22, no. 5, pp. 743–757, 2011.

[2] J. He, L. Cai, J. Pan, and P. Cheng, "Delay analysis and routing for two-dimensional vanets using carry-and-forward mechanism," *IEEE Trans. Mobile Comput*, vol. 16, no. 7, pp. 1830–1841, 2017.

[3] C. Liu, H. Huang, and H. Du, "Optimal rsus deployment with delay bound along highways in vanet," *Journal of Combinatorial Optimization*, vol. 33, no. 4, pp. 1168–1182, 2017.

[4] A. Abdrabou and W. Zhuang, "Probabilistic delay control and road side unit placement for vehicular ad hoc networks with disrupted connectivity," *IEEE J. Sel. Areas Commun*, vol. 29, no. 1, pp. 129–139, 2011.

[5] A. Abdrabou, B. Liang, and W. Zhuang, "Delay analysis for sparse vehicular sensor networks with reliability considerations," *IEEE Trans. Wireless Commun*, vol. 12, no. 9, pp. 4402–4413, 2013.

[6] H. Seliem, R. Shahidi, M. H. Ahmed, and M. S. Shehata, "Drone-based highway-vanet and das service," *IEEE Access*, vol. 6, pp. 20 125–20 137, 2018.

[7] Z. Zhang, G. Mao, and B. D. O. Anderson, "On the information propagation process in mobile vehicular ad hoc networks," *IEEE Transactions on Vehicular Technology*, vol. 60, no. 5, pp. 2314–2325, Jun 2011.

[8] J. Härri, F. Filali, C. Bonnet, and M. Fiore, "Vanetmobisim: generating realistic mobility patterns for vanets," in *Proc. ACM VANET 06*, 2006, pp. 96–97.

Chapter 7

Conclusions and Future Work

7.1 Introduction

Most of the existing routing protocols for VANET use the carry-and-forward strategy as one of the routing strategies to counter network disconnection. However, the packets suffer from long end-to-end delay in a carry-and-forward strategy, especially in low vehicular densities. Some VANET applications have an end-to-end delay constraint. Consequently, end-to-end delay is a very important issue in VANET routing design. In this final chapter, we summarize the contributions presented in this dissertation and discuss several potential extensions to our work.

7.2 Conclusions

The following conclusions can be drawn from this dissertation:

- We proposed a new routing protocol called multi-copy intersection-based routing (MCIR) [1] for vehicular ad-hoc networks (VANETs) in urban areas. MCIR is an intersection-

based routing protocol that forwards multiple copies of the packets in different road segments.

- We proposed a closed-form expression for the probability distribution of the re-healing delay conditioned on the gap distance between those two clusters on a one-way highway [2].

- We proposed a closed-form expression for the unconditional probability distribution of the re-healing delay [2].

- We proposed an analytical model to study the end-to-end delay in a one-way VANET and derive an analytical formula for the probability distribution of the end-to-end delay.

- We proposed a closed form expression for the lower bound on the end-to-end delay probability distribution.

- We proposed a closed form expression for the upper bound on the end-to-end delay probability distribution.

- We presented a routing protocol that uses infrastructure drones for boosting VANET communications to achieve a minimum vehicle-to-drone packet delivery delay.

- We propose a closed-form expression for the probability distribution of the vehicle-to-drone packet delivery delay on a two-way highway [3]. Based on that closed-form expression, we can calculate the minimum drone density (maximum separation distance between two adjacent drones) that stochastically limits the worst case of the vehicle-to-drone packet delivery delay.

- We proposed a drones-active service (DAS) [3] that is added to the location service in a VANET. This service dynamically and periodically obtains the required number of active drones based on the current highway connectivity state by obtaining the maximum distance between each two adjacent drones while satisfying a probabilistic constraint for vehicle-to-drone packet delivery delay.

- We propose an analytical expression for the probability distribution of the vehicle-to-drone packet delivery delay on a two-way highway where we consider the vehicle wireless communication range and the cluster length in the analysis.

7.3 Future Works

Despite the large number of research activities and the rapid and significant progress being made in VANET routing in recent years, numerous avenues for further research remain. The following research issues are outlined for future investigation:

- Bi-directional highway: Our analysis in Chapters 3 and 4 considers one way highways. Therefore, extending this analysis for bi-directional highway can be considered as an interesting area for future research.

- Drone-placement: In Chapter 3, the drones are uniformly distributed over the highway. In addition, DAS update the distance between them based on the highway status. Formulating the problem as an optimization problem to calculate the optimal location for each drone (drone-placement problem) to obtain a minimum number of drones with the highest VANET connectivity, this point can be viewed as an interesting area for future investigation.

- Drones with uniform vehicle speeds: In Chapters 5 and 6, we considers constant speed for vehicles in the forward and backward direction. Considering a uniform distribution for the vehicles' speed can be considered as an interesting area for future research.

- Implementations: The contribution on this dissertation have been evaluated through theoretical analysis and simulation. Further investigation and improvements to the current implementation approaches are identified as areas for future work.

REFERENCES

[1] H. Seliem, M. H. Ahmed, and M. S. Shehataa, "Multi-copy intersection-based routing for vanet in urban area," *International Journal of Technology and Engineering Studies*, vol. 3, no. 5, pp. 204–212, 2017.

[2] H. Seliem, R. Shahidi, M. H. Ahmed, and M. S. Shehata, "Probability distribution of the re-healing delay in a one-way highway vanet," *IEEE Commun. Lett*, vol. 22, no. 10, pp. 2056–2059, Oct 2018.

[3] ——, "Drone-based highway-vanet and das service," *IEEE Access*, vol. 6, pp. 20 125–20 137, 2018.

Appendix A

Lower Bound for the End-to-end Delay PDF

We can assume the first term in Eq. (4.1) that has in the denominator $t(v_{\max}+v_{\min})\left(\lambda+\frac{2(\lambda v_{\min}-\lambda v_{\max})}{v_{\max}+v_{\min}}\right)^2$, is equal to $e^{-\left(k_2+k_1+\lambda t+\frac{2\lambda(r-v_{\min}t)}{v_{\max}+v_{\min}}\right)}(A)$. Now, we wish to prove that

$$e^{-\left(k_2+k_1+\lambda t+\frac{2\lambda(r-v_{\min}t)}{v_{\max}+v_{\min}}\right)}(A) > -\frac{v_{\max}+v_{\min}}{\Delta v}e^{-(k_2-k_1)} \tag{A.1}$$

After simplification, this is equivalent to

$$A > -\frac{v_{\max}+v_{\min}}{\Delta v}e^{\lambda t+k_1+\frac{2\lambda r}{v_{\max}+v_{\min}}} \tag{A.2}$$

Then, substituting A by its value and multiplying both sides by -1

$$\frac{(\Delta v)^2\lambda\left(e^{k_2}+e^{k_1+\lambda t}\left(\lambda t-1-\frac{2\lambda t\Delta v}{v_{\max}+v_{\min}}\right)\right)}{\lambda^2 t(v_{\max}+v_{\min})^2\left(1-\frac{2\Delta v}{v_{\max}+v_{\min}}\right)^2} < e^{\lambda t+k_1+\frac{2\lambda r}{v_{\max}+v_{\min}}} \tag{A.3}$$

Then, dividing both sides by $e^{\lambda t+k_1}$

$$\frac{(\Delta v)^2\left(e^{k_2-k_1-\lambda t}+\left(\lambda t-1-\frac{2\lambda t\Delta v}{v_{\max}+v_{\min}}\right)\right)}{\lambda t(v_{\max}+v_{\min})^2\left(1-\frac{2\Delta v}{v_{\max}+v_{\min}}\right)^2} \quad < e^{\frac{2\lambda r}{v_{\max}+v_{\min}}} \tag{A.4}$$

This can be expressed in the equivalent form

$$(\Delta v)^2\left(e^{k_2-k_1-\lambda t}+\lambda t-1-\frac{2\lambda t\Delta v}{v_{\max}+v_{\min}}\right) < \lambda t e^{\frac{2\lambda r}{v_{\max}+v_{\min}}}(v_{\max}+v_{\min})^2\left(1-\frac{2\Delta v}{v_{\max}+v_{\min}}\right)^2 \tag{A.5}$$

However, we have $1+x \leq e^x$, so we can replace $e^{k_2-k_1-\lambda t}$ by $1+k_2+-k_1-\lambda t$ as follows

$$(\Delta v)^2\left(k_2-k_1-\frac{2\lambda t\Delta v}{v_{\max}+v_{\min}}\right) < \lambda t(v_{\max}+v_{\min})^2\left(1-\frac{2\Delta v}{v_{\max}+v_{\min}}\right)^2 e^{\frac{2\lambda r}{v_{\max}+v_{\min}}} \tag{A.6}$$

In addition, the term $\left(k_2-k_1-\frac{2\lambda t\Delta v}{v_{\max}+v_{\min}}\right)=0$. Consequently, inequality Eq. (A.1) will be true whenever

$$\lambda > 0 \tag{A.7}$$

From the system model, λ always is greater than zero. Therefore, Eq. (A.1) is always true.

Appendix B

Upper Bound for the End-to-end Delay PDF

Here, we wish to prove that

$$e^{-\left(k_2+k_1+\lambda t+\frac{2\lambda(r-v_{\min}t)}{v_{\max}+v_{\min}}\right)}(A) < \left(\frac{-2\left(-\Delta v+\frac{(2\Delta v)^2}{4v_{\max}+v_{\min}}\right)}{(v_{\max}+v_{\min})\left(1-\frac{2\Delta v}{v_{\max}+v_{\min}}\right)^2}\right) e^{-\left(k_2-k_1+\frac{2\lambda r}{v_{\max}+v_{\min}}\right)}. \quad \text{(B.1)}$$

After substitution of A and multiplication of both terms by $(v_{\max}+v_{\min})\left(1-\frac{2\Delta v}{v_{\max}+v_{\min}}\right)^2 e^{\left(k_2+\lambda t+\frac{2\lambda r}{v_{\max}+v_{\min}}\right)}/2$, Eq. (B.1) can be expressed as follows

$$\frac{\Delta v\left(-e^{k_2}-e^{k_1+\lambda t}\left(\lambda t-1-\frac{2\lambda t\Delta v}{v_{\max}+v_{\min}}\right)\right)}{\lambda t} < \left(\Delta v-\frac{(2\Delta v)^2}{4v_{\max}+v_{\min}}\right) e^{\lambda t+k_1} \quad \text{(B.2)}$$

Then, dividing both terms by Δv

$$\left(-e^{k_2}-e^{k_1+\lambda t}\left(\lambda t-1-\frac{2\lambda t\Delta v}{v_{\max}+v_{\min}}\right)\right) < \lambda t\left(1-\frac{4\Delta v}{4v_{\max}+v_{\min}}\right) e^{\lambda t+k_1} \quad \text{(B.3)}$$

Then, dividing both terms by $e^{\lambda t+k_1}$

$$-e^{k_2-k_1-\lambda t}-\lambda t+1+\frac{2\lambda t\Delta v}{v_{\max}+v_{\min}} < \lambda t\left(1-\frac{4\Delta v}{4v_{\max}+v_{\min}}\right) \quad \text{(B.4)}$$